DIPARTIMENTO DI INGEGNERIA INDUSTRIALE
CORSO DI LAUREA MAGISTRALE IN INGEGNERIA CHIMICA E DEI PROCESSI INDUSTRIALI

Tesi di Laurea Magistrale in Ingegneria Chimica e dei Processi Industriali

MICROSTRUCTURED FOOD POWDERS PRODUCTION BY SPRAY DRYING

Supervisors

Prof. Andrea Claudio Santomaso

Prof. Bipro Nath Dubey

Author

Patrick Roncato

Sessione Febbraio
Anno Accademico 2018/2019

Riassunto.

Durante i sei mesi trascorsi alla Sheffield Hallam University (UK) nei laboratori del MERI (Material and Engineering Research Institute), e grazie al dipartimento del NCEFE (National Centre of Excellence for food engineering), è stato eseguito uno studio sulla produzione di nuove strutture controllate a livello della microscala, impiegabili nell'industria alimentare. L'obiettivo del progetto è stato quello di includere nella struttura delle polveri micrometriche dei composti che non apportassero un aumento del valore nutrizionale ma che allo stesso tempo aiutassero ad integrare l'assunzione di nutrienti normalmente carenti nella dieta.

Diverse fibre alimentari sono state prese in considerazione, la sfida maggiore riguardante la produzione delle polveri alimentari attraverso spray drying, ha riguardato l'insolubilità delle fibre nella fase continua. Dopo la preparazione di alcune emulsioni olio in acqua, è stata eseguita una simulazione fluidodinamica per cercare di predire il comportamento di queste all'interno dell'ugello dello spray dryer. Sono state testate diverse condizioni operative quali temperatura e portata volumetrica dell'aria, portando a raggiungere una soddisfacente dimensione delle particelle, e buone proprietà riguardanti la loro densità e scorrevolezza. Le polveri più promettenti sono state quelle che includevano fibre di mela.

La parte finale di questo lavoro è stata quella di studiare la fattibilità economica del processo di produzione di una delle polveri prodotte, su larga scala. La valutazione è stata eseguita ad un livello di studio, quindi l'intervallo di incertezza è del 20 %, tuttavia il risultato ottenuto è incoraggiante.

Abstract

During the six months passed at Sheffield Hallam University (UK) in MERI laboratories (Material and Engineering Research Institute), and thanks to NCEFE department (National Centre of Excellence for food engineering), a study on new microstructured food grade powders has been conducted. These powders may be employed in the food industry. The objective of this project was achieving the inclusion in the microstructure of the powders, some components that cannot bring an increase in the nutritional value of the final product, but that at the same time that they could help to integrate the assumption of nutrients normally lacking in our diets.

Different dietary fibres were taken in account, the major challenge has been the one concerning the production of the powders through the spray drying technique, since some of the fibres were insoluble, and they were causing clogging problem in the nozzle. To avoid this problem as much as possible some fluid dynamics simulations were performed, trying to predict the behaviour of the oil in water emulsions prior the spray drying experiments. Different experimental conditions were tested, leading to reach a satisfying particle dimension, and good properties regarding their density and flowability. The more promising powders have been the ones containing apple fibres.

The final part of this work regards the study of the economical feasibility of the production process of one of the produced powders, on a large scale. The evaluation has been done at a study level, so the uncertainty is 20 % of the final result, which remains still encouraging.

Contents

List of Figures

List of Tables

Introduction

Human diet is changing and obesity is one of the major problems affecting some populations. To reduce the hunger feeling, without compromising the regular calories intake and without adding any nutritional value, fibers can help. Between their beneficial effects there is also the one concerning the aid provided during the digestion.
Food waste is another of the major problems in the occidental society. Every year an average of 270 kg of food waste per capita are produced [9]. Some food waste can be reprocessed to reduce this amount of waste and at the same time adding a new piece to the circular economy. Inside this macro group, a large percentage is coming from vegetables and fruit, and the waste is mainly composed by fibers.
But how to create a safe and deliverable product, coming from wastes ?
Spray drying is a well known technique that has been used for two centuries in the food industry. Its capability of deliver food grade powders on a large scale has been improved and more complex structures can be created through it. The success of this technique is that it's easily scalable and each module can be replicated several times, being controlled with an unique strategy.
At the moment, one of the main field of research around this technique applied to food industry, is the micro and nano encapsulation of some nutrients. If these particular nutrients that might be particularly sensible to oxidation, are encapsulated in microstructure, they could not only being better preserved, but also released in a more controlled way in the organism.
The key challenge of incorporating bioactive ingredients into functional foods is to keep the constituents stable and to release them into the target site of human bodies. Microencapsulation is broadly utilized also in industry and it can be pursued via spray drying, coacervation, and other routes. For a scale up of the production, a continuous process like the spray drying saves cost, time and energy and thus offers more advantages than the batch process, but it's not always feasible. Indeed, these different routes have specific conditions e.g., high temperature, shear force, that in fact affect the ingredients preservation.
The structure around those nutrients may be composed then by those fibers cited above. The main challenge is that most of them are not soluble and they might cause some problems in the operations. The purpose of this study is therefore trying to achieve the feasibility of this type of production.

Structure of the work

In the first chapter the theory behind the emulsions and their formulation is explained, as well as the one of the spray drying process. The second chapter reports the description of the materials and the equipment used to perform the experiments that led to produce the particles, reported in Chapter 4. The third chapter instead was dedicated to analyze the nozzle of the spray drying equipment to get some preliminary results, exploiting the fluid dynamic simulation, in order to reduce the number of experiments. Chapter 5 is entirely focused on the proposed design at a study level for the scale up of the powders production.

Chapter 1

State of the art

1.1 Food emulsions

According to [19], food emulsions, such as mayonnaise and salad dressings, are two-phase systems of immiscible liquids with limited stability. One phase is in the form of finely divided droplets of diameters generally larger than 0.1 μm. This dispersed, internal, or discontinuous phase is suspended in the continuous or external phase. Emulsion systems can be divided into two categories:

- those consisting of droplets of oil dispersed throughout an aqueous medium, which are usually referred to as oil-in-water emulsions;
- those in which droplets of water are dispersed throughout an oil or fat medium, which are termed water-in-oil emulsions. Most food emulsions are of the oil-in-water type.

There are then double emulsions, whose dispersed phase in containing part of the continuous phase (or similar to it). They are mostly used in biology, and they can be created by using two steps or one step. Emulsion properties generally depend on the nature of the continuous phase and the proportion of this phase to the dispersed phase

1.1.1 Food Emulsions formulation

The first stage of the process includes the dispersion, mixing and dissolution of the ingredients in the phase that is more capable to solubilize them. The order with which the ingredients are added has a relevant impact on the result, as well as the physic-chemical properties of the continuous phase and the type, intensity and duration of mixing.
The homogenization step involves the usage of a mechanical device, called homogenizer. Primary homogenization consists in the creation of a coarse emulsion starting from two separate phases, usually using a high shear blender. The secondary homogenization provides a size reduction of a pre-existing emulsion, by using different techniques such as colloid mill, high pressure valve homogenizer, rotor stator. The two types of homogenization could be used together, and the equipment used depends on the droplet size distribution objective, the materials to be processed, the cost of purchasing and running the (scaled) equipment.

1.1.2 Physical principles

The final droplet size distribution depends on the balance between droplet disruption and droplet coalescence, which are competing one against the other. The interfacial forces that hold the droplets together must be overcome by the disruptive forces given by the homogenizer. Since disruptive forces are proportional to the reciprocal of the droplet diameter, the smaller the particle size, the

more the disruptive force to be applied. The shape of the droplets tends to be spherical because the contact area between the two phases is minimized.

1.1.3 Emulsifiers

An emulsifier is a compound that has an hydrophilic and an hydrophobic part. Its primary role consists in creating a stable interface between the continuous and the dispersed phase. While the emulsification operation is performed, the time taken by the droplets to coalesce should be less than the one used by the emulsifier to form a layer around the droplets. Another role expected by the emulsifier to be played is the reduction of the interfacial tension, so that smaller droplets can be formed applying the same disruptive force. The concentration of emulsifier used is another factor that must be taken in account. Nowadays there is not a general classification schema that indicates which is the best emulsifier to be used according to a specific case, but the functional properties of the emulsifiers can be evaluated and compared exploiting some parameters, like the minimum droplet size, the minimum emulsifier load and the stability index. The major challenge about emulsifiers remains the correlation between more fundamental process parameters to the following physical characteristics:

- Surface load, Γ_{sat}, usually expressed as mg/m^2. It provides an indication about the minimum quantity of emulsifier required to generate an emulsion with a given droplet size (or surface area).
- Minimum surface pressure. It's the net amount of surface tension that can be reduced by using a sufficient amount of emulsifier: the higher this value, the smaller the droplet size that can be reached providing the same energy input.
- Adsorption kinetics is a measure of the average time taken by the emulsifier to be fully absorbed on the droplet surface. It is difficult to measure because the same dynamic conditions inside the homogenizer should be reproduced to achieve an accurate value.
- Binding affinity produces an indication about how strong an emulsifier is absorbed to the interface. It is usually expressed as the concentration of emulsifier when the surface pressure is half of the maximum one.

After the emulsion has been created, it could undergo through different treatments like pasteurization, cooling, to reduce the microbial population or to achieve a longer shelf life. Dehydration through spray, freeze or roller drying could be done to obtain solid powders from the liquid emulsion.

1.1.4 Emulsion stability

The overall interaction between droplets which is the major responsible for emulsion stability, depends on the sign, the magnitude and the range of several different types of interactions. The most important ones are described below.

Van Der Waals Interactions

These attractive forces can be calculated according to

$$w_{VDW} = -\frac{A}{6}\Big[\Big(\frac{2r^2}{h^2+4hr}\Big) + \Big(\frac{2r^2}{h^2+4hr+r^2}\Big) + ln\Big(\frac{h^2+4hr}{h^2+4hr+r^2}\Big)\Big] \tag{1.1}$$

Or, if the radius of the droplets r is much larger than the distance between them, the equations can be simplified to:

$$w_{VDW} = -\frac{Ar}{12h} \tag{1.2}$$

A is the Hamaker function, that can be calculated numerically as:

$$A = \frac{3}{4}kT\sum_{s=1}^{\infty}\frac{1}{s^3}\left(\frac{\epsilon_1-\epsilon_2}{\epsilon_1+\epsilon_2}\right)^{2s} + \frac{3hv_e}{16\sqrt{2}}\frac{(n_1^2-n_2^2)^2}{(n_1^2+n_2^2)^{3/2}} = A_{v=0} + A_{v>0} \tag{1.3}$$

ϵ the static relative dielectric constant, n is the refractive index, h is the Plank constant and v_e is the major electronic absorption frequency in the ultraviolet region. It can be noted that the use of emulsifiers reduces the strength of v.d.W interactions so that the stability is improved. The relations reported above overestimates anyway the attractive forces, because they do not consider the effects of electrostatic screening, retardation and the interfacial layer on the Hamaker function.

Electrostatic Interactions

Ionic or ionized absorbed compounds can lead to the formation of charged droplets, whose interaction can be approximately be described by Eq. 1.4, assuming that the interactions are not strong and the surface charge density is constant.

$$w_{electrostatic} = -2\pi\epsilon_0\epsilon_R r\Psi_\delta^2 ln(1-e^{-kh}) \tag{1.4}$$

where

$$k = \left(\frac{\epsilon_0\epsilon_r kT}{e^2\sum c_i z_i^2}\right) \tag{1.5}$$

k is the thickness of the electric double layer, with c_i and z_i molar concentration and valence of ions of the i-th species, ϵ_r is the relative dielectric constant of the medium around the droplets, while ϵ_0 is the dielectric constant in the vacuum. k is the Boltzmann constant, T is the absolute temperature, Ψ_δ is the surface potential of the droplets. Electrostatic interactions have a positive impact preventing aggregation, since usually all droplets have the same charge, so a repulsion is verified. For same biopolymers like proteins, the charge is changing with pH variation above or below their isoelectric point, and this has major consequences for the protein-coated droplets stability.

Hydrophobic Interactions

Although oil in water emulsions are usually coated with emulsifier so that their behaviour is hydrophilic, there might be some zones not covered by the emulsifier, especially during the homogenization, or there could be the presence of hydrophobic groups on the surface (e.g. protein unfolding causes exposure of non polar groups). These interactions are described with Eq. 1.5.

$$w_{hydrophobic} = -2\pi r\gamma_i\phi_H\lambda_0 e^{-h/\lambda_0} \tag{1.6}$$

λ_i is the interfacial tension between the continuous phase (water) and non-polar groups, λ_0 is the decay length of interaction, not greater than 2 nm, ϕ_H is the measure of hydrophobicity of the droplets, from 0 to 1, with 1 being a fully non polar surface.

Short range forces

This type of interaction is difficult to predict, since it depends on may factors like size, shape, conformation, packing, interactions, mobility and hydration of molecules in the absorbed layer. However, in a first approximation, they can be described with the following relation:

$$w_{SR} = \begin{cases} \left(\frac{2\delta}{h}\right)^{12} & x < 2\delta \\ 0 & x \geq 2\delta \end{cases} \tag{1.7}$$

where δ is the thickness of the absorbed layer of emulsifier molecules surrounding the droplets.

1.1.5 Emulsion instability

Depending on the environmental conditions, the physicochemical characteristic of the emulsion, and the processing conditions used to create it, the instability of the final product can manifest itself immediately or after a long time. The major mechanisms that bring to an instability are flocculation, creaming, Ostwald ripening, coalescence and phase inversion. Most of the time they are interacting each other, but usually one of them is prevailing. The knowledge of the dominant mechanism allows to prevent and control better the stability duration. Sometimes the emulsion is not required to be stable for a long time, since it is an intermediate product: that is the case of this thesis work, in which the emulsion can be used after its creation. Nevertheless it might be necessary to store the emulsion for short times before processing it, so some considerations must be done.

Creaming and Sedimentation

Creaming occurs when droplets are lighter than the continuous phase. On the contrary, sedimentation happens when droplets tend to move downwards. Oil in water emulsions tend to suffer creaming the most, since the density of many oils is less than the one of water. Creaming velocity can be calculated in a first approximation with Stokes equation (1.8).

$$v = -\frac{2gr^2(\rho_2 - \rho_1)}{9\eta_1} \tag{1.8}$$

v is the net velocity and if velocity is positive, the movement will be upwards. The greater assumption is that droplets are isolated spherical rigid particles that move through a Newtonian fluid. As suggested by Dickison (1992), an emulsion with a creaming rate less than 1 mm/day can be considered to be stable toward creaming. For food emulsions, Stokes equation needs to be modified, taking in account the non Newtonian behavior of the continuous phase, the Brownian motion, the absorbed layer, droplet aggregation and hydrodynamic interactions.

Flocculation and Coalescence

When two droplets collide, depending on the prevailing force, they may remain aggregated together or bounce and move apart. In the first case two types of aggregation can be distinguished: flocculation (droplets remain and coalescence. In both cases the collision frequency and efficiency determine the rate at which the droplet aggregate together. For quiescent and stirred systems, the collision frequency has been calculated according to 1.9 and 1.10 respectively:

$$N = \frac{4kTn_0^2}{3\eta} \tag{1.9}$$

$$N = \frac{16}{3}Gr^3n_0^2 \tag{1.10}$$

n_0 is the number of particles after homogenization at time 0, per number volume, r is the droplet radius, G is the shear rate and kT is the thermal energy. Depending on the nature of the interface and the interaction potential, the collision efficiency can vary between 0, corresponding to no aggregation, to 1 (aggregation occurs fast). Extensive coalescence can lead to the so called *oiling off*, the formation of free oil on the top of an emulsion. Although many food emulsion are stable to coalesce, they can become unstable when subjected to high shear forces, during aeration, when they are centrifuged or when droplets remain in contact for extended periods. Partial coalescence may arise when two partly crystalline droplets are aggregating forming a new particle with an irregular shape. Sometimes it may be a wanted effect to increase the viscosity of the emulsion.

Ostwald ripening

This phenomenon is described as the growth of bigger droplets at the expense of the smaller ones. It occurs because of the diffusion of dispersed phase particles through the continuous medium, and because the material inside the droplet becomes more soluble in the continuous phase when the droplet size diminishes. Phase inversion can be verified after a temperature, pH, change or a mechanical stress is applied. It the food field, it can be divided in the one promoted by fat crystallization and the one promoted by surfactant transitions.

1.2 Microencapsulation

Microencapsulation is a technique which is applied to preserve some nutrients inside a microsized structure (from 1 to 1000 μm). The components inside the capsule is defined core material, while the external structure is called shell/matrix material. There are different possible structures of microcapsules: one classification can be the distinction between mono-core shell, multi-core shell and matrix type at which the core material is dispersed as small droplets within the matrix material. The core material must be still active and useful after encapsulation, therefore various properties must be considered prior operating: the molecular structure, the physical properties, the biological behavior, the optical properties and the chemical stability of the shell must be compatible with the ones of the core material. For food ingredient production, the typical core materials are liquids and solids. Ideal encapsulant materials are supposed to be biocompatible, bio-degradable, non-toxic, and low cost.
According to the type of materials, various mechanisms can be identified, concerning the formation of the shell. Four main categories have been identified. Polymer chains are interconnected by covalent crosslinking into a hydrogel likemembrane. Lipids are stabilized by hydrophobic and Van der Waals interactions. Proteins are held together through hydrophobic interaction and covalent disulphide crosslinking [20]. Dense matrixes are obtained after the hydrolization and polycondensation of sol-driven metal alkoxide sand silica. The core material is released as well through a series of different mecahnisms, going from physical fragmentation to chemical or enzymatic degradation. The functionalities of cores and shells that can be modified allowing various applications. It is important to develop microencapsulation strategies by screening on active constituents with desired benficial effects, formulating shell materials with expected functional properties, and selecting encapsulation techniques, adjusting the processing conditions suitable for the core materials. Certain microcapsules have been incorporated into commercial food products, however most remain in the research stage where the functional properties of microcapsules like encapsulation efficiency and storage stability have been optimized but the evaluation of controlled release and bio-availability has rarely been studied. At present, there are two possible trends:

- reducing the size of capsules from microscale to nanoscale;
- employing shell materials with specific functionality

The first can potentially improve bio availability, controlled release, and precision targeting of core materials. The latter involves the usage of shell materials with higher nutritional values like proteins or with certain characteristics like non digestible dietary fibres. In summary, microencapsulation of bioactive ingredients offers opportunities for the functional foods industry.

1.3 Spray drying

Spray drying is an old technique which has been originally employed in the diary industry to produce milk powder. It has been optimized and modified along 150 years since it was tested for the first time in the United States. The stages of a spray drying process are mainly four:

- Atomization
- Hot gas sent in contact with the spray
- Evaporation
- Particle collection and separation

1.3.1 Atomization

Atomization is needed to reduce the resistance to the transfer of moisture from the droplet bulk to the transfer fluid (gas). The smaller the droplet, the faster the drying rate will be. There are different types of atomizers, but the physical principle behind is always the same: a liquid jet is falling thanks to the gravity force, then, after a critical value of length l is reached, a breakup is verified and a spherical droplet is formed, with a volume equal to the elongated cylindrical jet portion of diameter d.

$$4.51ld\left(\frac{\pi}{4}\right) = \frac{\pi}{6}D^3 \text{ with D = 1.89 d, D is the sphere diameter} \tag{1.11}$$

This is a simplification, proposed by Rayleigh, since it does not take is account for some important properties such as the viscosity, the surface tension, the surrounding air and the inertial forces. The Ohnesorge number is giving an indication about the ratio between viscous forces and the contribution of inertia and surface tension.

$$Oh = \frac{\sqrt{We}}{Re} = \frac{\mu}{\sqrt{\rho\sigma L}}, \text{ with } \textit{We} \text{ is the Weber number, } \textit{Re} \text{ the Reynolds number} \tag{1.12}$$

The turbulence in the liquid jet and the air forces compete to create the disruption of the liquid, while the droplet fission is achieved thanks to the shear stresses realignment.

Atomizers type

Rotary atomizers are driven by high velocity discharge of liquid from the edge of a wheel or disc. The high speed is accelerating centrifugally the feed, with a peripheral velocity of 200 m/s. Pressure nozzle atomizer instead are facilitated by discharge of liquid under pressure through an orifice. Kinetic energy is generated from pressure energy. In this case the diameter of the droplet is directly proportional to the viscosity, the feed rate, and inversely influenced by the pressure. The two fluid nozzle atomizer exploits compressed air to create a shear field. The only drawback of this nozzle type is that the droplets have poor homogeneity (large particle size distribution). Ultrasonic atomizers are using vibrating piezoelectric disks to lower the surficial tension. Here the velocity of the droplets after the atomizer is up to two order of magnitude lower with respect to the other equipment described above. The last type of atomizer is the electrohydrodynamic atomizer, or electrospray. This recent technique is including the usage of high voltage up to some kV, which is responsible for the creation of a conical shape of the liquid meniscus. The droplet size is related to the conductivity through the following law:

$$d_D = \alpha \left(\frac{Q^3\epsilon_0\rho}{\pi^4\sigma\gamma}\right)^{1/6} \tag{1.13}$$

1.3.2 Spray-air contact

After the droplets are created, they must be brought in contact with the hot gas, usually air. The particle formation then starts with this stage, since the moisture is evaporated rapidly from the surface of the drops, in an uniform manner. The ideal condition would be to achieve an uniform

Figure 1.1: a. Part of a rotary atomizer and b. Two fluid nozzle atomizer

distribution also of the gas along the drying chamber. That's the reason for which particular attention should be paid to the air disperser, whose function is to create pressure drop. The difference in pressure is achieved thanks to the through perforated plates or vaned channels. The drying chamber has usually a conical bottom, and the ratio between diameter and height influenced by the final application.
The hot air can be supplied in two ways, co-current or counter-current (only for heat resistant products) to the liquid flow. The contact time between the two fluids is anyway of few seconds, and the gas flowrate, and its temperature, must be deliver enough thermal energy to allow the evaporation. There is a third configuration of air flow, including both co-current and counter-current, but this implies that the outlet temperature is higher and is suitable only for free flow powders.

1.3.3 Evaporation of moisture

The evaporation in the spray drying process must be divided in constant rate period and falling rate period. A mathematical model can help to describe the drying kinetics of the process, which is also important to determine the heat and mass transfer prediction. From the initial temperature T_0, the evaporation rate is constant until the equilibrium evaporation temperature T_{eq} is reached. The wet bulb temperature is reached when the drying gas is saturated with vapour: at this point the droplet shrinks. At this stage the evaporation rate is given by:

$$\frac{\partial C}{\partial r} = Pe \cdot C \text{ ,where } \textit{Pe} \text{ is the Peclet number:} \tag{1.14}$$

$$Pe = \frac{k}{D} \text{ , with } k \text{ evaporation rate, } D \text{ diffusion rate} \tag{1.15}$$

The crust formation starts immediately after, giving a start to the falling rate period. The particle starts to heat up but it never reaches an higher temperature than the one of the inlet gas. The reason behind is that the bottom of the chamber is not a so high temperature. During this period a phenomenon defined as bubble formation could take place inside the particles, due to the rapid heating an inflation is created and a void space remains at the centre, causing a random distribution for the shape.

1.3.4 Particle separation

Also the particle separation is divided in two phases. The first happens at the bottom of the drying chamber (most of the times conical to facilitate the collection), and the delivery to the second stage is helped through pneumatic systems or a screw conveyor. The dry collectors are the equipment for the second part, and they include a cyclone separator, a filter bag, and an electrostatic precipitator,

according to the particle size. The gas, saturated with vapor, is dragged from the bottom and discharged aside.

Cyclone separator

The centrifugal force is the key force that acts inside this part located after the spray drier. The particles are reaching the cyclone and entering tangentially the barrel, which is the upper cylindrical part. The air the drives the solids downwards through the conical part, forming a vortex. The centrifugal force is increasing from top to bottom, and it helps the separation between solids, which are going to fall into the collector at the bottom, and the gas.

Bag Filter

The bag filter is essential for continuous operations. It is placed after the cyclone: the air, containing the finest particles that did not deposit in the collector, must be cleaned prior discharging. When the differential pressure across the bags is too high, the compressed air acts to clean the filters.

Electrostatic precipitator

A high voltage is applied to the discharge wires and it ionizes the surrounding air. The particles passing between the collecting plates and the ionizing wires are charged, and the air which is conveying them is purified, since the Coulomb force attracts the solids towards the plates. Then the particles are removed in different ways, according to their fragility and wettability.

1.3.5 Morphology

The process spray drying parameters are often decided according to the final particle morphology which is desired. The particle size distribution is related to the morphology, as well as the flowability and other key qualities such as the density and the moisture content. The process parameters are affecting each other for the whole process, so the main obstacle is to correlate the effect of a single variable on the particle shape. However one clear indication is given by the drying kinetics, which influences the two main routes: dry shell, similar to the shrinking core model, and wet shell, which leads to the formation of hollow and eventually inflated particles.

Defects

Spray dried particles are usually subjected to the phenomenon of blow hole formation, principally due to the permeable nature of the particle. The low resistance to the water in liquid and vapor form, from the interior to the surface allows to create a sufficient pressure from the core, potentially causing the shell rupture or blow holes in the shells. Sometimes, collision and adhesion forces are so strong that they cause the agglomeration of the particles. During the drying the viscosity of the droplet increases until it reaches a critical value of 10^7 Pa·s, which is related to stickiness: bridges between the particles are eventually formed, and the solubility of the material to be dried in water is also an influencing factor. In general, particles that are hardly soluble in the feed tend to agglomerate.

Chapter 2

Materials and methods

In this chapter all the equipment used to perform the experimental part, from the emulsion creation to the measurement of the particles properties is described, together with the principles ruling them and some operating procedures. Moreover, the ingredients used to run the experiments are listed, together with their main characteristics.

2.1 Ingredients

The first type of emulsion which has been studied is the oil in water single emulsion. Fig. 2.2 show the aspect of all the ingredients described in this section (except water).

2.1.1 Water

The food processing industry uses a huge amount of water, because it can be a major ingredient in many formulations. Water can potentially transfer directly diseases and still continues to cause significant outbreaks of disease all over the world. Water is just one route by which foods can be contaminated with pathogenic micro-organisms, foreign bodies or toxic chemicals. Moreover, the volume used in the food and catering industries means that the potential risk to the consumer can be very high from poorly maintained systems, including bacteria such as Legionella. There are several legal documents related to the water safety in both EU and UK, the most recent one is the Regulations 2010 (SI 2010/996), which relates to legally binding water quality improvement programs to meet drinking water standards (SHFT, 2014). All the water used at Sheffield Hallam University laboratories is drinking water and its properties are aligned with the standards given by the law. The reproducibility of some experiments could be related somehow also to the water physic-chemical properties (e.g. pH, conductivity, salt content) but since at the end all the water is supposed to evaporate during the spray drying, the final result should not be affected in this case. Beside this, there is no need in the food industry to use demineralized or deionized water: that could be reflect on higher production costs and additional equipment (resins, osmosis membranes) and humans usually assume drinking water.

2.1.2 Solid materials

To create an emulsion, different coating materials can be chosen, to separate the continuous phase from the dispersed one. For this thesis work a new formulation never tested before has been chosen. Previous researches has shown that a dual blend of protein and fiber (Qian Shen, 2014) was proven to be a good material with good encapsulating efficiency. Nevertheless, there is no record of more complex systems, that included three components, one of which was insoluble. All the solid materials were included in the aqueous phase.

Whey protein isolate

Whey protein isolate, from now to end WPI, is a well known protein derived from milk. Its extraction starts from the liquid that remains after the curd (for the cheese production) has been taken out from the inoculation bath. The liquid is pasteurized and then a series of evaporators allow to achieve the production of the solid WPI. This product is widely used for its capability of creating viscoelastic films at the interface of emulsion droplets. Sometimes its usage leads to unsatisfactory results in terms of emulsion stability [16], but the explanation is given by a synergism with another compound and if a low concentration is used. There are indeed a lot of cases that prove the protein efficiency in similar systems [8]. WPI adsorbed at an oil/water interface interacts with neighboring molecules adsorbed, via a combination of non-covalent bonds or covalent disulfide bonding, decreasing the coalescence rate. WPI has also been reported to possess antioxidant activity: than can be really useful in case of systems including components in the dispersed phase, easily depleted by oxidation. For this work WPI employed was kindly donated by Arla Food Ingredients (DK-Viby J), with a purity greater than 92.2 $\%$.

Fibersol-2

Fibersol-2 ® contains at least 90 % of dietary fiber (in accordance with AOAC method # 2001.03). This digestion-resistant maltodextrin is derived from corn and it acts as a low-calorie bulking agent. Its impact on taste and viscosity is null, even at high concentrations. Its production is done through spray drying, exploiting a proprietary method of controlled enzymatic hydrolysis of cornstarch. It has numerous starch linkages that remain undigested by enzymes of the human digestive tract. It has been recognized as GRAS (generally recognized as safe) by the Food and Drug Administration and certified Kosher and Pareve by the Orthodox Union. One of the main reason that has encouraged to try this compound is reported in the research done while assessing the digestion and absorption of lipids [11], which stated that a micelles emulsion was prepared with or without resistant maltodextrin, and their stability was compared. The results shown how Fibersol-2 stabilized the micellar structure, inhibiting the decomposition of micelles. Moreover, it is one of the most economical fiber sources available, and it may help to reduce hunger and increasing at the same time increasing satiety hormones when ingested with a meal [21]. For all the experiments, Fibersol-2 used was kindly donated by Prince International B.V (Emmeloord, The Netherlands).

Cellulose fibres

JELU-WERK, Josef Ehrler GmbH & Co. KG (Rosenberg, Germany) provided some free samples of cellulose fibers (commercial name: JELUCEL®-PF 30), classified as the food additive cellulose E 460ii. The raw materials are natural, purified fibre extracts from grain and bamboo stalks. The production process includes grinding methods, which follow after the fiber extraction, then the different sizes are separated through fractioning (screening process). Finally the product is ready to be employed directly in the food industry. JELUCEL® is said to be an improving agent for texture, stability, mouthfeel, shelf life extension, but there is no record found in any previous research regarding emulsion preparation.

Apple fibres

Apple fibers are coming from a waste derived product. Their usage was thought as alternative to the cellulose fibers, since they are partially not soluble in water (45 % insoluble dietary fiber). One of the main differences is the colour: apple fibre is brown while cellulose is white. That is affecting also the final color of the emulsion. The product VITACEL® Apple Fiber AF 401-30 exhibits fruity and sweet organoleptic properties characteristic of apples. It is used in baked goods and beverages, and it was supplied for free by Rettenmaier UK Ltd, (Surrey, UK). The average size of this fiber is said to be less than 30 μm, which is comparable with the cellulose fibers described above.

Name	Density ρ $[kg/m^3]$	T_{eb} [° C]	T_m [° C]	Average size, d_{50} $[\mu m]$
WPI	400.0	-	-	50
Fibersol-2	300.0	-	-	-
Cellulose	300.0	-	-	30
Apple fibers	400.0	-	-	30
Sunflower oil	918.8	120	-17	-
Palm stearin	942	-	52.0	-

Table 2.1: Fundamental properties of the ingredients

2.1.3 Oil phase

The oil phase for the single emulsion was entirely constituted by sunflower oil, nevertheless, for future researches some liposoluble micronutrients could be included. Double emulsions required an emulsifier to separate the inner aqueous phase from the oil phase: palm stearin as nanocrystals were used as an attempt to stabilize the secondary emulsion.

Sunflower oil

KTC Sunflower oil was bought from Morrisons Groceries. It contains some E vitamin, to prevent rancidity in short time after the container is opened. In the past, some researches about emulsions containing sunflower oil has been done, to study some pH effects, the stability of an emulsifier [10], the antioxidant activity of carotenoids [6], and the influence of pectin on sunflower/linseed oil in water emulsion [4], to enhance the antioxidant capacity. However, pectin shown also a destabilizing effect on the emulsion even at low concentrations (0.1 % m/v) causing coalescence and flocculation problems. This is an important result to be consider for this work, especially when apple fibers are used, since they contain pectin.

Palm stearin

Palm stearin is a triglyceride, characterized by an high content of palmitic acid (50-68 % w/w), oleic acid (20-35 % w/w) and a mixture of other fatty acids: among them linoleic, stearic and myristic acids are the most important ones (average amount 7, 5 and 1.5 % w/w respectively). It is obtained from oil palm, after a refining process, followed by a bleaching and deodorizing treatment. Finally, its fractionation at low temperature, its crystallization and filtration lead to the commercialized product, presented a white-yellow solid. The palm stearin used for the experiment was a gift from AAK Ltd. (UK).

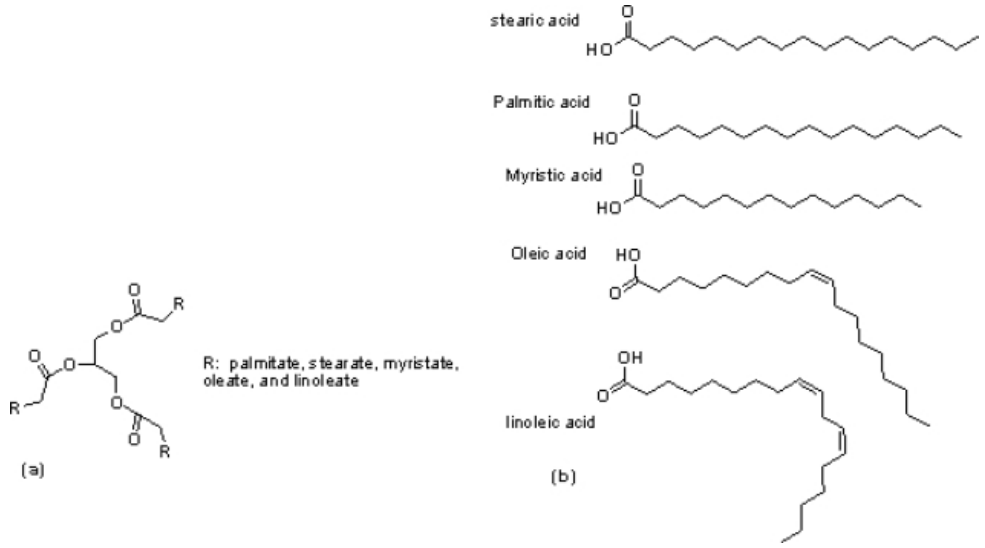

Figure 2.1: Palm stearin main fatty acids

Figure 2.2: Ingredients used for the experiments

2.2 Homogenization equipment

Before creating the emulsion, all the solid ingredients must be well homogenized in the aqueous phase. After that, the pre emulsification process takes place. Finally, a device to break down the particles is employed, to create the final emulsion.

2.2.1 High shear blender

The mixer to generate the pre-emulsion presents a 4 pitched blade turbine, with a 45 degrees slope. It is an axial impeller type, suitable to not segregate the mixture in the zones above and below the impeller. The blender used comes from the company IKA®, the model is identified as Eurostar 60 and it's shown in Fig. 2.3. All the parts in contact with the mixture are made off high quality AISI 316L stainless steel (DIN 1.4404). The speed range goes from 20 to 1200 rpm, and the maximum batch size is 80 l. For the experiments the maximum rotational speed used is 400 rpm, and the maximum batch size was 3.5 l, so for this work purposes, the blender is suitable. As additional tool, a temperature sensor is coupled (PT 1000, measure range -10 - +350 °C). To clean the shaft and the blades (they can be easily disjointed from the motor) hot water and detergent are sufficient.

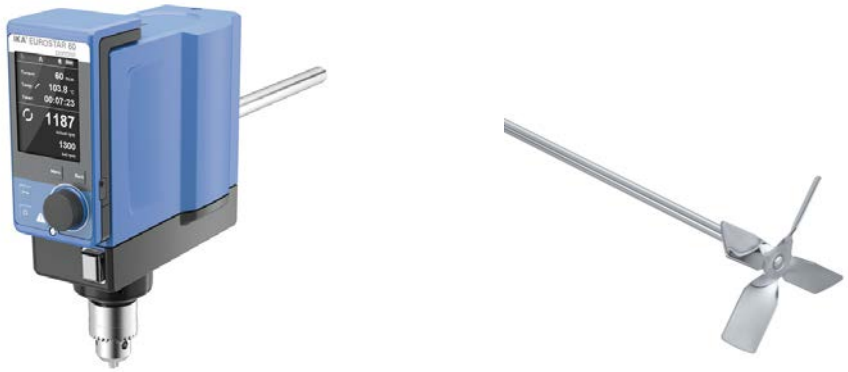

Figure 2.3: Ika Blender: control panel with the knob to set the speed and shaft with blades

2.2.2 High Pressure Homogenizer - HPH

The high pressure homogenizer used for this work is a C-50 EmulsiFlex, purchased from Avestin (commercialized by BioPharma, UK). The purpose of this equipment is to reduce the droplet size by passing the pre-emulsion through a valve. The liquid is moved thanks to the action of a primary pressure (pneumatic), which can be regulated through a knob. The counter action of a secondary pressure (compressor), modulated by another knob, causes the stem movement of the homogenizing valve; after the depressurization through the valve, droplets are disrupted. The side consequence is a temperature increase: a 1000 bar P increase corresponds to an increment of 17-21 °C. The combination of the two pressures allows to reach a maximum value of 2000 bar, so the maximum temperature increment is 42 °C: this could lead to undesired partial evaporation, coalescence of droplets immediately after emulsification etc. In Fig. 2.4 the schema of the equipment is represented: the two sections are working in parallel, but there is only one hose for the inlet and one for the outlet. Depending on the final purpose, the inlet and outlet hoses can be put in the same beaker, so the solution is recirculating. In addition a little mixing effect is provided, helping to avoid phase separations in the early stages. The outlet hose can be temporarily removed from the beaker to collect some samples after the desired number of passes through the homogenizer. This can eventually provide the size evolution with the number of passes and the minimum number of passes can be determined. The minimum amount to be processed is 25 ml, since the hold back volume is less than 4 ml.

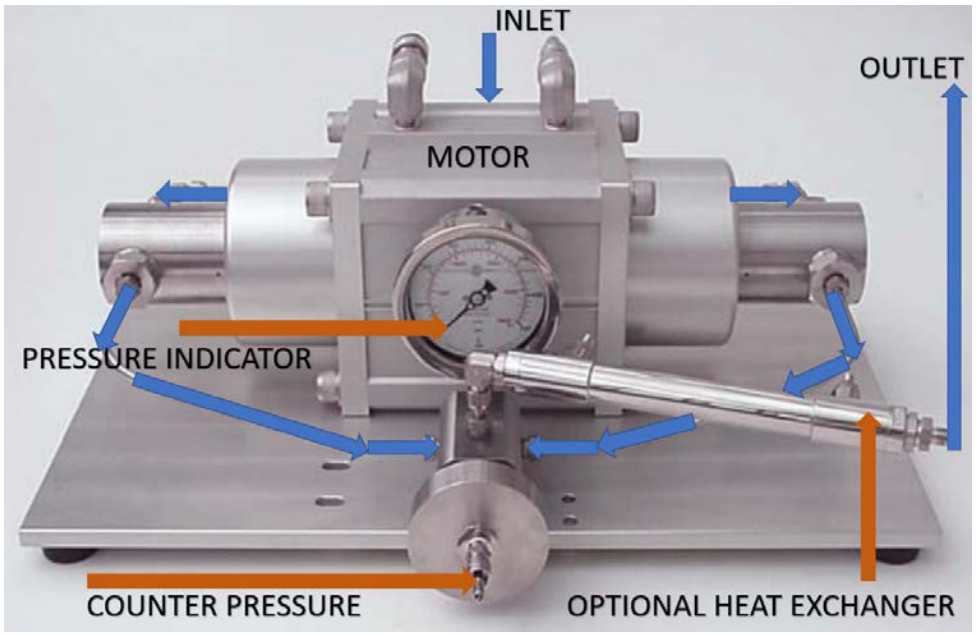

Figure 2.4: Avestin C50 emulsifier. Schema with the main parts

This patented technology has been already used many times for research purposes, from lab scale for emulsions' production [12], to the pilot scale [17], for testing nanoparticles, that's the reason why it has been thought to be used for the emulsification stage. However, there's no record about its usage in case of liquids containing solid. The physical principle behind this type of equipment is that the pressure applied has to overcome the Laplace pressure to break a droplet. The smaller the size, the higher the P required, according to the formula:

$$p_c = \gamma(\frac{1}{r_1} + \frac{1}{r_2}) = \gamma\frac{4}{d} \tag{2.1}$$

where γ is the interfacial tension, d the droplet diameter. A dimensionless number that indicates the power of disruption is the Weber number, *We*, defined as the ratio between drop disrupting and maintaining forces (We = τ/p_c): droplets must be exposed to a tangential stress for a sufficient amount of time. The emulsifier role, beside preventing coalescence, is to facilitate breakup, lowering the interfacial tension, and to form a resistant membrane around the droplet once it is created. After a certain concentration of emulsifier, the droplet size will depend only on the energy input of the homogenizer, however, this limit can be determined only experimentally since it is depending on the type of emulsifier.

Operating procedure

Open the air valve for the line connected to the control panel and to the motor (the starting pressure to be supplied to the instrument must be 7.5 bar). Then turn on the electric power, and push the start button on the control panel (not displayed in the figure above). Start increasing the pressure using the second knob (counter pressure) until 2 bar is reached on the analog indicator. Do the same for the first knob, until also the second analog indicator is set on 2 bar. After that, the pressure is usually fluctuating between 0 and 500 bar on the main pressure indicator, and by operating the two knobs an higher pressure (or flowrate) can be achieved. While operating adjust the knobs to maintain a steady pressure: fluctuations may be due to a viscosity and density change, to pressure line disturbances, nozzle clogging, or a combination of these factors. After the experiment the equipment can be cleaned with steam up to 120 °C, however, for this work only a solution with a detergent has been passed through the tubing and the equipment, first keeping an high pressure, then releasing it while recirculating the cleaning solution. After five minutes the procedure has been repeated with water several times until the outlet liquid is showing no emulsion nor detergent traces.

2.2.3 Rotor Stator

The Silverson® Rotor Stator, model L5M-A (sold by Silverson Machines Ltd., UK) allows to homogenize thanks to the high shear created between the static part (external) and the helix moving at high speed (max 10000 rpm). The shape of the head allows to break down easily the droplets, and the reduction power is similar with respect to the homogenizer (considering pressures above 1000 bar). Different head shapes can be tested, but the one chosen for the set of experiments for this work is the Square Hole High Shear Screen^{TM} (see Fig. 2.5). This stator thanks to its configuration and internal tolerances provides exceptionally high shear rates, ideal for the rapid size reduction of both soluble and insoluble granular solids, so it is suitable for emulsions preparation.

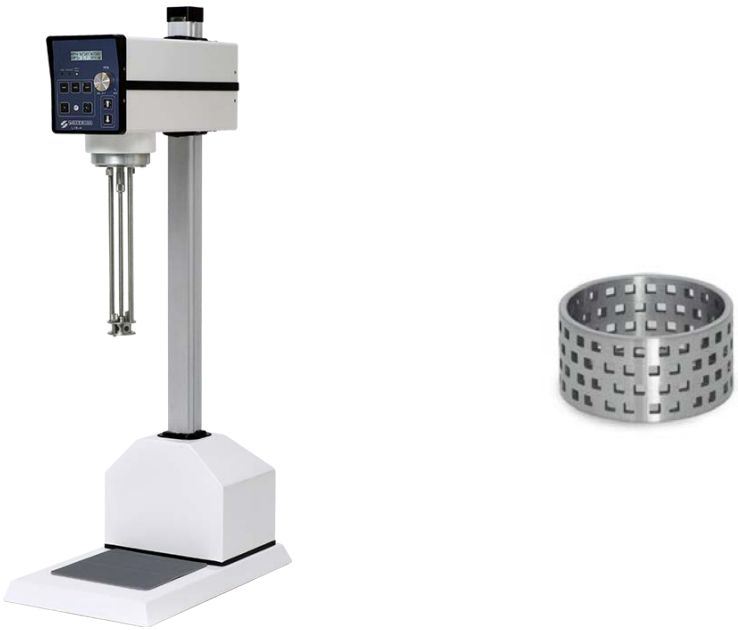

Figure 2.5: Silverson L5M-A. On the right, type of head chosen for the experiments.

Stages of emulsification

- Stage 1. The rotor blades, rotating at high speed inside the workhead boundaries, create a relevant suction. Both liquids and solids are drawn upwards, until they reach the centre of the workhead.
- Stage 2. The materials are moved towards the periphery's workhead and milling action acts on them in the clearance between the ends of the rotor blades and the wall of the stator.
- Stage 3. The materials are ejected though the holes of the workhead, subjected to the intense hydraulic shear. Then they are circulated into the main body of the mixer.

- Stage 4. The materials are accelerated radially through the bulk in the mixing vessel. In the meanwhile, fresh material is continually drawn into the workhead maintaining the mixing cycle. The liquid path has been designed to avoid aeration caused by the disturbance of the liquid's surface.

Further considerations

There are some advantages with respect to the HPH. The most immediate one is related to the easiness of the operations and cleaning procedures. After the steady state has been reached, there is no need to adjust the knob to maintain the rotational speed close to the set point: this leads also to a better reproducibility of the experiments. For the cleaning, only 2 minutes of stirring into a detergent solution, and 5 minutes of stirring in clean water repeated two times are sufficient to entirely clean the workhead. Another advantage is to include the possibility to process more viscous solutions, without clogging any part. The main disadvantage consists in the fact that it cannot be installed as an in-line mixer to make the process continuous, (Silverson is providing those types of mixers anyway, if needed).

2.2.4 Ika Magic Lab

The Magic LAB® is a unique and multi-functional small-scale laboratory machine. It is able to mix, disperse, wet mill and incorporate powders into liquids. The magic LAB® is most frequently used for developing new products or for optimizing existing process techniques, in a wide range of industries including food manufacturers. This machine can be used both for continuous, circulating and batch processes, thanks to its interchangeable modules. Moreover, the magic LAB® ensures a reliable scale-up by offering the possibility to work with the same method from formulation development to mass production. The basic in-line machine is equipped with the single-stage dispersing module ULTRA-TURRAX® UTL. It is best suited for batch applications and can be adapted for the manufacturing of dispersions from coarse to fine. Compared to a conventional stirrer, the mixing time is reduced by up to 50%. Depending on the application, the basic unit can be modified quickly with different working modules. The magic LAB® is admitted to temperatures up to 80 °C even for continuous processes, while the maximum working pressure is 2.5 bar. In short-term operation, the seal materials are resistant for temperatures up to 120 °C. With an engine power of 900 W, the basic configuration with the module UTL performs 26,000 revolutions per minute and a throughput of 130 l/h.

Figure 2.6: IKA Magic lab a) cooling and heating baths b) box for transportation c) main part of the equipment

Advantages of the magic LAB®:

- Thanks to its flexibility and ease of use, this machine suits for many applications and variety of processes.
- Optimum mixing, dispersing and wet milling results due to rotor tip speed up to 40 m/s and therefore high energy input into the working area.
- Simple heating or cooling of all modules is provided by two baths (see Fig. 2.6.a)
- Together with inline machines of 2000 series enables seamless transition of processes from laboratory to production while retaining the product quality.

- Easy and quick exchange of the modules as well as conversion to a complete working plant.
- User-friendly operation via the magic LAB® control panel
- Practical transport and storage packaging (see Fig. 2.6.b)

Disadvantages:

- The cleaning time for different batches is more than the homogenization time for the experiment, for small batches.
- The space occupied by the equipment (including the added cooling and heating modules) is relevant if compared to Silverson Rotor Stator.

Magic LAB® was used in previous researches involving the production of some emulsions [3], but for this work, the machine has been used to produce fat nanocrystals, which are emulsified at the process conditions, but they are solid at ambient temperature: this equipment is perfect to stabilize the temperature thanks to the heating bath.

2.3 Analysis equipment

In this section all the equipment used for assessing the emulsions stability, the particle shape, size and flow ability, are described, from the physic principles to the operating procedures.

2.3.1 Particle size analyzer

The particle size analyzer in Fig.2.7 is a Master Sizer 3000E, purchased from Malvern Instruments (Malvern, UK). This instrument can determine the particle size distribution of both solids and liquids, exploiting two different modules. It has been developed not only to measure particle size from 0.01 μm to 3500 μm, but also to develop different measurement methods. Different categories of particle disperser can allow to measure the size of emulsions and particles. The user-friendly software allows to set up the methods, using the correct parameters and to follow the measurements from the initialization to the cleaning process.

Figure 2.7: Master Sizer 3000. a) Wet module b) Dry module

Particle sizing

A particle is defined as any condensed-phase tridimensional discontinuity in a dispersed system (NIST). This covers droplets in air or in a liquid medium, solids in air or in a liquid medium, gas bubbles in a liquid medium. Particles could have non-regular shapes, but they must be described as well in the best way. There are different equivalent diameter types.

- d_{max}: sphere of same maximum length
- d_v: sphere of the same volume (used by the M.S.)
- d_{min}: sphere of the same minimum length
- d_w: sphere of the same weight
- d_s: sphere of the same surface area
- d_{sed}: sphere having the same sedimentation rate

Diffraction system

The diffraction pattern is presenting different zones at different intensity, starting from the centre (more intense bands) and proceeding radially through the outer part of the circle. The system will measure the intensity of the scattered light as the function of the angle from the incident laser beam. He-Ne laser, with a wavelength of 633 nm (red), passes through the cell, the dispersion unit sends the particles inside the cell and then they are hit by the laser. The light therefore is scattered, and different detectors are recording the signals according to the intensity of the light that they are receiving (see Fig.2.8.b). There is another light source, at 470 nm (blue), to extent the measurement range and improve the precision for submicron particles. In this case only side scatter and back scatter detectors are used. Once data are collected, the scattering pattern is transformed into an initial guess of the size distribution. Mie theory is then used to generate backward the scattering path again, and the two scattering patterns (experimental and theoretical) are compared. This is an iterative procedure that is repeated until the difference between the two scattering patterns is minimized. Finally the size distribution is displayed.

Mie Theory

This model accounts for the interaction of the laser with the surface of the particle, and it can predict the scattered and refracted light. It can work with any wavelength and intensity. The Inputs required are the absorption factor of the material and the refractive index of both the particle material and the dispersant. Refractive index is not always available in the databases or in the literature, but some good guesses can be done by looking at similar materials and to previous publications. Absorption index instead is much more difficult to be determined, but thanks to some microscope observations the order of magnitude for this parameter can be certainly be obtained. Emulsions usually have an index of 0.001, while slightly coloured powders have 0.1. Crystalline milled powders instead have 0.01. Alternatively, to Mie Theory, Fraunhofer approximation can be used; it only takes in account the scattering phenomenon. It works for larger particles, and with high refractive index difference between the dispersant and the particle material. It works bad for particles with a size less than 50 μm.

Results

Why laser diffraction is used instead of more traditional techniques? Let's have a look at some comparisons. Comparison between laser diffraction and sedimentation. Information based on the velocity can be obtained by knowing the density and measuring the particle sedimentation velocity, some good guesses about the size can be achieved.

$$v = \frac{(\rho_{particle} - \rho_{liquid})gd^2}{18\eta} \tag{2.2}$$

where v is the terminal velocity, ρ stands for density, g is the gravitational force, d the particle diameter, and η is the liquid viscosity. Comparison between laser diffraction and sieving. Sieving is more reproducible for spherical particles, while for elongated particles their smallest side is allowing some of them to pass through the sieve, while laser diffraction is reading the 2^{nd} largest dimension, so some mismatches could be encountered for this reason.

Wet module - Hydro EV

Initialize instrument to align the laser, measure background to subtract later the dispersant signal. After having added the sample until obscuration is in range, the measurement can be performed, and then repeated eventually for a pre-defined number of times. The rotational speed of the disperser (impeller) has been set to 2400 rpm. This speed has been decided thanks to the indicative plot in Fig. 2.9: after that value the size is not affected too much, and at the same time is not to high to break eventually the droplets. The obscuration chosen is always in the range 7-15 %, considering some references [5], [13]. For each sample, a series of 3 measurements has been set, duplicated and averaged thanks to the averaging tool available in the software.

Dry module - Aero S

Although wet dispersion is really used for particle size distribution, the real benefit of rapid measurements with laser diffraction are best realized with dry powder measurements. Changing module takes about one minute only, and the software is able automatically to recognize which module is installed. Large volumes of

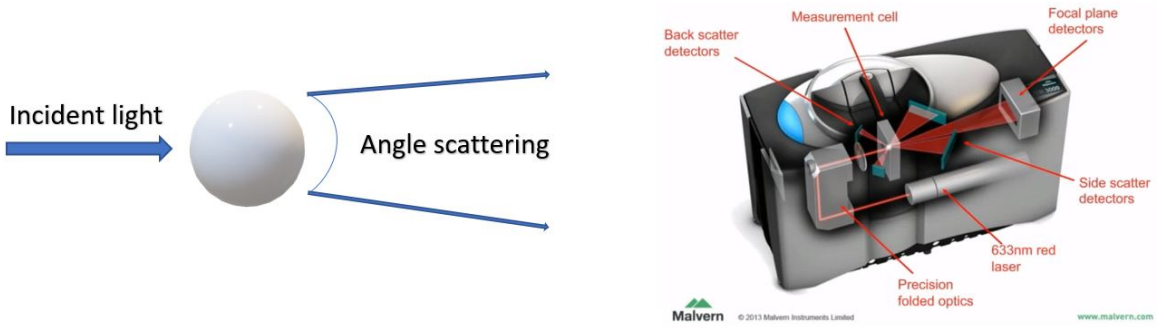

Figure 2.8: a. Smaller particles have weaker scattering, and the peaks will be not so distinct. Bigger particles have high scattering capability, and the peaks will be more focused at the centre. b. Different parts of the measurement system.

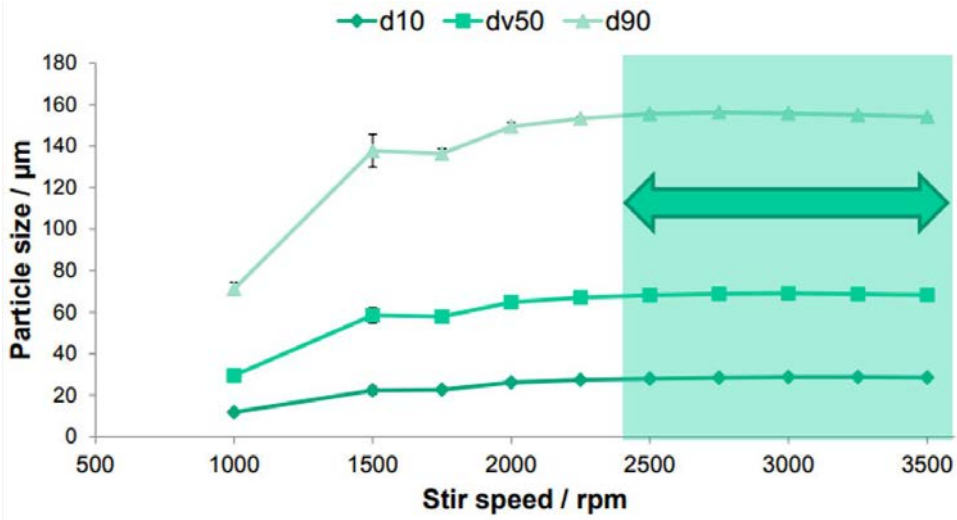

Figure 2.9: Variation of the particle size based on different rotational speeds. Source: malvern.com

sample can be measured (up to 10 ml). The sample tray and the hopper can be regulated to change the flow through the analysis cell. The measure runs until all the sample is undergone through the cell. For the general operating procedure, sample is loaded into the hopper; the compressor air is turned on (5 bar is enough). After the instrument is initialized and the background measured, the sample tray starts to vibrate, and the powder is carried to reach the cell, where it is floating thanks to the dispersant (air).

Diameter measurements

The software gives automatically the particle size distribution based on the D_{10}, D_{50}, D_{90} values. The D_{10} is indicating that the 10 % of particles in the sample have a diameter less than D_{10} (the same reasoning is applied to D_{50}, D_{90}). The diameters calculated are d_{43}, d_{32}, volume based and surface based respectively, defined according to:

$$d_{43} = \frac{\sum_1^n d_i^4}{\sum_1^n d_i^3} \tag{2.3}$$

$$d_{32} = \frac{\sum_1^n d_i^3}{\sum_1^n d_i^2} \tag{2.4}$$

These two values should be the most similar as possible, that means the particles that have the most frequent diameter have also the largest mass fraction. Another indication of monodispersity is the span, defined as:

$$Span = \frac{D_{90} - D_{10}}{D_{50}} \tag{2.5}$$

If this value is grater than 1, the sample shows a poly-dispersed emulsion. The software automatically calculates this values and an average between all the measurements can be added through the interface.

2.3.2 Centrifugation

The centrifuge is an equipment made essentially by three parts: the rotor, the drive shaft and the motor. The rotor holds the equipment together with the samples, and it is mounted on the shaft. The motor is connected with the shaft and it provides the movement. The interactive forces in centrifugation are the sedimenting force, which is opposed by the friction force and the flotation force. The net force is given by:

$$F_{net} = (m_p - m_s) \cdot r \cdot \omega^2 - f \cdot v \tag{2.6}$$

so the greater the distance from the centrifuge centre, the higher the force. The centrifuge acceleration can be expressed also in G units, where G is calculated through:

$$G = \frac{4\pi^2 rpm^2 r}{3600} \tag{2.7}$$

2.3.3 Milling

Milling is a well known technique to mechanically reduce the size of solids. For this work the machine shown on Fig. 2.10.a has been used. The operating procedure is counts really few steps. First, the solids are loaded between the void spaces between the three cylinders shown in Fig. 2.10.b, then a metallic cap is applied and put inside the milling machine. The rotational speed is set together with the treatment time, through the display on the machine. At the end of the operation, the cylinders are taken out and the fine powder can be transferred into a container. Cleaning the cylinders can be done by using isopropanol, while the machine is cleaned through a cloth or in certain cases, using an hoover. The minimum size that can be reached is not smaller than 20 μm, independently of the material milled.

2.3.4 Rheology

This important physical property is determining either if an emulsion can be spray dried or not. Indeed, a product which is too thick would cause a nozzle clogging and a frequent interruption of the operations for a single batch. The limit imposed for this series of experiments is 44*10^3 cP. This indication is given by [14], where the viscosity of the spray dried solution was below the value reported above, and it is the highest registered so far. The instrument used for the experiments is Physica MC R 301, provided by Anton Paar (UK). The module used is a plate-plate geometry. The cone-plate geometry was not available, the coaxial cylinders instead would require at least twice the sample used for the parallel plates (plus they were unavailable during the whole period of the project).

Figure 2.10: a. Milling machine. b. cylinders containing the sample

Figure 2.11: Rheometer used for the experiments

Viscosity determination

The software allows to set a program of variable shear rates, including a pre-shear to distribute the sample in a more homogeneous way before the data sampling starts. The ramp of shears can be set on a linear

or logarithmic basis, including the possibility of verifying hysteresis, returning to low shear values at the end of the measurement. All the measurements must be done at constant temperature, since the viscosity can be affected by temperature variations: this is prevented by a thermo-regulated plate under the sample measurement plane. The viscosity is determined indirectly, as ratio between the shear stress and the shear rate raised to the n-th power. It is fitted using a power law of this type:

$$\mu = K\dot{\gamma}^{n-1} \tag{2.8}$$

Another important parameter that can be measured is the complex viscosity: the trend of this parameter that can vary with the frequency with which a shear stress is applied, can give an indication about the viscoelastic behavior of the emulsion. To set up the frequency program (defined as frequency sweep), two previous passages must be performed. First a strain sweep is executed. The stress corresponding to a percentage of the strain

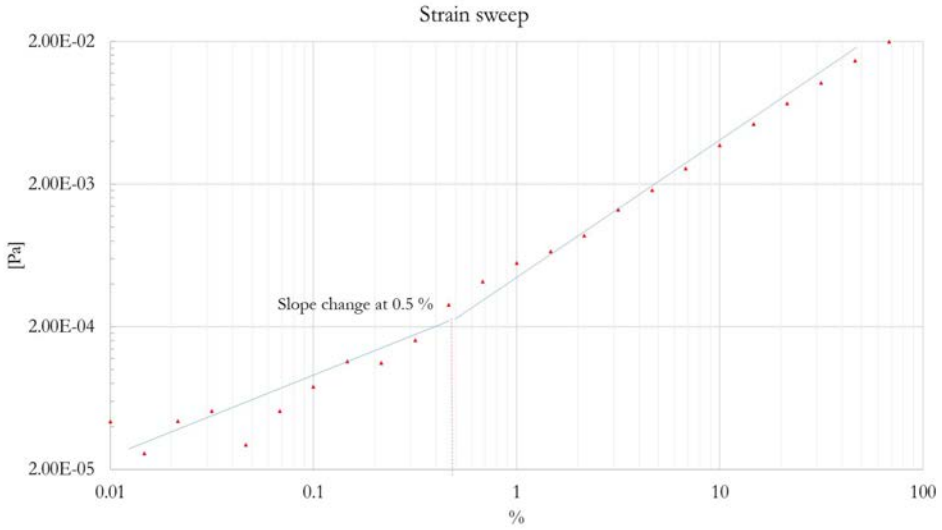

Figure 2.12: Strain sweep plot

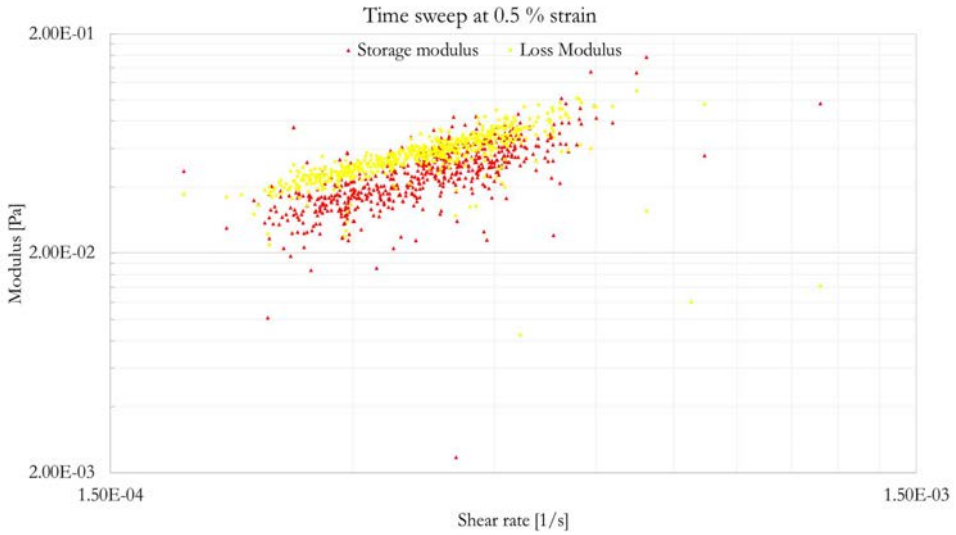

Figure 2.13: Time sweep plot

is recorded. A slope change in the trend indicates a tentative value of the strain to be used for the next step. Fig.2.12 shows that a good guess value is corresponding to 0.5 % of strain chosen. Then the time sweep is executed: if no significant changes of the storage modulus *G'*, and the loss modulus *G"*, are noticed by varying the shear rate, (applying the strain determined in the previous step), then the same strain will be used to assess the complex viscosity for all the emulsions produced. Fig.2.13 confirms that the strain chosen

is suitable to be used for the series of experiments: if there was a sudden slope change, another shear stress must be tested. The relation stated on Eq. 2.9 indicates the relation between the variables discussed above.

$$\tau(\omega, t) = G' \cdot \gamma_0 \cdot sin(\omega t) + G" \cdot \gamma_0 \cdot cos(\omega t) \tag{2.9}$$

2.4 Spray drying

In the previous chapter, the general principles and operations concerning the spray dryer equipment and process have been analyzed. In this section The spray dryer used for the experiments is illustrated: the model is a 4M8-TriX Spray Dryer, purchased from ProCepT, Belgium. Fig. 2.14 shows the main components of the equipment, and the two possible configurations: the height of the column can be increased by adding an extra glass cylinder to the basic structure.

2.4.1 Operations

Once the spray dryer is turned on, it is possible access the control panel (touch screen monitor) that manages all the parameters of the machine. First of all, the emulsion must be put on the scale. Then the scale is turned on and it will read a value equal to 0 (a maximum weight of 2 kg can be put on it anyway). The second thing to be activated is the air that will be heated. Its range varies from 0 to 1 m^3/min, but its maximum value is depending also on the pressure line which the spray dryer is connected to (so it could be less than 1 m^3/min, eg. for this work the maximum available was 0.5 m^3/min) The heater must be turned on after the air is active and while the temperature set point (the maximum T is 200 °C) is achieved and its value reaches a steady state. Also the cyclone air can be turned on (in the range 0 to 3 bar) at this point. The nozzle air can be turned on at the same time (range from 0 to 4 bar) and only at the end the pump can be turned on, carrying the liquid until it reaches the nozzle section. The speed pump can be regulated from 10 to 160 rpm, it can operate both forward and backward. The mass flowrate, considering a fixed rotational speed, varies depending on the viscosity and density of the liquid. During all the spraying time data can be collected by recording the value of all the variables mentioned before, plus some additional variables, measured through temperature probes (Pt1000) and pressure sensors. At the end of the spray drying operation, powder can be collected by unscrewing the glass at the bottom of the cyclone. All the powders less than one micron size are sent to a filter, which must be periodically checked and eventually cleaned. All the column and the glass parts can be removed and cleaned with hot water and eventually a detergent. If the residual dried material is stick on the glass surface, scratching it using a spatula or a sponge can be helpful.
Once the powder have been produced, they must be analyzed in terms of flow ability and shape (microstructure).

2.4.2 Flowability

The flowability is defined as the capability of a powder to flow under a specified set of conditions (among them the pressure on the powder, the humidity of the air around the powder and the equipment the powder is flowing through or from). The most simple indication of a particle behavior is the angle of repose. It is the angle that an hopper needs to ensure the flow. It is typically 30°, but it is not precise for non free flowing particles; this because the cohesive structure formation is not taken in account. The bulk density is the combined density of the powder and the void space, defined as:

$$\rho_b = \rho_s(1 - \epsilon) \tag{2.10}$$

so neglecting air density and fraction contribution. ϵ is the porosity, and this parameter increases as the shear increases, because of the dilatancy property, until the critical porosity is reached. When a powder flows, there is not a linear increase in pressure with depth of particle as it happens for a fluid. The pressure is stable after a short distance and the rate of discharge from a hopper will be:

$$M_p = \frac{\pi}{4}\rho_b\sqrt{gB^5 2tan\theta_H} \tag{2.11}$$

with B opening diameter, θ_H hopper half angle (see Fig.2.15). However this is an approximation: powders may form arches, segregated zones in which there's no flow, or the density changes. A silo is composed by a

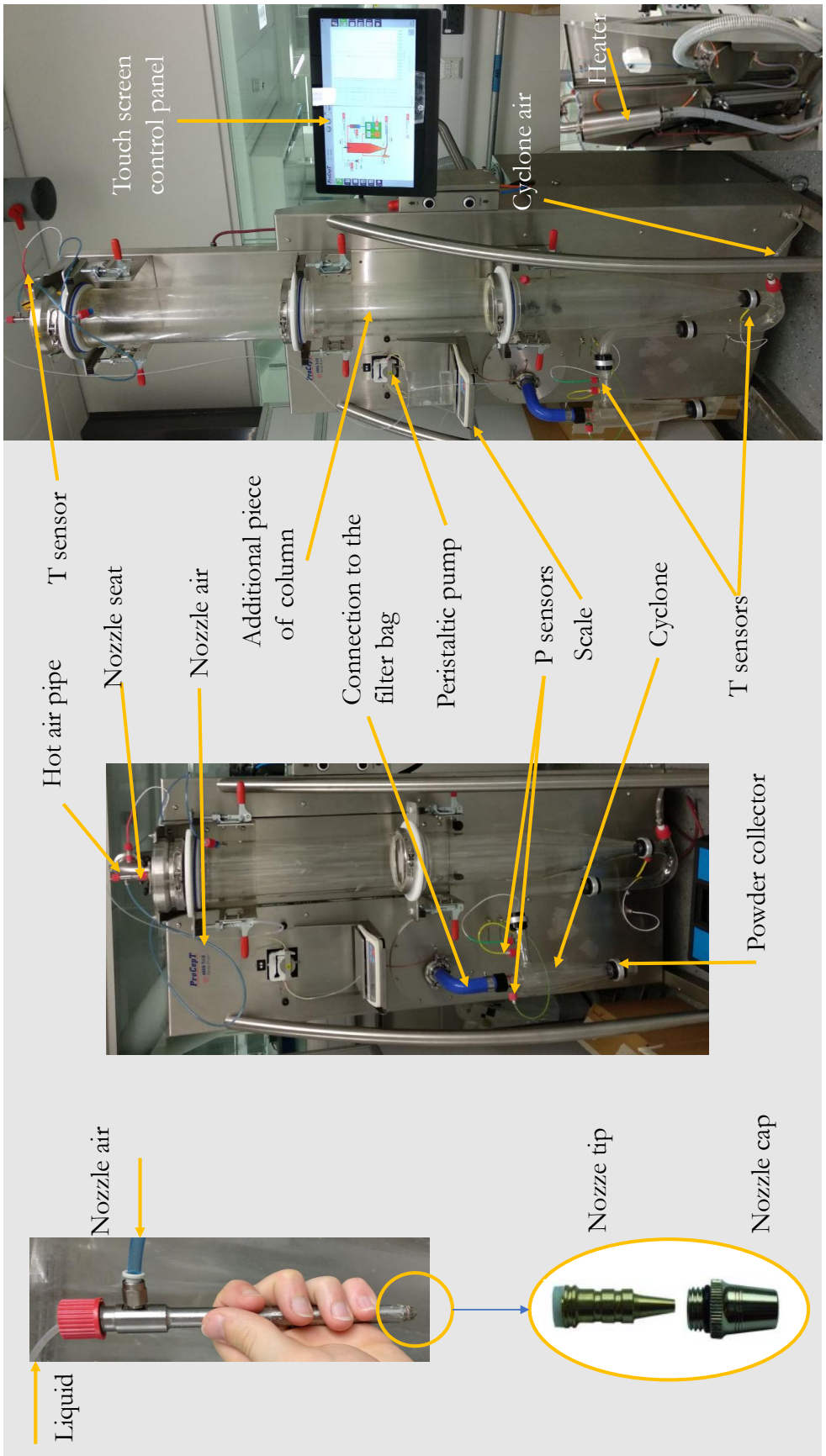

Figure 2.14: Principal parts of the spray dryer. Details around the nozzle section

cylindrical bin and the terminal part called hopper. Powder stresses in a hopper can be studied through the Janssen's method. Considering a section dz at a certain height z, the solid stress is:

$$F_p = \frac{\pi D^2}{4}(P_v + \delta P_v) - \frac{\pi D^2}{4}P_v = \frac{\pi D^2}{4}\delta P_v \tag{2.12}$$

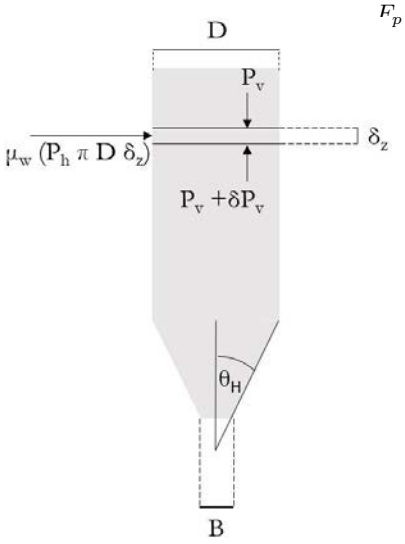

Figure 2.15: Forces acting on the silo's structure

Another force is the one coming from the wall. The horizontal stress at the wall is defined with P_h, the coefficient friction μ_w and then the wall support force is:

$$F_w = \mu_w(P_h \pi D \delta z) \tag{2.13}$$

The solids exert a force equal to

$$F_g = \frac{\pi D^2}{4}\delta z \rho_b g \tag{2.14}$$

Combining the forces:

$$\frac{\pi D^2}{4}\delta P_v + \mu_w(P_h \pi D \delta z) = \frac{\pi D^2}{4}\delta z \rho_b g \tag{2.15}$$

and rearranging:

$$\frac{\delta P_v}{\delta z} + \frac{4\mu_w P_h}{D} = \rho_b g \tag{2.16}$$

As stated before, powders have some void spaces between themselves, therefore they assume a behavior between a solid and a fluid. To transfer this concept into the equations, the horizontal pressure becomes: $P_h = k_J P_v$, where k_J is in the range]0,1[if the state is not passive (otherwise it can be greater than 1). Substituting this equivalence inside Eq. 2.16 and integrating:

$$P_v = \frac{\rho_b g D}{4\mu_w k_J}[1 - e^{\frac{-4\mu_w k_J z}{D}}] + P_{vo}\, e^{\frac{-4\mu_w k_J z}{D}} \tag{2.17}$$

P_{vo} is the pressure at z=0, the uniform stress in the top of the powder. If its value is negligible and for high values of z:

$$P_v = \frac{\rho_b g D}{4\mu_w k_J} \tag{2.18}$$

An hopper must be designed by taking in account the capability of the powder to form stable arch that acts like an obstacle to the flow. The unconfined yield stress f_c is the value of the force to be applied to break the arch and let the powders flow. B is the opening diameter, L is the linear distance interested by the arc action, A is the cross sectional area.

$$\begin{cases} f_c\ A\ L = W\ \frac{B}{2} \\ W = A\ \Delta h\ \rho_b\ g \end{cases} \tag{2.19}$$

$$f_c \rho_b\ gB\frac{\Delta h}{2L} = \frac{\rho_b\ gB}{H(\theta)} \quad \text{Therefore the opening needs to be:} \tag{2.20}$$

$$B = \frac{H(\theta) f_c}{\rho_b g} \tag{2.21}$$

Now the objective is to find the unconfined yield stress for a powder into a hopper, and to know the function $H(\theta)$. The Mohr's circle can represent the normal and shear stresses on a plane. By looking at the Fig. 2.16.a, the centre C_e of the circle is given by: $\sigma_y + r$. $r = 1/2(\sigma_x - \sigma_y)$. Substituting:

$$C_e = \frac{1}{2}(\sigma_x + \sigma_y) \tag{2.22}$$

Exploiting the Pythagoras' theorem for triangles:

$$\tau^2 + (\sigma - C_e)^2 = \left[\frac{1}{2}(\sigma_x - \sigma_y)\right]^2 \quad \text{Using 2.22} \tag{2.23}$$

$$\tau^2 = \left[\frac{1}{2}(\sigma_x - \sigma_y)\right]^2 - \left[(\sigma - \frac{1}{2}(\sigma_x + \sigma_y))^2\right]^2 \tag{2.24}$$

The normal and shear stresses can be represented by Eq.2.24 if principal planes of length l and width m are considered (see Fig. 2.16.b, on which there is no shear acting. the resulting values are defined as maximum

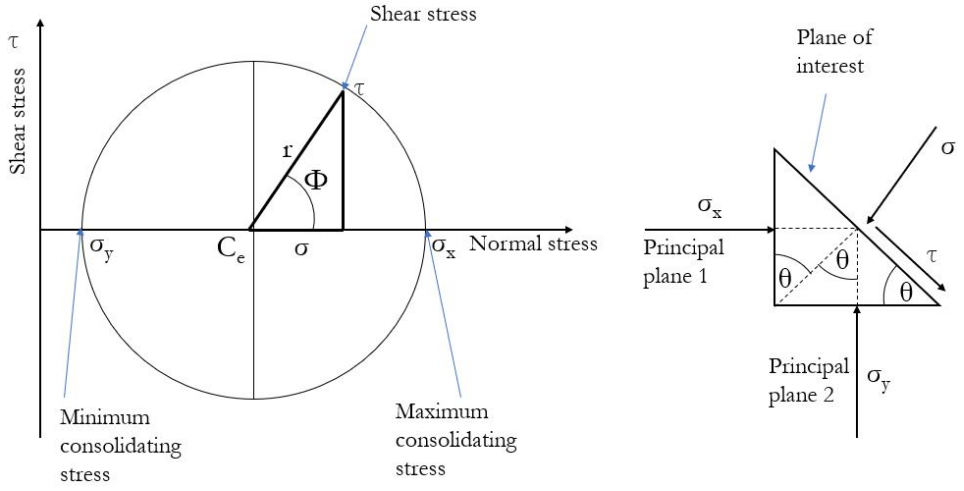

Figure 2.16: a) Mohr's circle. b) Plane of interest.

and minimum principal stresses. Please consider that for the sake of simplicity the two major directions are coincident with the reference system (x,y), but this is not true in general. The two planes are anyway orthogonal to each other. The two force balances, horizontally and vertically are:

$$\begin{cases} l\ m\ sin\theta\ \sigma_x + l\ m\ cos\theta\ \tau = \ l\ m\ sin\theta\ \sigma \Rightarrow \sigma_x \ + \ \frac{\tau}{tan\theta} \\ l\ m\ cos\theta\ \sigma_y = l\ m\ cos\theta\ \sigma + \ l\ m\ sin\theta\ \tau \Rightarrow \sigma_y \ = \ \sigma \ + \ \tau\ tan\theta \end{cases} \tag{2.25}$$

Combining the two equations:

$$tan\theta = \frac{\sigma_y - \sigma}{\tau} \Rightarrow \tau^2 = (\sigma - \sigma_x)(\sigma_y - \sigma) = \sigma\sigma_y - \sigma^2 - \sigma_x\sigma_y + \sigma\sigma_x \tag{2.26}$$

$$\text{Therefore, after rearranging: } \tau^2 = \left[\frac{1}{2}(\sigma_x - \sigma_y)\right]^2 - \left[(\sigma - \frac{1}{2}(\sigma_x + \sigma_y))^2\right]^2 \tag{2.27}$$

The minimum is at τ = 0, corresponding to σ_y, the major principal plane is at the top end of the circle, corresponding to σ_x.

$$tan\theta tan\theta = tan^2\theta = \frac{\tau}{(\sigma - \sigma_x)}\frac{(\sigma_y - \sigma)}{\tau} \tag{2.28}$$

using the trigonometry rule:

$$tan(2\theta) = \frac{2tan\theta}{1 - tan^2\theta} \text{ and substituting the result above, we obtain:} \tag{2.29}$$

$$tan(2\theta) = \frac{\tau}{\sigma - 1/2(\sigma_x + \sigma_y)} \text{ Knowing that } tan\phi = \frac{\tau}{\sigma - C_e} = \frac{\tau}{\sigma - 1/2(\sigma_x + \sigma_y)} \tag{2.30}$$

We can conclude that $2\theta = \phi$, so the principal plane angle is half the one given by Mohr's circle. To build the powder flow function, different stresses are applied. To these stresses, different unconfined yield stresses and maximum/minimum yield stresses are related and can be found graphically (see Fig. 2.17). The yield locus is built by using the following equation:

$$\tau = \sigma tan\theta + C_y \text{ ,with } C_y \text{ defined as cohesion, similar to a yield stress} \tag{2.31}$$

The ring shear tester is one of the tool used to measure the flow ability of solid particles. A normal force is applied together with a shear or rotational stress on the lower ring, containing the sample. When the stress is sufficient, the top ring will slide, and the value of shear is then recorded as a yield locus. Different tests using a series of normal forces will give a plot from which the angle of friction can be determined. The resistance of a powder is also greatly influenced by the prevailing humidity. Hence it is important to perform the tests under controlled humidity conditions, comparable to the ones used for the powders storage.

Operating procedure

The instrument used for this work is a Brookfield Powder Flow Tester (Brookfield, UK). This equipment (see Fig. 2.18) is fully controlled by a software. The standard method, pre-set by the software, was used for all the

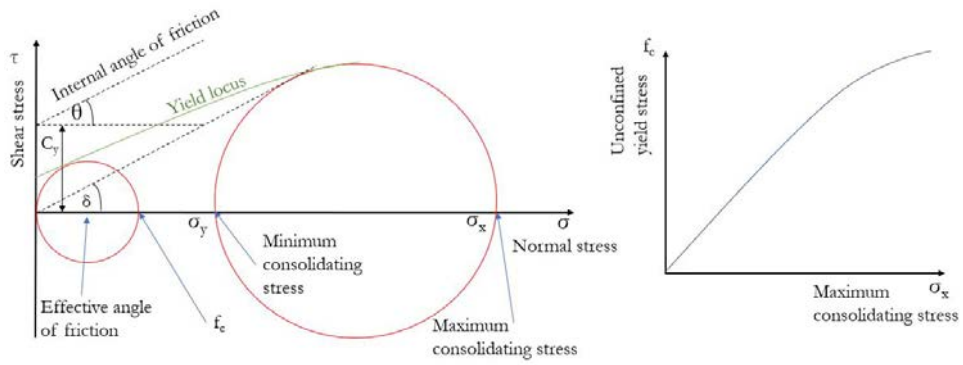

Figure 2.17: Construction for the required data for the powder flow function

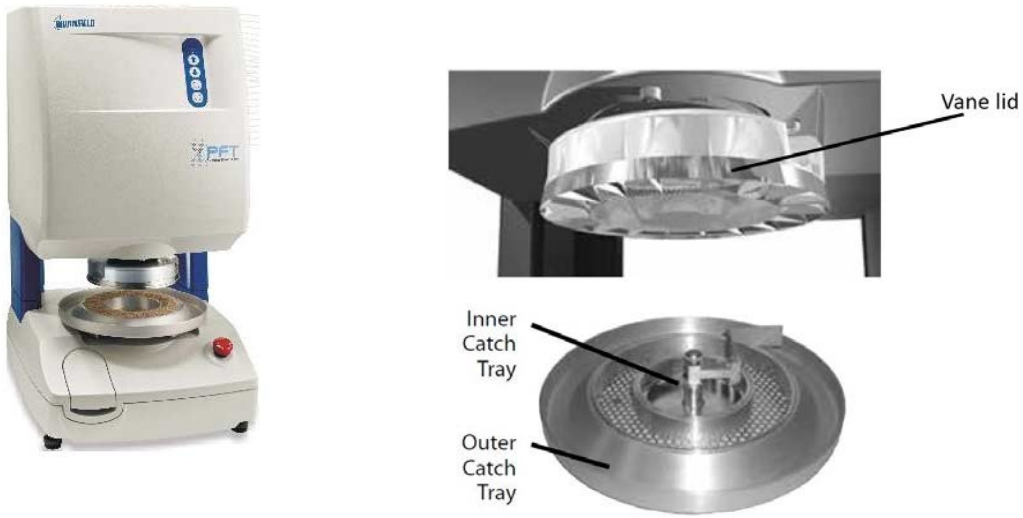

Figure 2.18: a) Powder flow tester used for the experiments. b) Details: vane lid, sample through and inner catch tray.

trials. The resulting data will be a good representation of the flow behavior of the material as a function of consolidation. No specific choices for test parameters are necessary: the values are embedded into the test, and can be eventually modified for personalized tests. With this type of test exploits 5 consolidation stresses, using geometric spaces between each stress. To fully explore the complex behavior of the powder, 35 conditions are tested. The first operation to be done manually is to completely fill the lid with the powder. Then use the inner catch tray to distribute the sample and remove the excess powder. Before installing the lid on its seat, the powder sample must be weighed, by using an analytic scale. Finally, the lid type (small or large) must be selected through the software interface: this data will be useful to determine the density. To start the test, click the “Run Test” button on the Main Screen. The lid will descend to a position slightly above the sample in the trough; the instrument will perform an autozero; then the lid will sense the sample and the test begins. The standard test takes approximately 30 minutes; after it is complete, the lid will raise a distance sufficient to allow its removal. Then the cleaning can be done by using the cleaning brush; also a small hoover for more stuck powders could be useful. For powders that remain on the lid, after the cleaning, the only option is to wash the piece, although is not recommended. After washing, no other analysis can be performed until the metal is fully dry.

2.4.3 Scanning electronic microscope

The scanning electronic microscope (from now to end indicated with the acronym SEM), indicates all the range of microscopes which operates with an electron beam to reveal an image of a sample on a specimen. The SEM

used for this work is a Quanta SEM (Quanta instrument, UK). The instrument general structure is displayed in Fig.2.19.

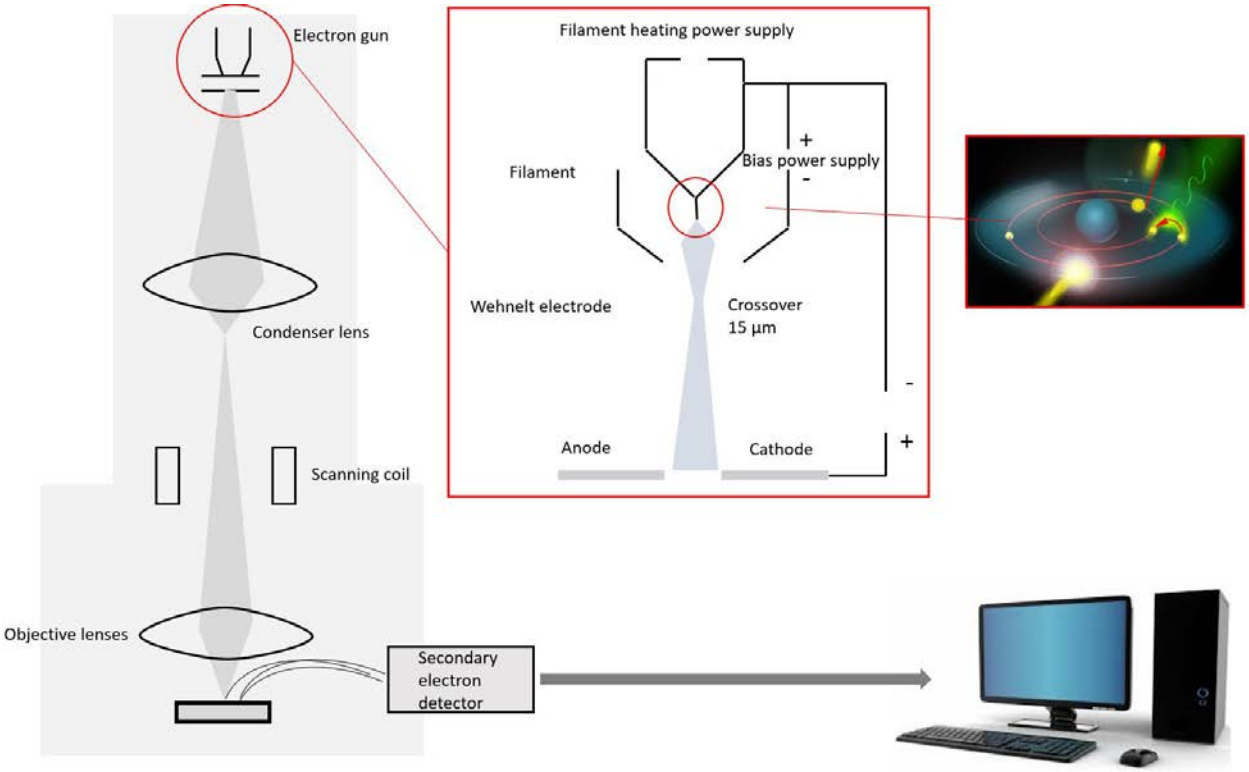

Figure 2.19: Schema of the instrument. Detail of the electron beam functioning.

Electron gun

A filament of tungsten is heated up to 2800 K, and starts to emit thermoelectrons. A positive voltage is applied (1 to 30 kV) and the electrons start to flow into an anode metal plate). The current of the electron beam can be adjusted by placing another electrode (called Wehnelt electrode) between anode and cathode (the most used cathode is a LaB_6 crystal). The crossover is defined as the finest point of the beam, and its width is in the rage 15-20 μm. An alternative electron gun is the Schottky-Emission type.

Lenses

Usually a magnetic lens is used. The lens action on the electron beam is generated when a rotationally magnetic field is created by passing a direct electric current though a coil shaped electric wire. By changing the current passing through the coil, also the strength of the lens is changed. This is one of the advantage of using a lens of this type, since optical lenses cannot have this property.
The diameter of the electron beam can be adjusted if a lens is placed below the electron gun.

Specimen

The specimen is the objective of the observation. It can be observed at high magnification, using different point of views, thanks to the capability of the stage to be moved in the three directions and to be rotated around the support holding the specimen. Before performing the observation, the sample can be coated by using different materials if it is made of a non conductive material. One of the most effective materials is Au: for this work 10 to 20 nm of coating have been applied to each sample, by using an high vacuum technique. The specimen chamber must be kept under vacuum conditions (10^{-3} to 10^{-4} Pa). The vacuum is applied after the specimen is inserted, and air is pumped again for the removal of the sample, and prior to the chamber opening.

Secondary electron detector

This detector is used to determine the electrons coming from the specimen. An high voltage (eg. 10 kV) is applied to a fluorescent substance (scintillator), coating the detector tip. When the scintillator is hit by the secondary electrons, which are attracted by the high voltage, generates some light. The light is conveyed through a light guide to a photo-multiplier tube. The light signal converted into electrons is then amplified and sent to the PC for data acquisition.

2.4.4 Moisture content

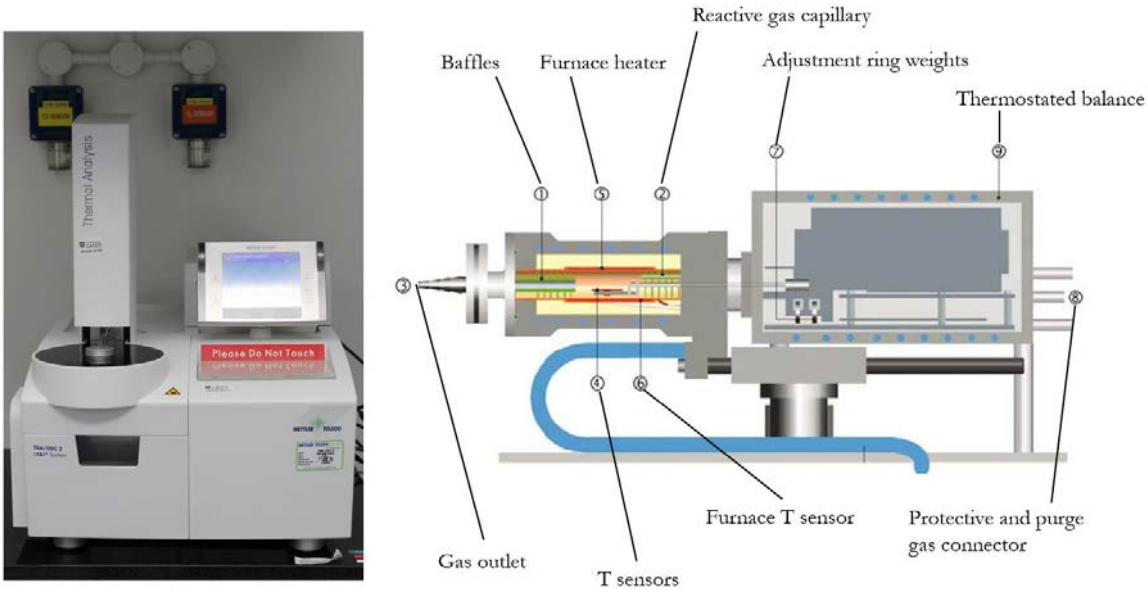

Figure 2.20: Image and schema of the instrument.

The flow ability of a powder is influenced by its moisture content. To measure this physical property, a termogravimetric analysis (TGA) has been performed. The instrument used for this analysis is given by Mettler Toledo (see Fig. 2.20). First of all a temperature program must be set. Since only the water must be evaporated, a temperature of no more than 100 °C must be set for a sufficient long time (until there is no weight variation).The atmosphere that can be used is either oxidative or inert (N_2 or Ar is sent through the chamber). Some tentatives must be done before setting the definitive program that will be used. Once the T program is set, the next stage regards the pan weight, to obtain the tare. The crucible must be treated on a Bunsen flame until its colour switches to orange, to be sure there's no contamination coming from external sources or the previous samples. After the tare, some mg of samples are introduced on the pan and weighed. The program is finally run and data can be easily collected at the end of the experiment.

Chapter 3

Fluid dynamics simulation

The aim of this chapter is to understand the fluid dynamics behavior of the stable micro emulsions oil droplets before entering the spray drier. The main reason is that as will be discussed in the next chapter, the nozzle is a critical region in which the emulsion can rapidly solidify and then block the spray drying operations. Therefore, the interested region for the simulations is the nozzle, which geometry can vary according to the various tips provided with the spray dryer's support equipment.
The final purpose of the simulations is to choose the most appropriate nozzle sizes (if any), and the inlet velocity, so that the oil particles are not broken nor unevenly distributed.
The simulation is done before the spray drying operation because the amount of created emulsion is sufficient only for few trials. Beside this, the accuracy of the models used allows to obtain reliable results in a time which is much lower than the one taken by an experiment. The two software used for the simulation are AutoCAD 2016 and Ansys Workbench v.19 - Student release. In particular the tools used in Ansys are: Geometry, Ansys Fluent, Results (post-processing).

3.1 Geometry

The geometry of the nozzle is displayed in Fig. 3.1. The structure would count another inter space plus another upper cylinder before encountering the tubing carrying the emulsion, but this is not relevant for this analysis, since it would increase the computational power demanded for the simulation.

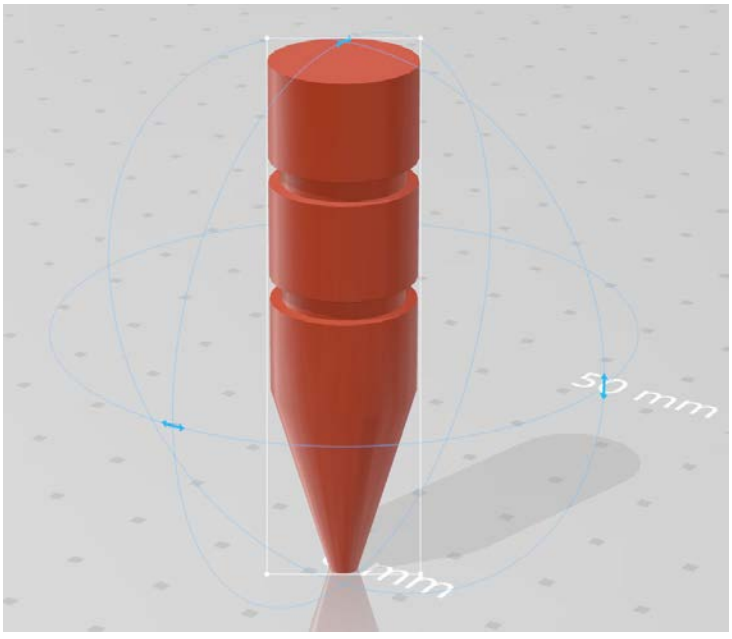

Figure 3.1: Nozzle geometry.

3.1.1 Mesh generation

After importing the geometry from Autocad to Ansys Workbench, a file with the .scdoc extension has been generated, in order to allow the readability of the figure into the meshing environment. Four solids have been automatically isolated. The first operation to be done is to assign an inlet face and an outlet face by creating two named sections. After that, it can be noticed that apart of the conical section, the other three solids are cylindrical, and for that type of geometry the best alternative turns to be defining a sweeping method. This is done through the following procedure:

- Select Mesh on the left menu, then Mesh Control and Method on the sub menu
- Select manually the body the method has to be applied to and select Apply on Geometry.
- Change the method from automatic to Swipe (for cylinders).

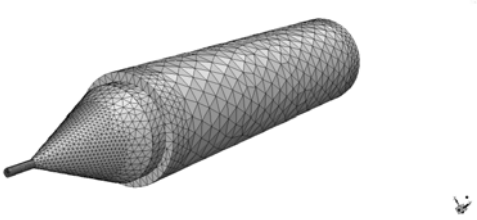

Figure 3.2: Mesh. Nozzle tip: 0.4 mm

For the conical shape an automatic method has been chosen. After that a refinement should be applied, however in this case a face sizing turned to be sufficient. Again, the procedure is very similar to the method application: select the face to size, and set a smaller cell dimension. After that update the mesh. More than 80% of the mesh is composed by tetrahedron cells, then the computational power required could be lower with respect to a mesh composed only by hexahedrons, but finally the result could be precise enough. The final result is displayed in Fig. 3.2 Two important parameters were assessed to determine the overall quality of the mesh.

Skewness

Skewness can be defined in two ways. Here below is reported the most suitable one for triangles and tetrahedrons.

$$\frac{optimal\ cell\ size\ -\ actual\ cell\ size}{optimal\ cell\ size} \tag{3.1}$$

The maximum skewness should never overcome the value of 0.9. The graph displayed in Fig. 3.3 is showing the results for the final mesh, composed by 452987 nodes, 125452 elements. Only 52 elements, representing less than 0.05% are presenting a skewness greater than 0.65. This consideration allows to proceed to the second parameter.

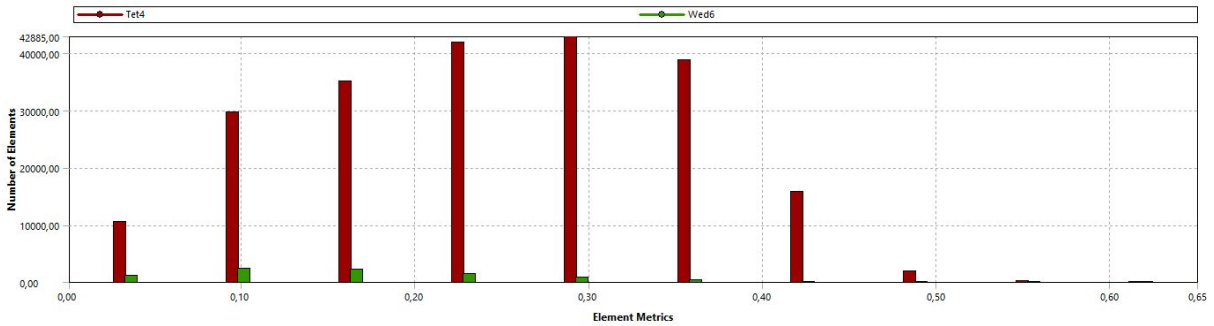

Figure 3.3: Skewness distribution along cells. Nozzle tip: 0.4 mm

Orthogonal quality

The orthogonal quality for each i-th face is computed as:

$$min\left[\frac{\overrightarrow{A_i}\cdot\overrightarrow{f_i}}{|\overrightarrow{A_i}|\cdot|\overrightarrow{f_i}|};\frac{\overrightarrow{A_i}\cdot\overrightarrow{c_i}}{|\overrightarrow{A_i}|\cdot|\overrightarrow{c_i}|}\right] \tag{3.2}$$

where $\overrightarrow{A_i}$ is the face normal vector, $\overrightarrow{f_i}$ is a vector from the centroid of the cell to the centroid of that face, and $\overrightarrow{c_i}$ is a vector from the centroid of the cell to the centroid of the adjacent cell that shares the face. The minimum orthogonal quality should never go below 0.1. The graph displayed in Fig. 3.4 is showing that only 52 elements, representing less than 0.05% are presenting an orthogonal quality less than 0.4, which is really far from the minimum limit of 0.1. Further refinements have been attempted but they all would bring to a lower quality of some cells. After this evaluation it is possible to import the mesh in Ansys Fluent.

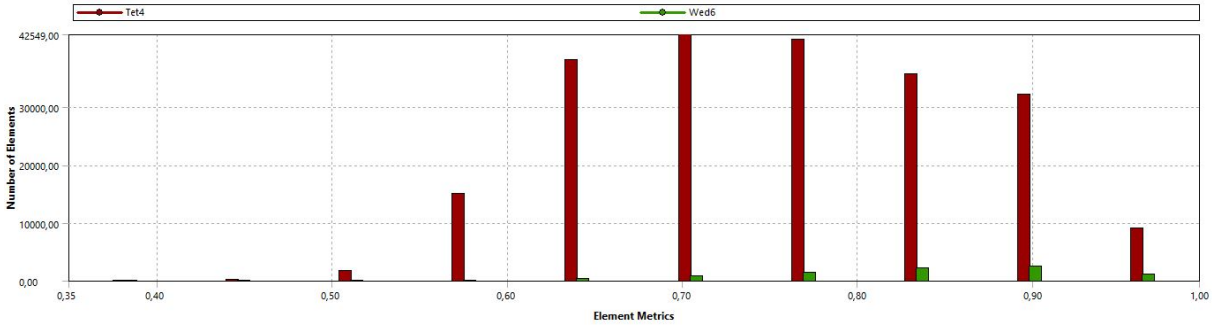

Figure 3.4: Orthogonal quality distribution along cells. Nozzle tip: 0.4 mm

3.2 Ansys Fluent

The simulation environment allows to guide the user step by step, from setting the general conditions and basic parameters until the initialization of the case. The following description is related to one specific simulation performed, to allow the repeatability for similar or analogue cases.
First of all the gravity has been set normal to the z-axis, with a negative sign. Units have been maintained. The mesh has been checked before proceeding with the model choice.

3.2.1 Setting the simulation

Materials

Under Fluid add water liquid from the Fluent database and engine oil. Now the engine oil properties must be changed according to the characteristics of sunflower oil. The density chosen is 918.8 kg/m^3, which is an average density for a vegetable oil. The viscosity has been determined this way. Three experimental points for dynamic viscosity at different temperatures were taken from 2 different sources ([22], [7]). Data were then fitted to an Arrhenius type law:

$$\mu = \mu_0 \, e^{(E/R \cdot T)} \tag{3.3}$$

where T is the universal gas constant, T is the temperature in Kelvin, E and μ_0 are the adjustable parameters. Once the law has been found through the minimum SSE (sum of squared errors), the viscosity at 360.15 K (typical T at the nozzle) is calculated. In Table 3.1 the experimental data and the calculated data are displayed. The second column has been obtained with a μ_0 of $4.9155 \cdot 10^{-6}$ kg/ms and an E of 22791 kJ/kg

Model

The model chosen is a realizable k-ϵ. This belongs to the category of RANS models (Reynolds average Navier Stokes), and it is considering the parameter C_μ not constant but it can vary. This parameter is useful to calculate the turbulent viscosity, μ_t. The model in general is performing better than the standard k-ϵ, especially for jets and boundary layers interested by particular conditions (strong pressure gradients, separations, recirculation). Since two phases are present, the one of the simplest model to start with is the Eulerian model.
After the Eulerian model, in order to verify the results, a Lagrangian model with particles injections (simulating the droplets movement) has been considered.

Boundary and cell zone conditions

The inlet section is crossed by the emulsion, so both phases are entering at time zero. The inlet velocity varies with the peristaltic pump speed, which in this case can operate within a range of 10 to 160 rpm, corresponding to 0.6 to 10.3 g/min (considering pure water). Taking an average value of mass flow of 3 g/min, the inlet velocity turns to be:

$$v = \dot{V} \ / \ A = \frac{3 \cdot 10^{-5}}{1.9625 \cdot 10^{-5}} \ m/s \ = 1.5287 \ m/s \tag{3.4}$$

The other two velocities tested are 0.55 m/s and 2 m/s, which are still within the range that the pump can operate. The cells must be emptied from the air and filled with the mixture, composed by 90 % aqueous

T	Experimental data [kg/m s]	Calculated Data [kg/ m s]
298.15	0.04914	0.04839
311.25	0.03230	0.03295
323.15	0.02340	0.02376
360.15		0.009940

Table 3.1: Sunflower oil dynamic viscosity vs T

phase and 10 % oil (the composition is set by indicating the volume fraction of the discontinuous phase). The outlet conditions remain unchanged since the underpressure after the nozzle is negligible with respect to the atmospheric pressure. All the nozzle walls are set to 360 K, since the nozzle is inside the spray chamber and it must be at the same temperature.

Calculations

All transient simulations have been performed with a time step size of 0.01 s, and 7000 time steps. For each time step the maximum number of iterations is 10. The initialization type chosen is standard, before starting the calculations the volumetric fraction of the second phase is patched to all the cell zones.

3.2.2 Results

Eulerian

The results reported in Figs. 3.5 - 3.7, show that there is an even distribution around the sections, from the inlet to the outlet. The worst case scenario is reached when the velocity is higher e.g. 2 m/s. This consideration must be taken in account for the spray drying operation. It can be evinced that the oil particles are not accumulating near to the wall.

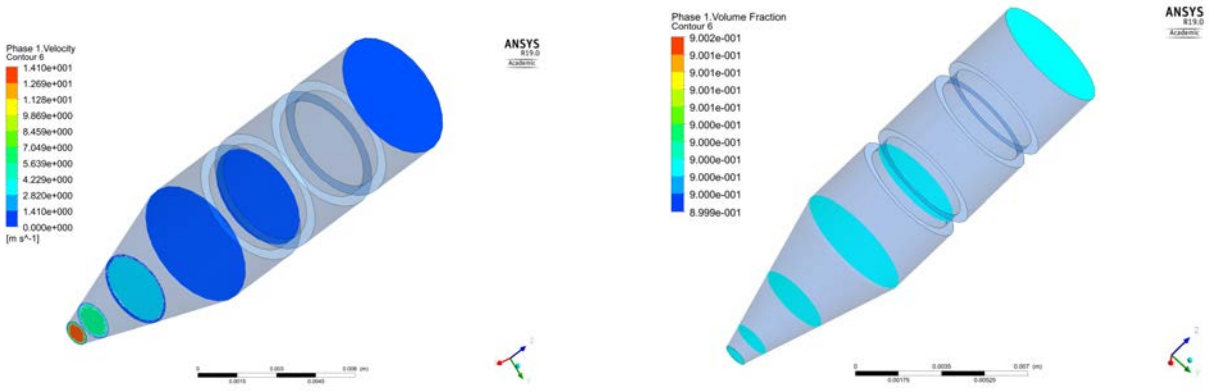

Figure 3.5: Velocity profile and phase distribution profile of the continuous phase. Inlet velocity: 0.55 m/s

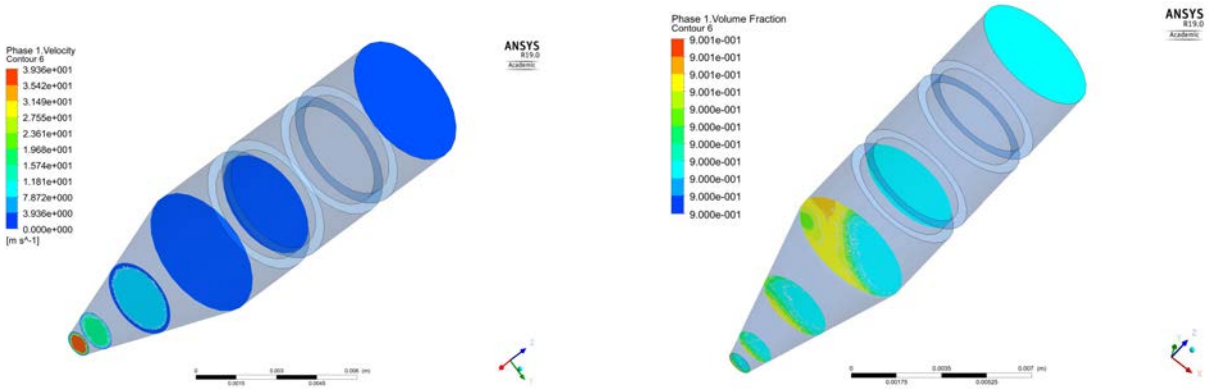

Figure 3.6: Velocity profile and phase distribution profile of the continuous phase. Inlet velocity: 1.5287 m/s

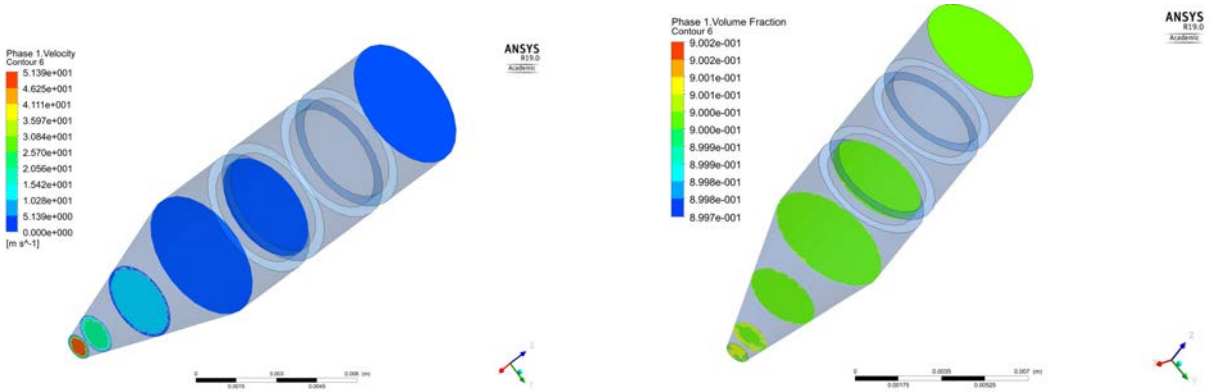

Figure 3.7: Velocity profile and phase distribution profile of the continuous phase. Inlet velocity: 2 m/s

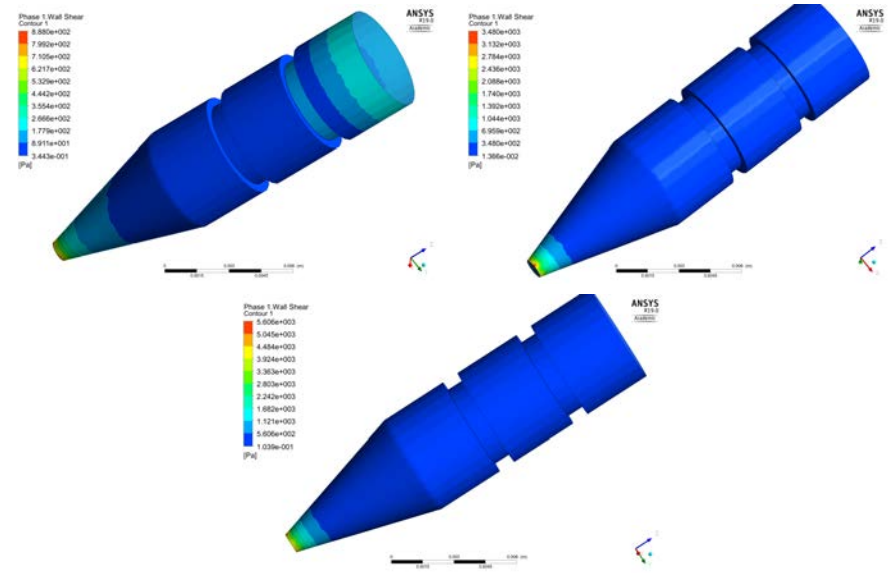

Figure 3.8: Wall shear stress for the three tested velocities

As it can be noticed in Fig. 3.8, the shear stress is increasing along the nozzle for all the three cases, and the highest value is reached for the highest inlet velocity, as expected, This could be beneficial for the spray conditions: an higher shear stress can bring to a viscosity change so that the clogging will be less probable.

3.3 Population Models

Another hypothesis that has been made (but not verified) is that the particle size distribution (PSD) is not constant inside the nozzle, due to the birth an death of new droplets. A confirmation of this has been searched exploiting the Population Balance Models (PBM). They are used to characterize the distribution of particles, droplets or bubbles, including some mechanisms related to the PSD.
PSD is important because it affects the product quality. From a mathematical point of view, the equation representing the change in the number of the particles is the following one:

$$\frac{\partial n}{\partial t} + \nabla \cdot (v_i n) + \nabla \cdot (v_e n) = B \; - \; D \tag{3.5}$$

where *B* is the birth rate term due to aggregation and breakup, *D* is the death term, v_e is the convective term, v_i is the growth term.

$$B = B_{brk.} + B_{ag.} = \int_v^{V_{max}} p\beta(v/v')g(v')n(v';X,t)dv' + 1/2\int_0^V a(V-V')n(V-V')n(V')dV' \tag{3.6}$$

$$D = D_{breakup} + D_{aggregation} = g(v)n(v';X,t) + 1/2\int_0^\infty a(V,V')n(V)n(V')dV' \tag{3.7}$$

where *g(v)* is the breakage frequency, β is the probability breakup distribution function, v is the size of the droplet, *V* is the volume, *X* is the set of internal and external coordinates. In Fluent there are different models to define the aggregation, the one used for this purpose is the free molecular model, that relates the frequency of collision to the aggregation rate:

$$a_{ag}(L_i, L_j) = \frac{2k_B T}{3\mu}\frac{(L_i + L_j)^2}{L_i L_j} \tag{3.8}$$

where L_i, L_j are the relative quantities of two distinct bin sizes.

3.3.1 Solving Population Balance Equation

After having enabled the PBM through: define – models – addon-user – 5, the next step is to choose how to solve the equations. There are two types of methods: Discrete and Method of Moment. For this simulation the homogeneous model, belonging to the first category should be chosen. It divides the particle population into a finite set of size intervals.

$$\alpha_i = N_i V_i = \int_v^{v_{i+1}} n(v;X,t)dv \tag{3.9}$$

In the simulation there are only two phases and inside a cell all the particles have the same velocity. A Sauter mean d_{32} could be used to complete the coupling of PBM with fluid dynamics. The data measured thanks to the particle size analyzer have been introduced inside this model.

Chapter 4

Experiments and results

In this chapter, all the relevant experiments that have been performed, leading to the final formulation, are described. Different types of emulsions were tested, by using different ingredients and/or different ratios of ingredients. The final objective is the creation of solid microstructures embedding sunflower oil, so the quantity of surfactant and thickener must be studied, as well as the robustness of the structure and the critical parameters to be adjusted during the spray drying operations.

4.1 Experiment 1

The first objective of the first experiment is to identify the effect of the HPH on the particle size and compare it with the one of the Rotor-Stator (Silverson L5MA, from now to end RS). The second objective is to check if there is an influence on the particle size distribution (from now to end: PSD) given by a change of the ratio solids to oil. The composition of the first emulsion is displayed in Fig. 4.1. The quantities produced are sufficient to characterize the product and eventually to spray it. The ratio between surfactant and thickener has been

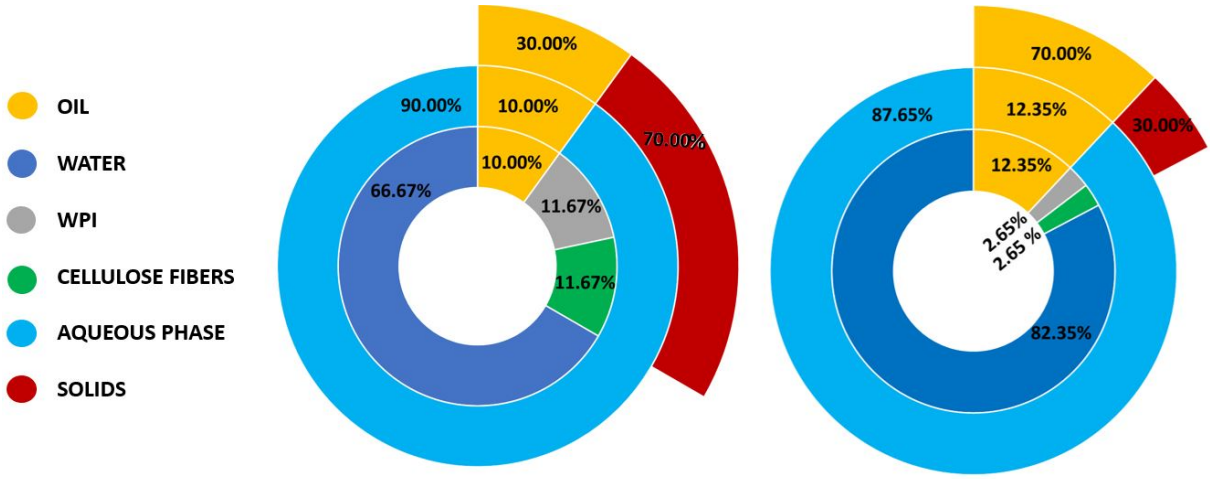

Figure 4.1: Composition of the emulsions, highlighting the ratio between oil and solids and the ratio between oil and aqueous phase.

chosen according to [18]. After the ingredients were mixed at 300 rpm using the high shear blender, and the aqueous solution let rest overnight, the oil was merged using the high shear blender at 350 rpm, then the beaker containing the pre emulsion was moved to the HPH. A pressure of 800 bar was reached, but due to the high quantity of solids the HPH was blocked for a while and operations were stopped after the first pass was completed. Then one sample was taken and the emulsion was treated for other 10 minutes using the RS at 5000 rpm. After the experiment the HPH was unclogged by passing water and adjusting the pressure several times.

4.1.1 Particle size

The particle size distribution is bi-modal in both cases. The data, coming from an average of all measurement performed by the software, are displayed in Tab. 4.1. The following graphic (Fig. 4.2) is showing the evolution of the particle size according to the different passes or treatment used. Unsatisfactory results have been eliminated, to represent more precisely the droplet size distribution. Still by looking at Fig. 4.2 it can be

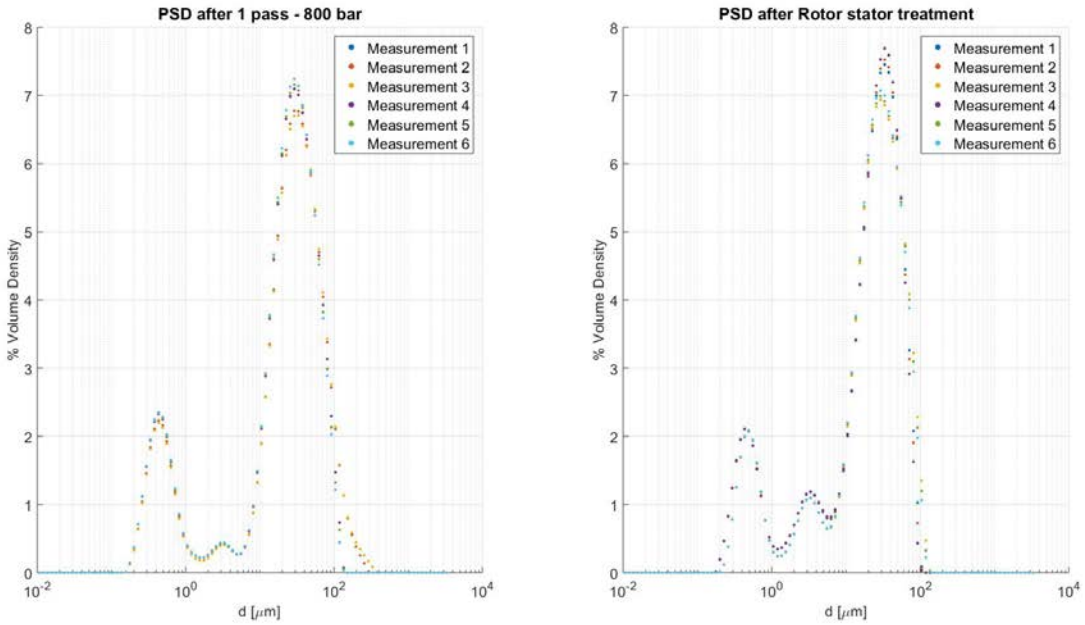

Figure 4.2: PSD after the passage at 800 bar and after RS, PSD after the RS for the first emulsion,

noticed that over the 6 measurements the deviation is not relevant, so for the next measurements only three repetitions have been done. The second important point is that the treatment with the rotor stator seems not to bring any advantage: after the first passage with the HPH the nanosize has been reached already for some droplets. In both cases the distribution is not unimodal, and this is an unwanted characteristic, that must be improved. For the second emulsion, only the RS has been used, and the droplet size is clearly bigger. This could be due to the fact that there was not enough emulsifier and stabilizer compared to the quantity of oil, or to the poor effect of the RS: since both the parameters were changed this cannot be determined with certainty, and other trials are therefore required. The previous emulsification led to consider the introduction of an ice bath while the homogenization is performed: if the temperature is increased due to the breakage of the droplets, the friction of the rotor stator and/or eventually the high pressure effect of the HPH, the probability of coalescence increases according to the number of collisions due to Brownian motion:

$$N_{collisions} = \frac{4kTn_0^2}{3\eta} \tag{4.1}$$

Diameter type	$Size_{emulsion1}$[μm]	$Size_{emulsion2}$ [μm]
d_{32}	2.83	12.4
d_{43}	27.9	64.2
D_{10}	0.626	10
D_{50}	24.0	47.3
D_{90}	60.2	148

Table 4.1: Diameter values for the two emulsions. Again, the second emulsion is presenting bigger droplets.

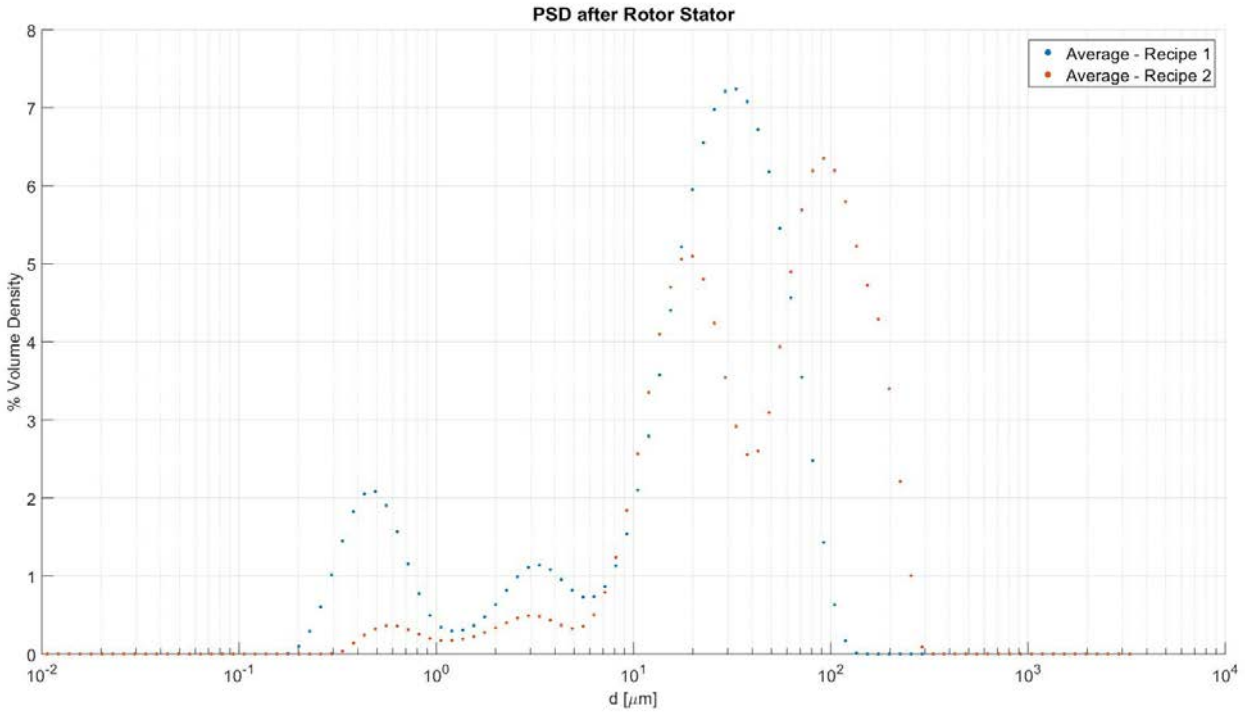

Figure 4.3: PSD after the passage at 800 bar and after RS for the first emulsion (average of the measurements) vs PSD after the RS for the second emulsion (average of the measurements)

4.1.2 Particle shape

The image collected with the camera on the microscope shows how the shape and the size of the droplets is varying, according to the results obtained with the Mastersizer (see Fig 4.4)

4.1.3 Creaming index

Three samples coming from the emulsions have been centrifuged for 1 minute at 1000 rpm. The result is an immediate separation between the insoluble cellulose fibers and the liquid part. No other layers can be distinguished within the liquid part. Fig. 4.5 is showing the result of the centrifugation A more dense layer can be distinguished within the liquid part. The creaming index can be calculated, considering as creaming layer the one on top, for both the emulsions

$$CI = \frac{height\ of\ the\ cream\ layer}{height\ of\ the\ emulsion} = 18\% \text{ (see Fig.4.5)} \tag{4.2}$$

4.1.4 Spray drying

For the first emulsion, no particles were produced. As soon as the emulsion was passed through the nozzle (0.8 mm nozzle tip was used), a clogging was verified, at any condition. The hypothesis is that the quantity of solids used in the emulsion was too high. For the second emulsion, different operating conditions were used, in a random way to identify the best conditions for future formulations. This time the spray was possible, because the quantity of solid in the whole emulsion was significantly reduced with respect to the previous formulation. However, sometimes during operations was necessary to interrupt the spray and clean the nozzle, which was about to be clogged. Tab. 4.2 is reporting the conditions used for this experiment, while Fig. 4.6 is displaying the aspect of the corresponding particles produced.

It can be noticed that the worst particles are produced with a lower temperature and an higher heating air flowrate: the dragging force was increased, so the residence time reduced, and particles are then less dried and stickier. Beside this, the quantity of oil in this formulation was excessive compared to the solid amount. That

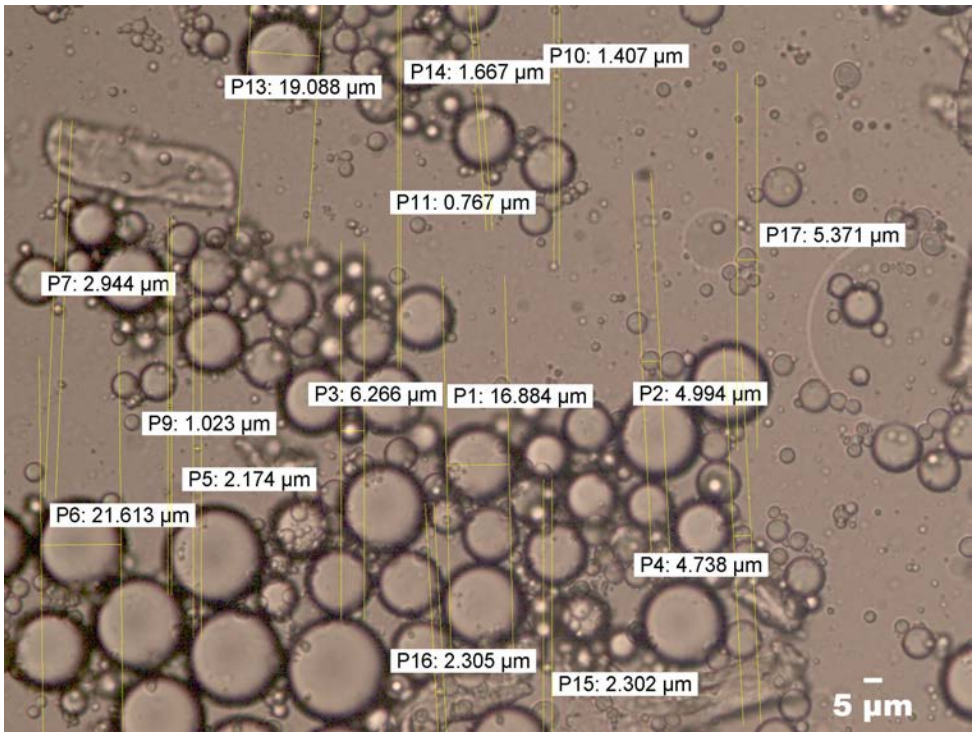

Figure 4.4: Particle size through the optical microscope. It can be noticed how the 2D shape is pretty much circular for each single droplet.

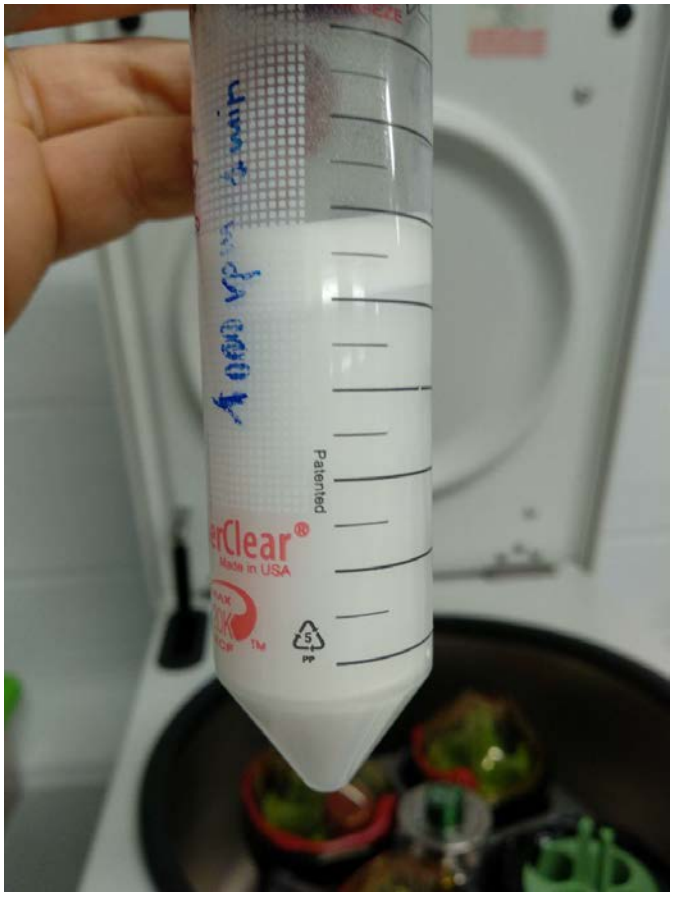

Figure 4.5: Centrifuged sample

A B C

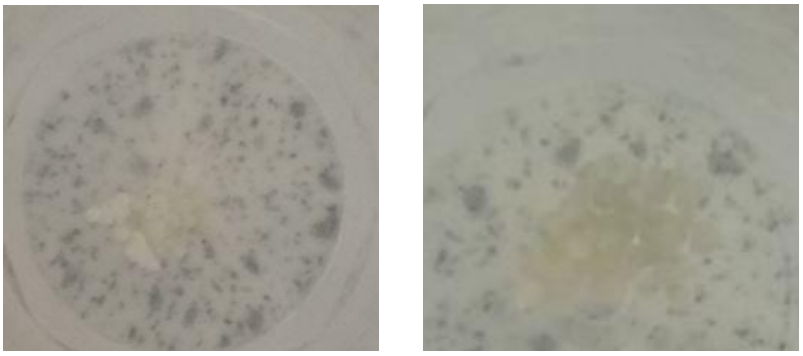

D E

Figure 4.6: Spray dried particles. Conditions A to E (see Tab. 4.2)

ID	Nozzle air P [bar]	Heating Air flow $[m^3/min]$	Inlet T [°C]	Pump speed [rpm]	Cyclone air P [bar]
A	3.5	0.5	120	160	0.75
B	3.5	0.35	160	160	0.75
C	0.5	0.5	160	160	0.75
D	0.7	0.5	120	160	2
E	0.3	0.25	160	50	0.7

Table 4.2: Spray drying conditions for the second emulsion

could be one of the reasons for which the particles were oily on their surface, and they coalesced easily (very big particles were collected for each condition, which was unexpected). For any process condition was achieved a sufficient amount to be analyzed in terms of flowability. The instability of the process can be noticed also through the plot in Fig. 4.7 generated by the data collected from the spray drying controller. The operations were stopped several times and to attain a new steady state 5 to 10 minutes were required.

4.2 Experiment 2

By looking at the PSD plots of the previous experiment, it can be noticed that one peak is centered around 30 μm for both the two emulsions created: this could be due to the presence of insoluble cellulose fibers that are not bonded to the droplet wall. This experiments wants to confirm this hypothesis by treating the cellulose separately, trying to reduce its average size. The procedure followed is described: a sample of fiber, with a concentration of 6% w/w in water was prepared. 1% w/w of Tween 20 has been added to facilitate the dispersion. After its preparation, the sample has been treated with 3 ml of NaOH 0.1 M, to reach pH 12. The sodium hydroxide agent is applied to try to reduce the size of the fibers, so that the final particle distribution could become unimodal. After each measurement, 0.5 ml of NaOH solution have been added, to maintain the pH stable. Unfortunately, as reported in Fig. 4.8, the particle dimension has not manifested any changes over

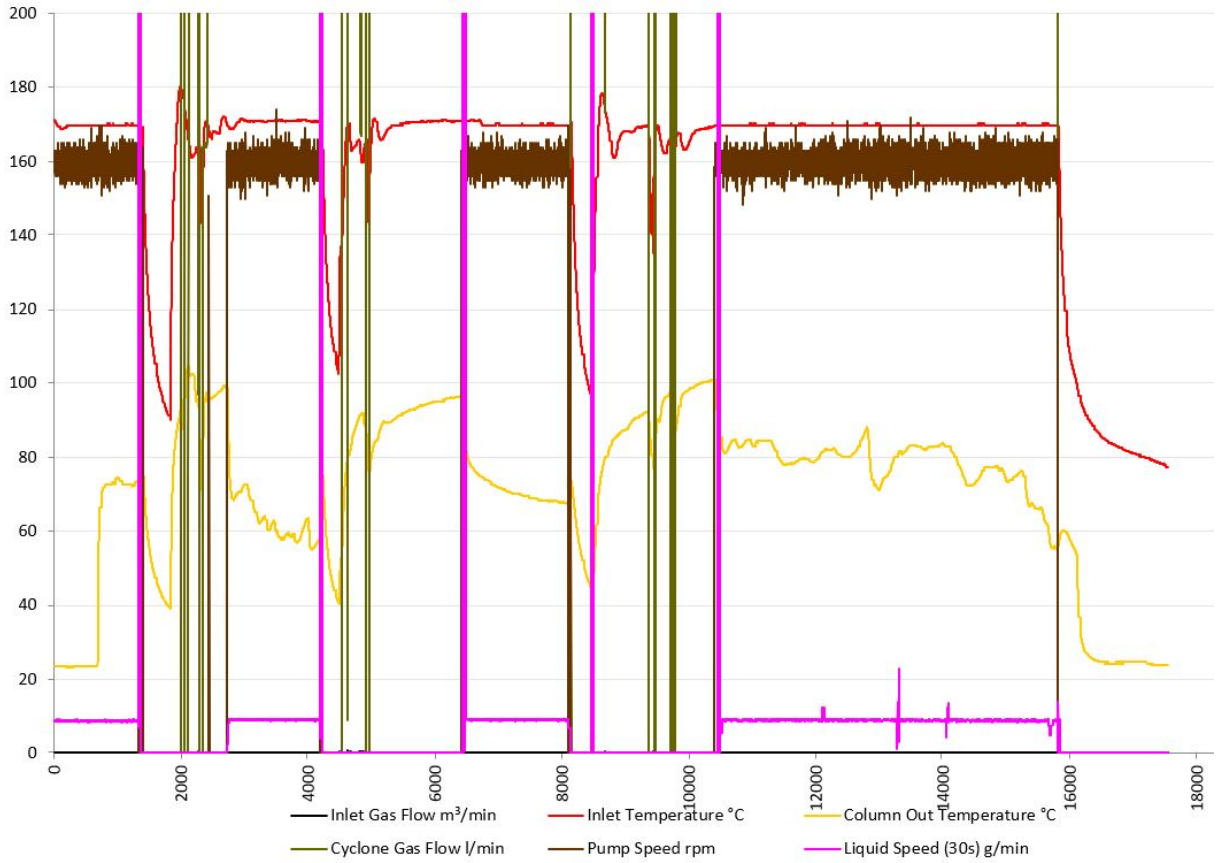

Figure 4.7: Spray dryer plot report. The number of maximum variables displayed is 6 and they can be selected time to time from the controller prior recording the whole run.

1 day of treatment, on the other hand the particle are stable and this may be a good characteristic for other applications. The same type of treatment was applied to some rice bran fibers, which have been treated before,

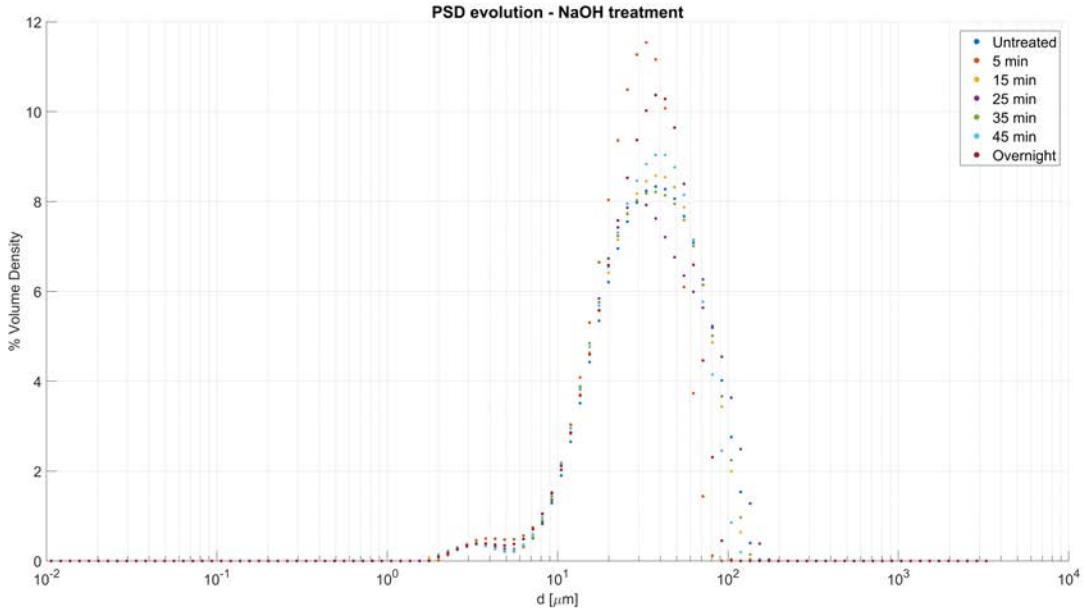

Figure 4.8: Cellulose fibers: size evolution with NaOH treatment

to remove all the fat and the protein present in the bran. These fibers are then mainly made of cellulose, of a different type of the one treated before. As shown in Fig. 4.9, their size is bigger, however, the fiber dimension is not reduced at all after one day of treatment.

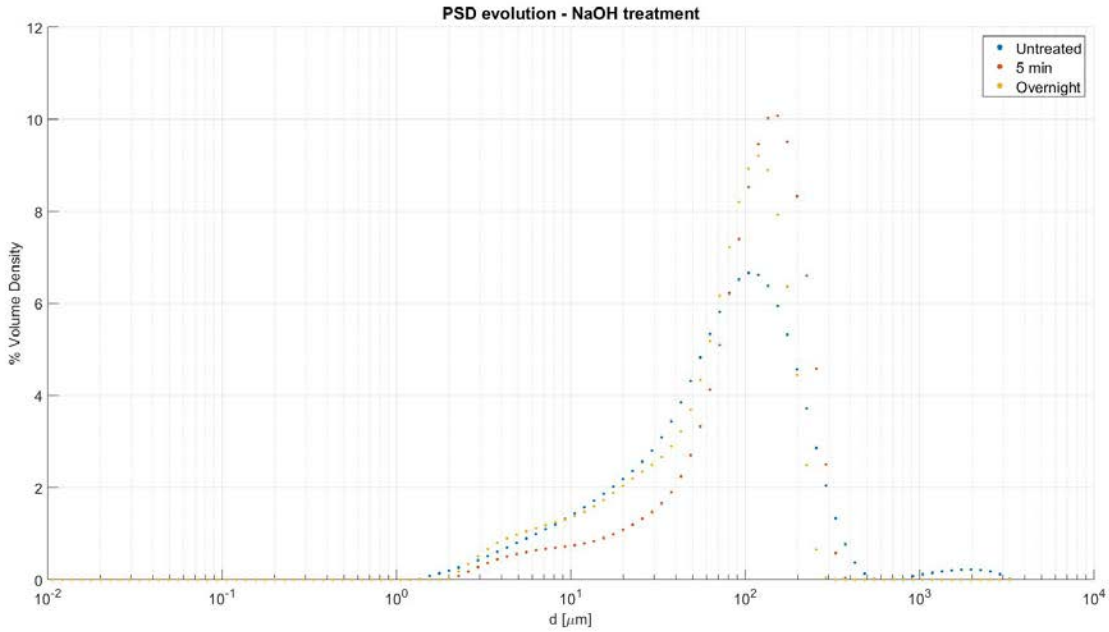

Figure 4.9: Rice fibers: size evolution with NaOH treatment

Fig 4.10 instead displays the size reduction achieved after 10 minutes of milling through the milling machine illustrated in Ch. 2. However, the size reduction is still not enough for this work purposes and further research should be done to find some solubilization methods for cellulose. After these trials apparently there

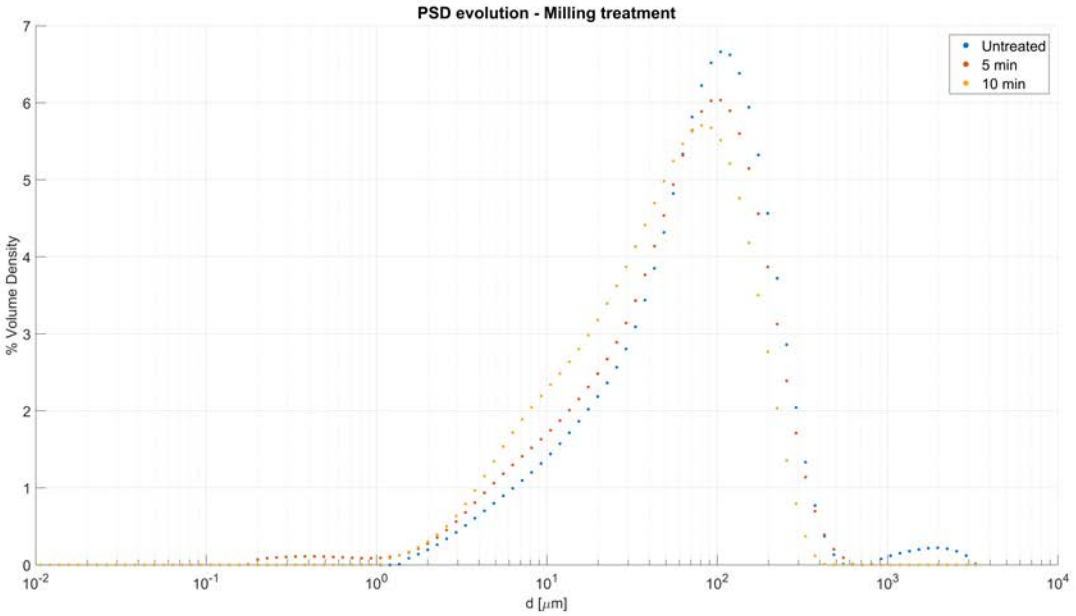

Figure 4.10: Rice fibers: size evolution with milling treatment

is no way to reduce the cellulose particles in size, s the only way seems to decrease dramatically their content in the next experiment.

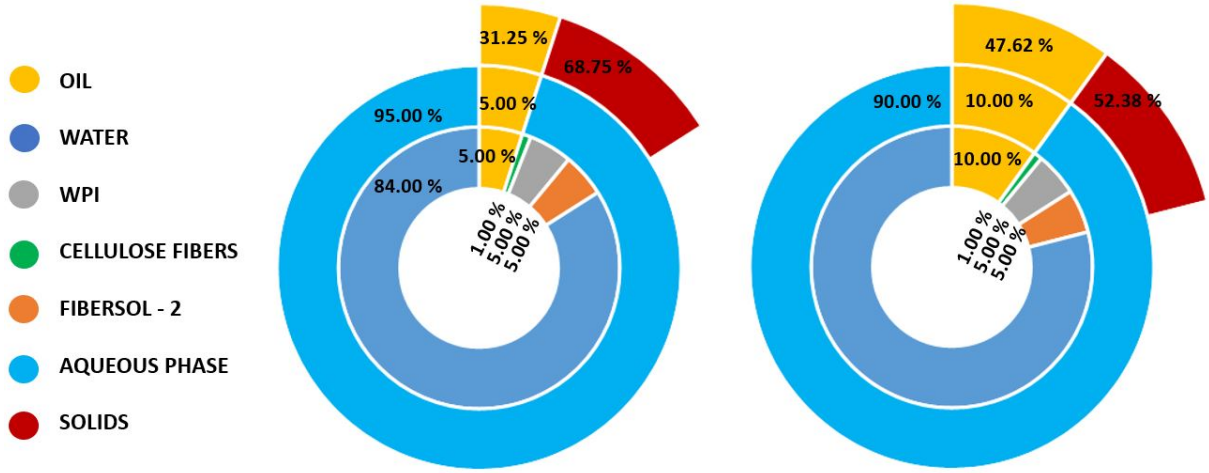

Figure 4.11: Composition of the emulsions E1 and E2

4.3 Experiment 3

This experiment wants to investigate further the effect of the quantity of oil compared to the one of the solids and at the same time, assess the rheological behavior of the emulsions produced, and the effect of the nozzle air on the PSD. Two emulsions were created, by varying the quantity of oil (and then the ratio oil to solids), trying to understand again the best combination of ingredients to produce a processable emulsion. From Fig. 4.11 it can be noticed that one additional component is present: Fibersol-2 is now allowing to maintain a reasonable amount of solids, and at the same time facilitating the spray since it is a water-soluble component. This time the emulsions were both produced with the HPH, and three passes at 800 bar were performed without interruptions caused by the clogging, but the quantity of cellulose fibres was negligible if compared to the one of Experiment 1. Therefore the cause of clogging is to be addressed to the excess of cellulose fibres.

4.3.1 PSD

Both emulsions were created with the HPH, by recirculating three times the whole batch. Fig. 4.13 is showing the evolution of the PSD for E1. From the first to the third pass there is not a size reduction, but the number of particles that has a lower size is increased. The little peak corresponding to the insoluble fibres is shifted to the right for the measurement of the third pass sample: this might be due to an error of the instrument, caused by the agglomeration of some particles that had not enough time to be dispersed before the measurement started. Fig. 4.12 is showing the PSD for E2 directly after the third pass. By making a comparison, the quantity of oil is not influencing the PSD, at least considering small quantities (5-10 %) in the emulsion, so for further experiments, at least 10 % of oil should be used, to increase the encapsulating power of the powders.

4.3.2 Rheology

The viscosity is clearly diminishing with a greater shear, denoting the non-Newtonian behavior of the emulsions (both are shear thinning). For shears greater than 80 1/s the difference in viscosity between the two emulsions is not so relevant, so they should have the same capability to be sprayed through the nozzle. For the complex viscosity for both E1 and E2 there is a change in the behavior, from viscous to elastic. For the emulsion containing more oil, the change in behavior is happening at a lower angular frequency (40 1/s): that could mean that there is a more resistance encountered in passing through the nozzle although the ratio oil to solid in E2 is lower than in E1.

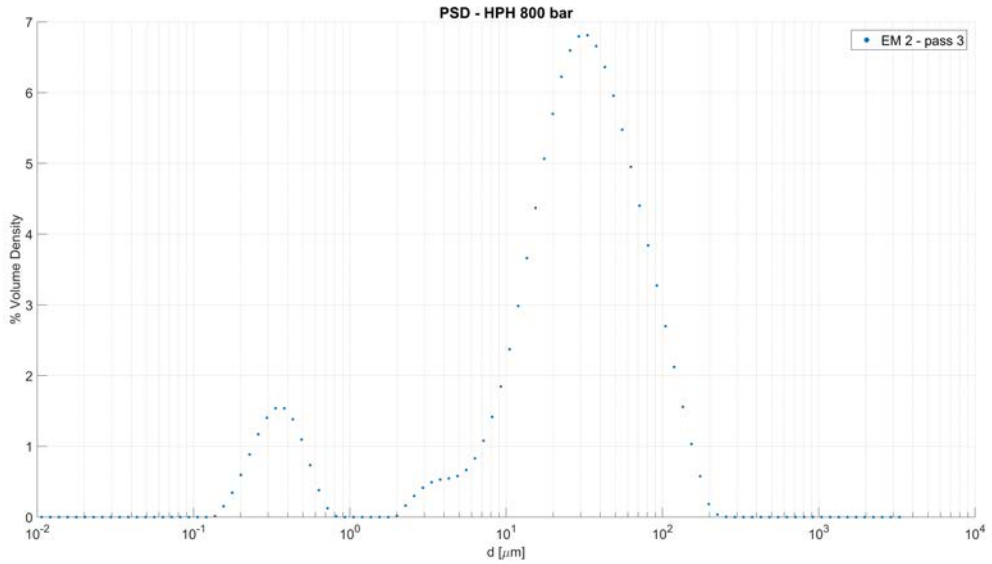

Figure 4.12: PSD for E1

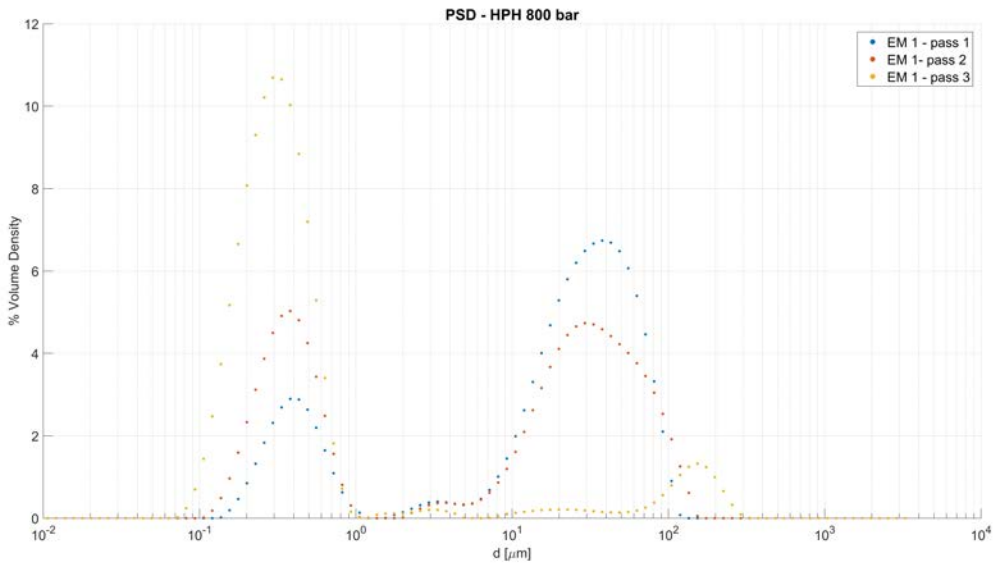

Figure 4.13: PSD for E2

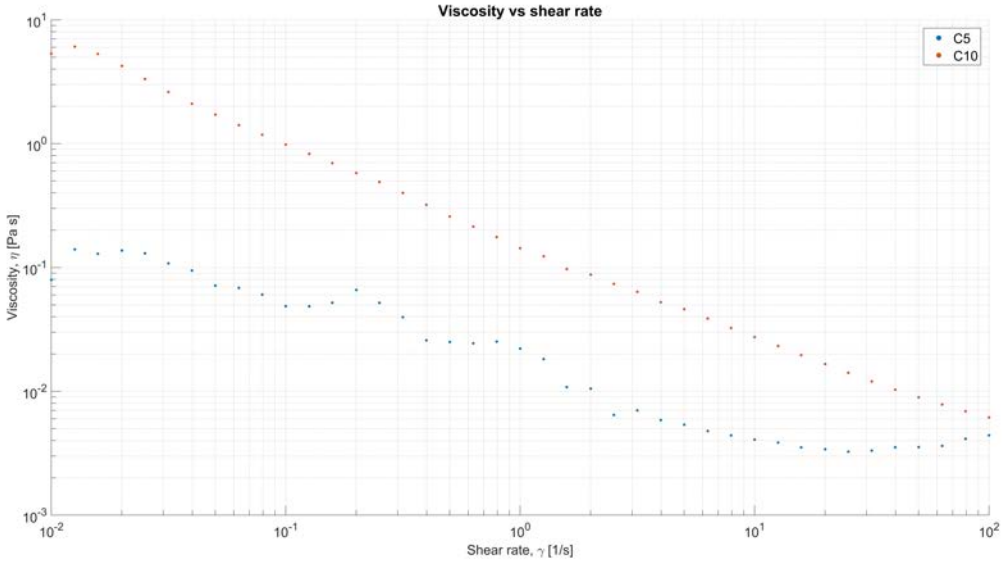

Figure 4.14: Viscosity vs shear rate for E1 (C5) and E2 (C10), where C5 and C10 indicate the percentage of oil in the emulsion.

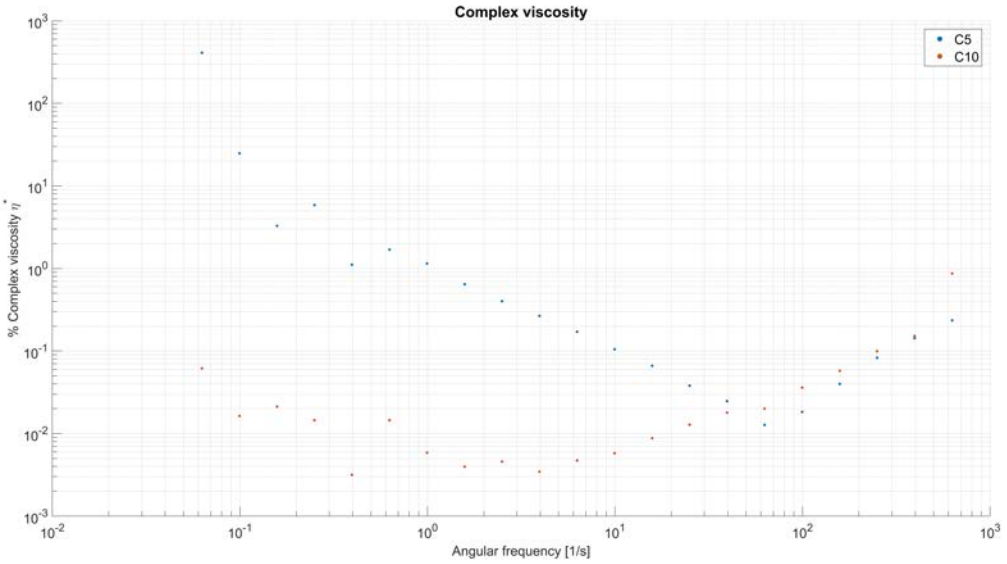

Figure 4.15: Complex Viscosity vs angular frequency for E1 (C5) and E2 (C10), where C5 and C10 indicate the percentage of oil in the emulsion.

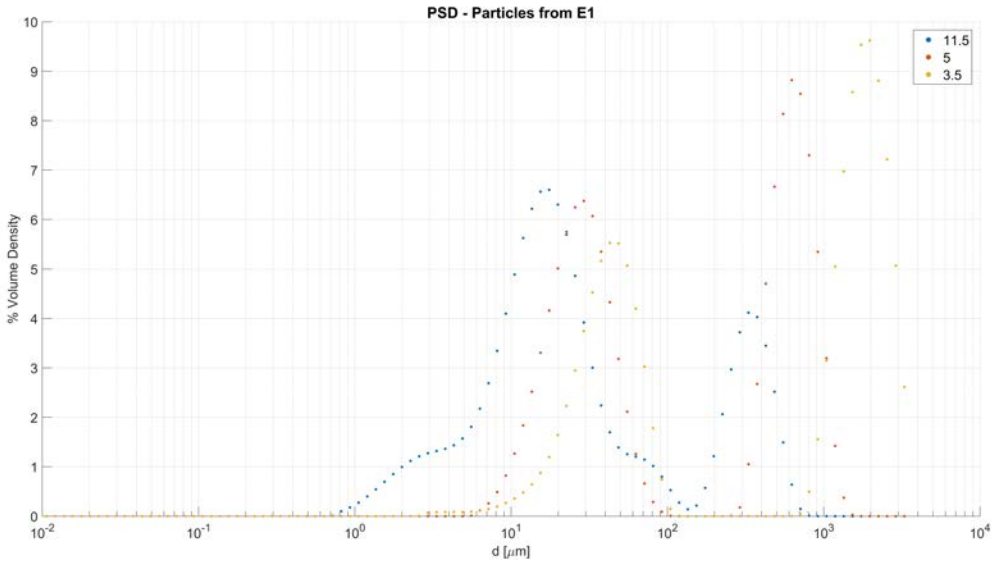

Figure 4.16: PSD for the particles coming from E1. The legend is reporting the flowrate of air provided to the nozzle in l/min

4.3.3 Spray drying

As stated at the beginning of this section, the only condition which was changed is the nozzle air flowrate. The other conditions are listed below here:

- Heating air flow: 0.35 m^3/min
- Inlet T: 160 °C
- Pump speed: 160 rpm
- Cyclone air P: 1 bar

Fig. 4.17 shows a clear trend about the PSD for the spray dried particles: by increasing the quantity of air provided to the nozzle, there is a corresponding decreasing of the average particle size. The same can stated for particles coming from E2, but in this case there is a bi-modal distribution: the final product was containing bigger particles for all the three conditions tested. This may be due to the greater elastic behavior of the E2, the more the residence time inside the nozzle, the greater the particle size. At the same time, an increment of the residence time inside the nozzle produces more frequent solidification and clogging of the nozzle: that's the reason why less conditions were tested. Also for this experiment, there was not a sufficient quantity of powder to assess the flowability of the product.

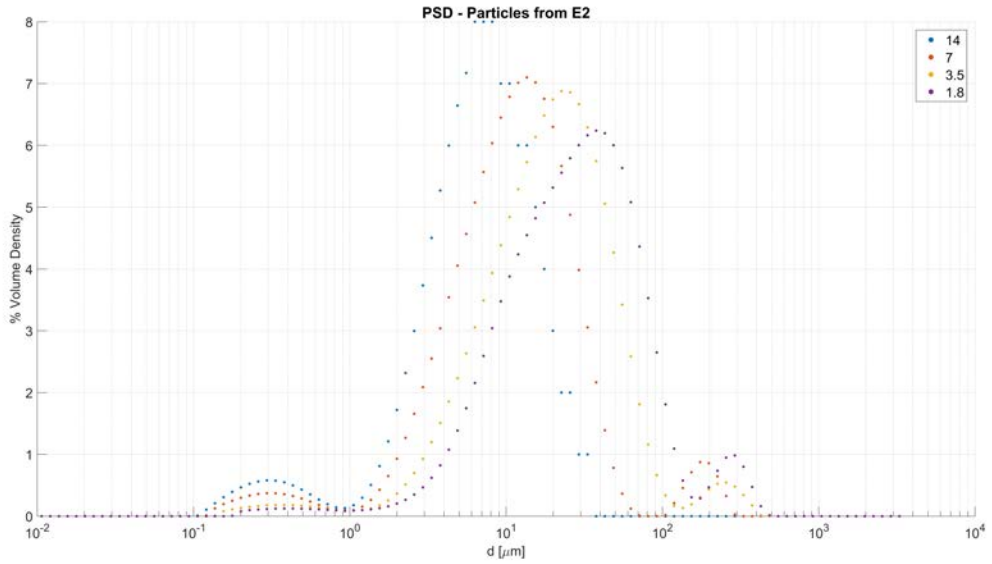

Figure 4.17: PSD for the particles coming from E2. The legend is reporting the flowrate of air provided to the nozzle in l/min

4.4 Experiment 4

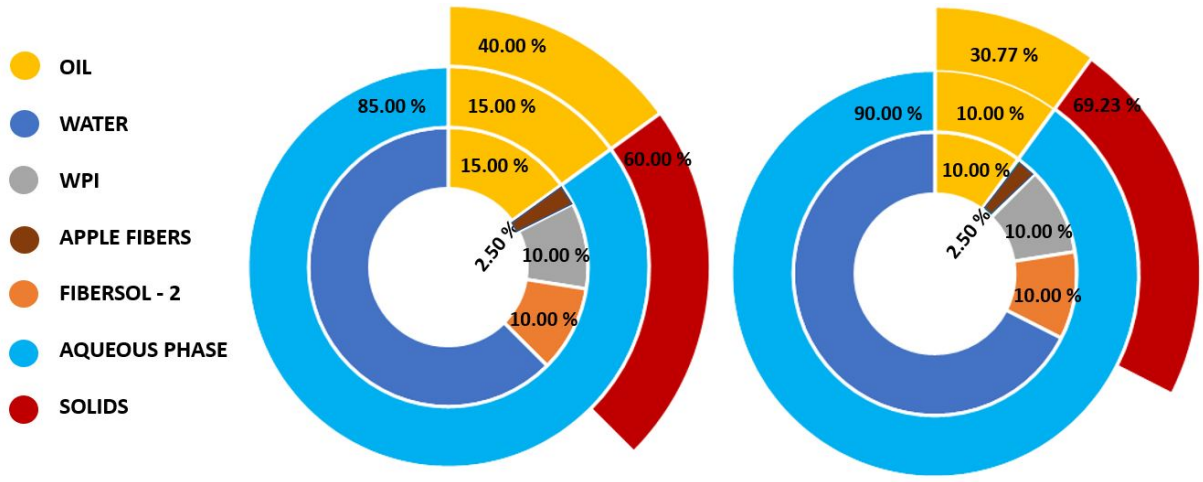

Figure 4.18: Composition of the emulsions E3 and E4

The objective of this experiment is to test the spray capability on two formulations, from now on called E3 and E4, containing apple fiber instead of cellulose. The quantity of solid has been raised again, because of the better dispersibility of this type of fiber, and for E3, also the oil percentage has been stressed a little bit as it can be evinced by looking at Fig. 4.18. The operative conditions have not been modified with respect to the previous experiment. Even if the materials have changed, the PSD distribution shown in Figg. 4.19, 4.20 is similar to E1 and E2. However, three passes are needed, since the first pass shown a poor yield in both cases (especially for E4, where no sub micron droplet was created after the first pass).

4.4.1 Rheology

The total quantity of solids has been more than doubled w.r.t. the previous experiment. Therefore also the viscosity manifested an increment, the quantity of oil is still significantly influencing this property: at the highest shear tested, Fig. 4.21 shows that the viscosity for E3 is almost the double of the one of E4. The

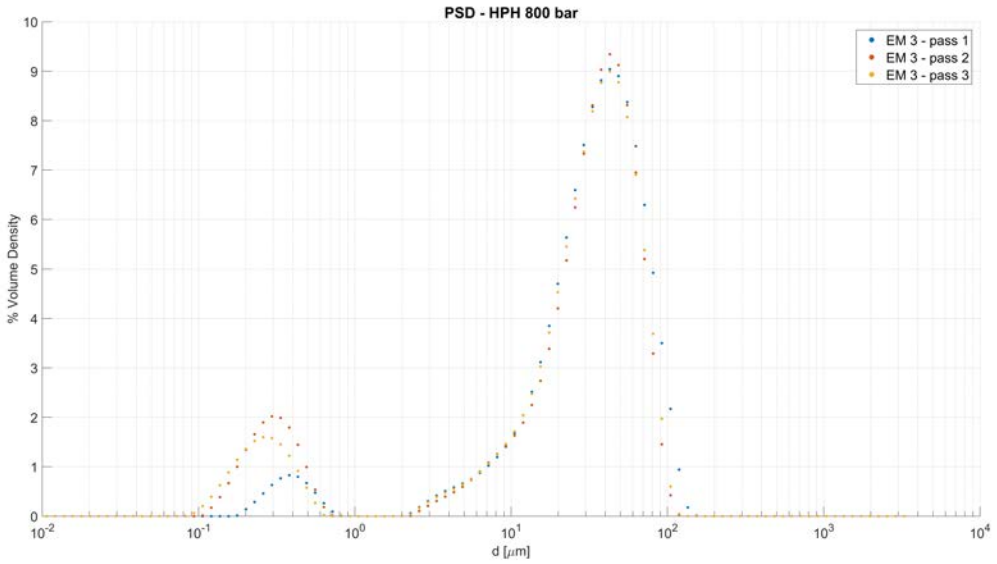

Figure 4.19: PSD for E3.

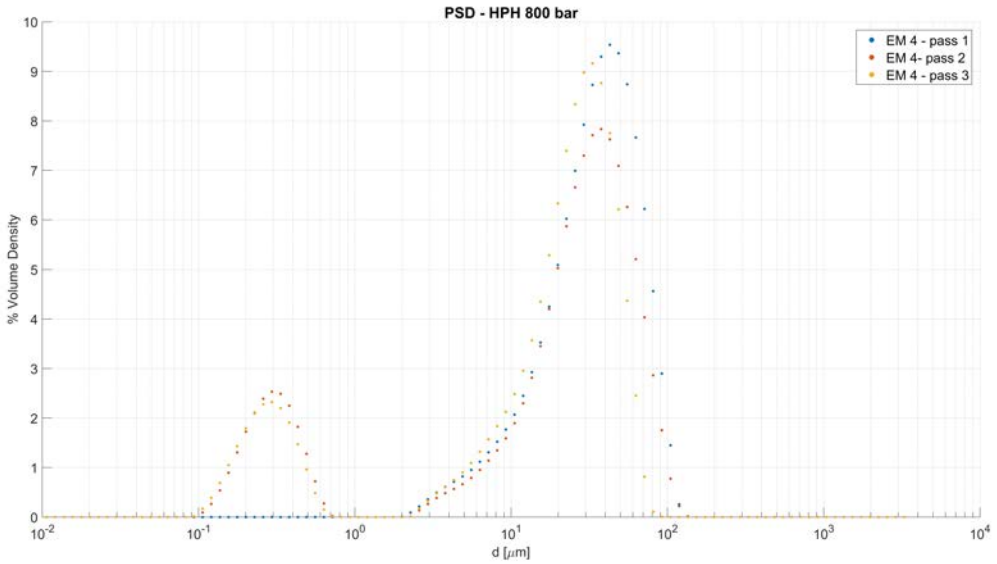

Figure 4.20: PSD for E4.

behavior is, again, shear thinning, and the elastic behavior appears at 250 1/s for both E3 and E4, later than E1 and E2: this is a positive result, and it could be a signal of a better spraying ability.

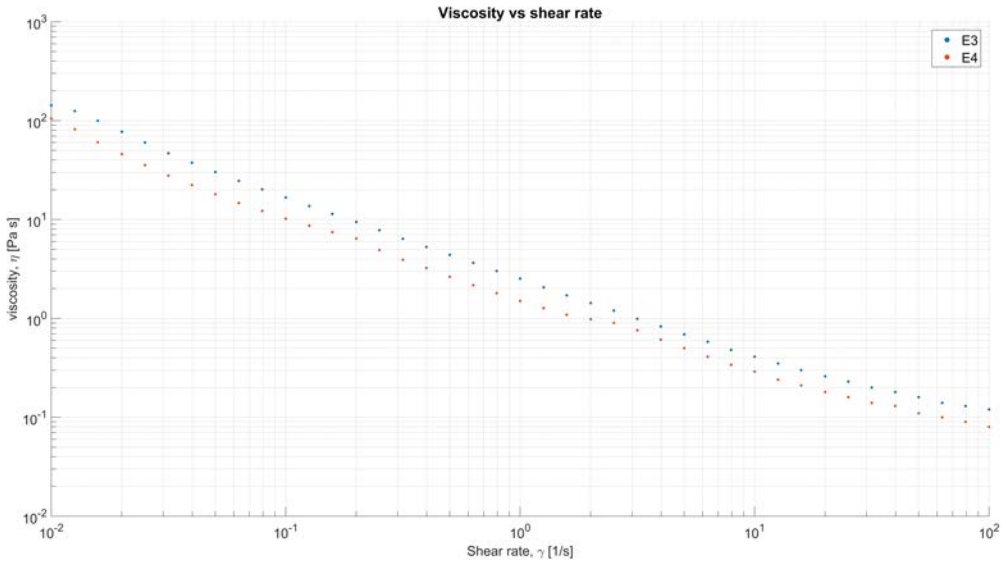

Figure 4.21: Viscosity vs shear rate, for E3 and E4.

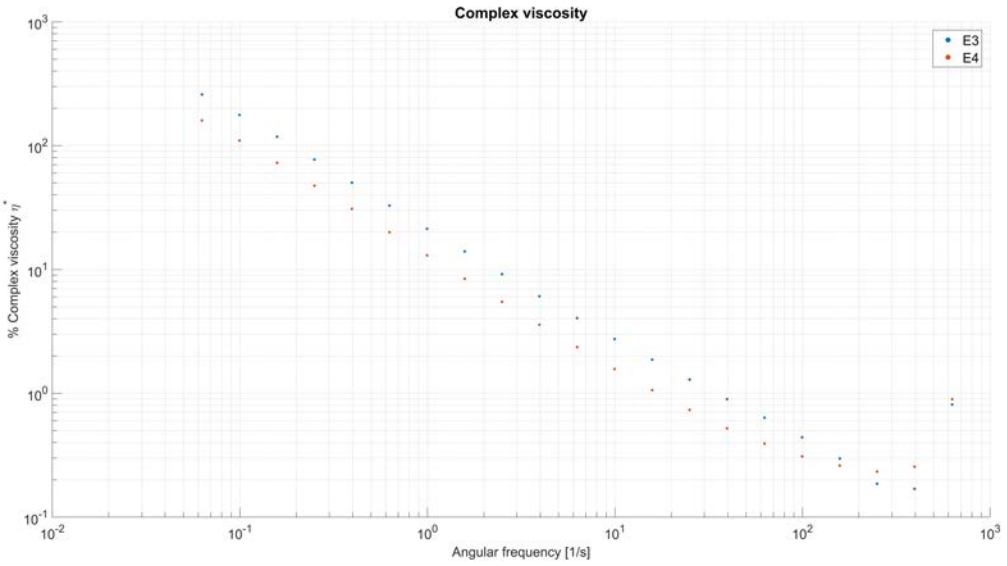

Figure 4.22: Complex viscosity vs angular frequency, for E3 and E4.

4.4.2 Spray drying

For this experiment an higher air temperature has been used, as an attempt to increase the dryness of the powders. Moreover, also the air cyclone pressure (and then flowrate) has been increased, while the pump rotational speed has been maintained to its maximum. The same nozzle air flowrates of the previous experiment were tested, to have a mean of comparison. Here below the operative conditions that were chosen are listed.

- Heating air flow: 0.35 m^3/min
- Inlet T: 170 °C
- Pump speed: 160 rpm
- Cyclone air P: 1.5 bar

Apart from the anomalous behavior of the third condition for the particles produced with E3, the trend found in the previous experiment is confirmed: even with these two recipes at higher air nozzle flowrates,

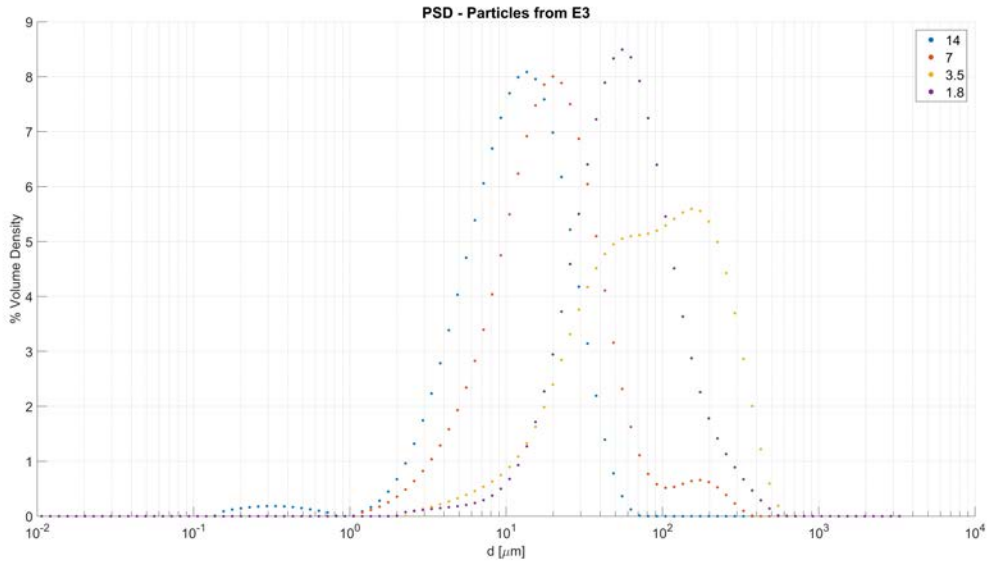

Figure 4.23: PSD for the particles coming from E3. The legend is reporting the flowrate of air provided to the nozzle in l/min.

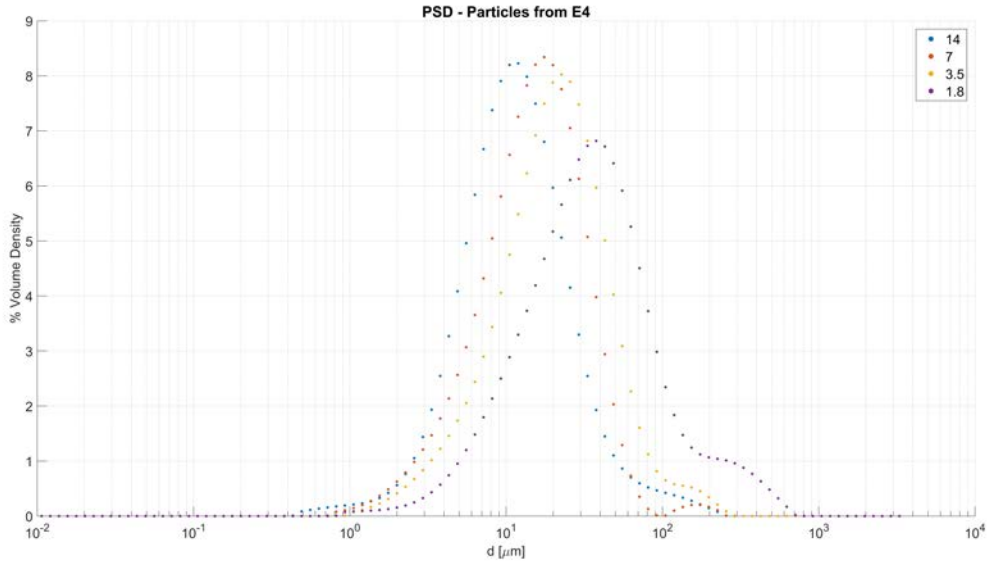

Figure 4.24: PSD for the particles coming from E4. The legend is reporting the flowrate of air provided to the nozzle in l/min.

smaller particles are produced. The quantity of oil seems not to influence the particle size, for any condition. Although the recipes has changed considerately w.r.t E1 and E2, the PSD is falling within the same range, with small deviations probably due to the change in the air temperature and the cyclone air pressure. One of the problem which is still persisting, is related to the moisture content of the powders and the small quantity produced, due to the weeping phenomenon happening inside the columns, causing a lost in the efficiency: powders attach to the wet walls, causing clogging in the restrictions and preventing the powder to end into the cyclone and then being collected. This causes a lot of interruptions and a depletion of the emulsion, that cannot be sprayed anymore.

4.5 Experiment 5

This experiment tried to solve the issue raised in the previous trial, without coming back to the nozzle clogging problem. Beside this, an equipment change for the emulsion creation was obliged, since the HPH was broken after the fourth experiment. First of all, the rheology of the aqueous phase was tested, to understand the best formulation to achieve the right ratio of viscosity between the oil phase and the aqueous phase: the value of the ratio must be between 0.1 and 4 [1], with the best ratio equal to 1. With the HPH this was not taken in account, since the emulsification efficacy was high anyway, but with Silverson RS, foaming problems, and emulsion stability problems can be encountered more easily. Fig. 4.25 shows the viscosity of two aqueous solutions containing 30 % of solids and 50 % of solids, with the same ratios of Experiment 4. The outcome is showing clearly that the ideal concentration of solids is closer to 50 %: the viscosity of sunflower oil at 20 °C is 0.068 Pa [22], and the ratio between the this value and the viscosity of the first solution is 2.34, while for the 50 % solution is 0.55, which is closer to 1. It can be also noticed that the 30 % aqueous solution has a Newtonian behavior, while the second one has a shear thinning behavior even before the emulsion creation. Please notice

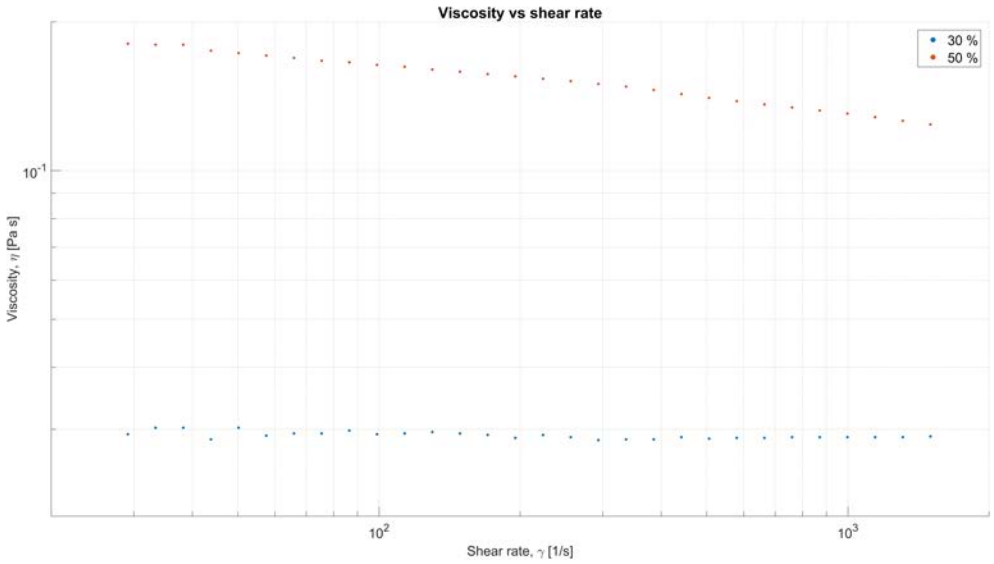

Figure 4.25: Viscosity vs shear rate for the 30 % and 50 % aqueous solutions.

that this time a different rheometer has been used, since the Anton Paar one was temporary unavailable. The mechanism behind this equipment is related to coaxial cylinders, and thanks to it, it has been possible to assess points at higher shear rates. The information coming from this experiment is fundamental for the creation of the recipes in the following one. A dramatic change in the quantity of solids will be applied (still taking in account the possibility of nozzle clogging).

4.6 Experiment 6

This experiment concludes the part regarding the formulation of powders starting from simple oil in water emulsions. The results of the previous experiment led to choose the three recipes reported in Fig. 4.26, from now called F1, F2 and F3. The only quantities that have been modified between the three formulations are the apple fibre and the Fibersol-2 content. The objective is to assess the behavior of the emulsions by changing the relative quantity of the solids, and at the same time finding the maximum quantity of insoluble solids that can be introduced without clogging the nozzle. All the emulsions have been created by using the Silverson RS, homogenizing for 10 minutes at 9000 rpm, using an ice bath to limit the temperature raise. The PSD measured immediately after the homogenization is displayed in Fig. 4.27: it can be noticed that the quantity of fibre is not influencing the particle size, and even if the quantity of water has decreased significantly w.r.t. the fourth experiment, the nanosize for the oil droplets surrounded by Fibersol-2 and protein was reached anyway. The only difference between the emulsions is the ratio between the volumetric density of nanosized particles, as

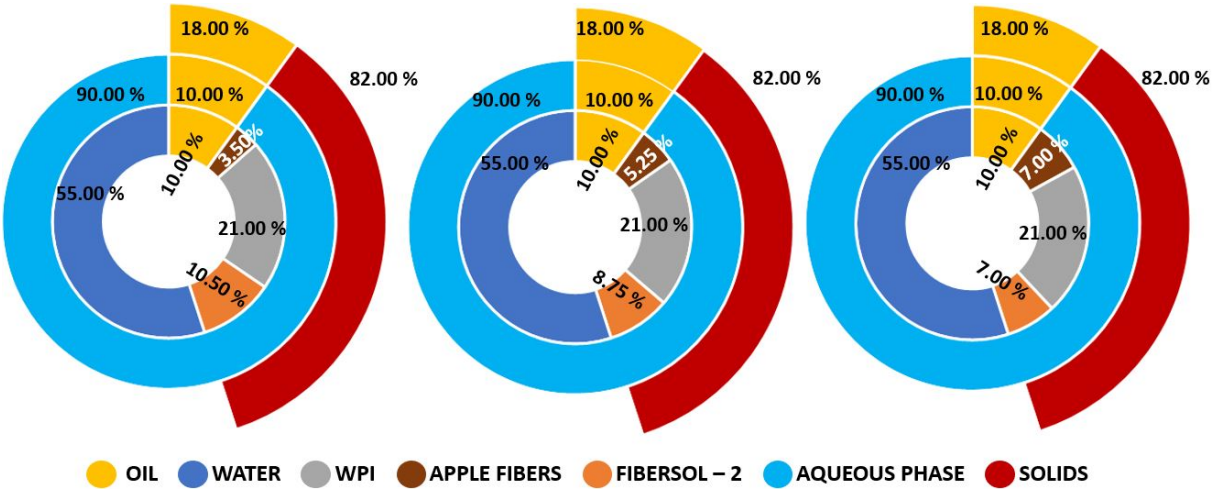

Figure 4.26: Composition of the emulsions F1, F2 and F3.

expected, F3 is containing more apple fibers and therefore the correspondent peak is higher (and decreasing from F3 to F1).

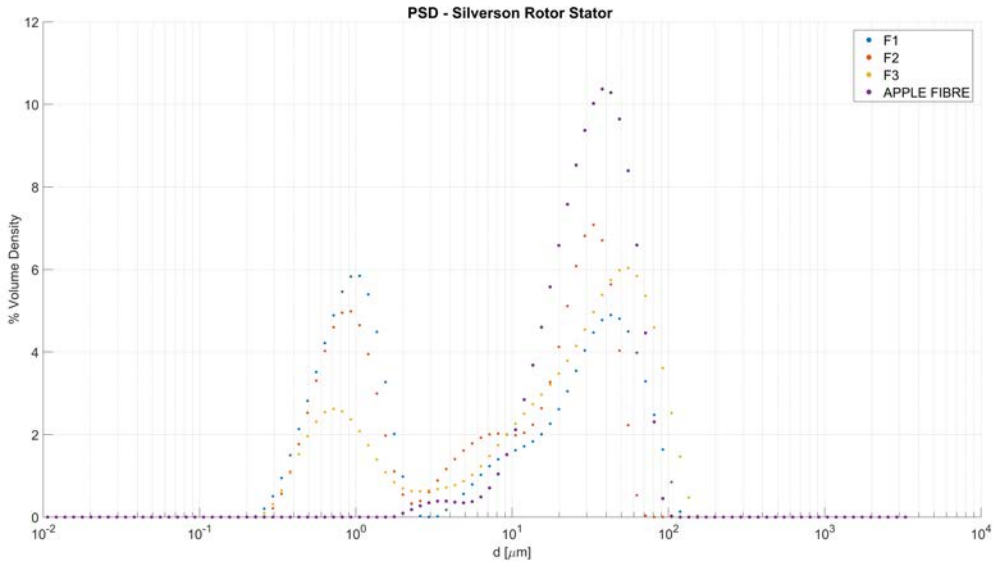

Figure 4.27: PSD for F1, F2 and F3.

4.6.1 Rheology

Also in this case, the rheological behavior trend found is the one expected: the more the quantity of fibers, the more viscous the emulsion. For all the three recipes the behavior remains shear thinning, and the viscoelasticity is still present, with a change of the behavior at 400 1/s for F2 and F3 and at 250 1/s for F1. This result indicates that an higher quantity of fibers produces a delay in the manifestation of an elastic behavior, because the viscous one has to be completely extinguished. However, once the change is reached, the increment in viscosity is more evident for F2 and F3 than for F1.

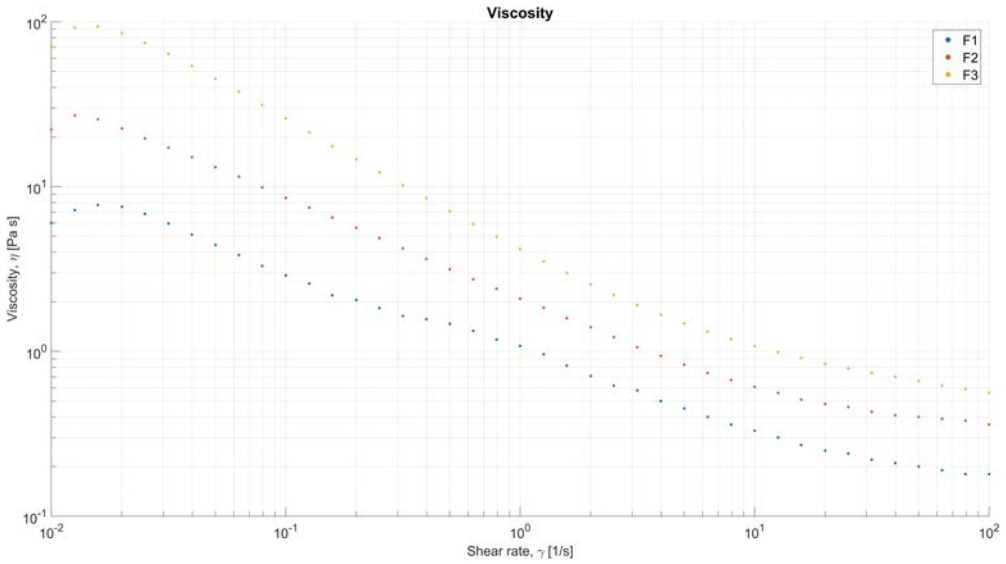

Figure 4.28: Viscosity vs shear rate, for F1, F2 and F3.

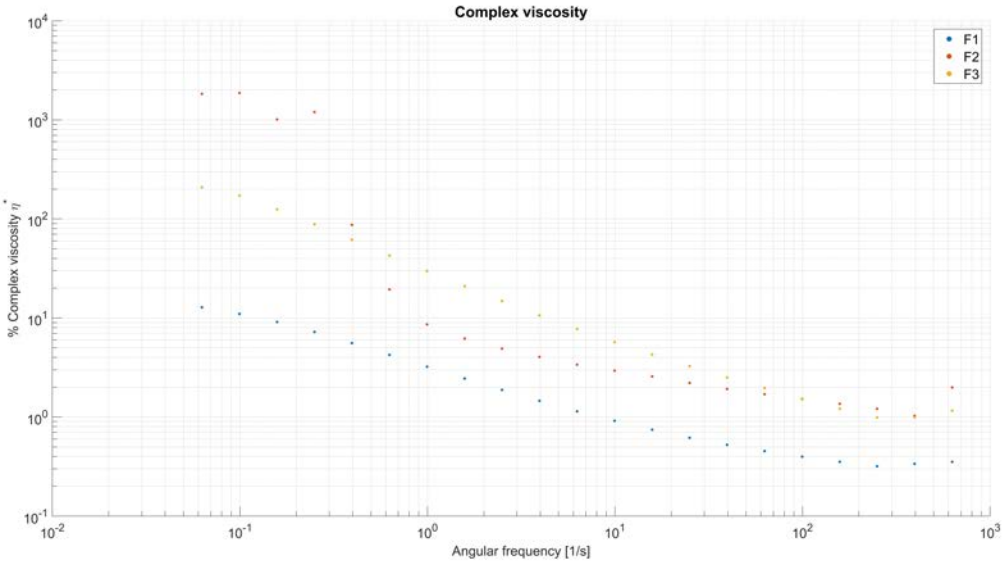

Figure 4.29: Complex viscosity vs angular frequency, for F1, F2 and F3.

4.6.2 Spray drying

For this experiment, the air temperature was maintained at 170°C, since qualitatively the aspect of the last powders produced was good. The air cyclone pressure (and then flowrate) has been decreased w.r.t. the fourth experiment, since an higher fresh air flowrate reduced too much the T at the bottom of the column, causing sometimes the condensation of some droplets and then generating caking problems. The pump rotational speed has been maintained to its maximum, but to increase the corresponding liquid flowrate, a double tubing was installed. This arrangement will decrease the air to liquid ratio, so that the final particle size will be increased. The following nozzle air flowrates were tested: 6.0, 3.0, 1.5, 7.5e-1 l/min. Here below the other operative conditions that were chosen are listed.

- Heating air flow: 0.35 m^3/min
- Inlet T: 170 °C
- Pump speed: 160 rpm

- Cyclone air P: 0.75 bar

The results are reported in terms of two dimensionless number: the ratio between the d_{50} and nozzle diameter versus the *Re* number, calculated according to the following equation:

$$Re = \frac{D_{eq}(v_{air} - v_{liq})\rho_{air,25°C}}{\mu_{air,25°C}} \tag{4.3}$$

The reason of considering an equivalent diameter is given by the fact that the air is flowing through an annular section and not a circular one. The velocity of the liquid is considered as the velocity inside the tubing, before the spraying, and although it is negligible should be considered, since it is different according to the different emulsions: a more viscous liquid is flowing at a lower velocity. Even for the same air flowrate, in the plot in Fig. 4.30 it can be noticed a deviation of the Re number. The major information that comes from this graph, is that over 5.25 % w/w the quantity of fibers cannot influence the particle dimensions too much, so it's not worth to keep an increase in the apple fibers because it would not be beneficial, instead, it would obstacle the processability of the emulsion in the spray drying phase.

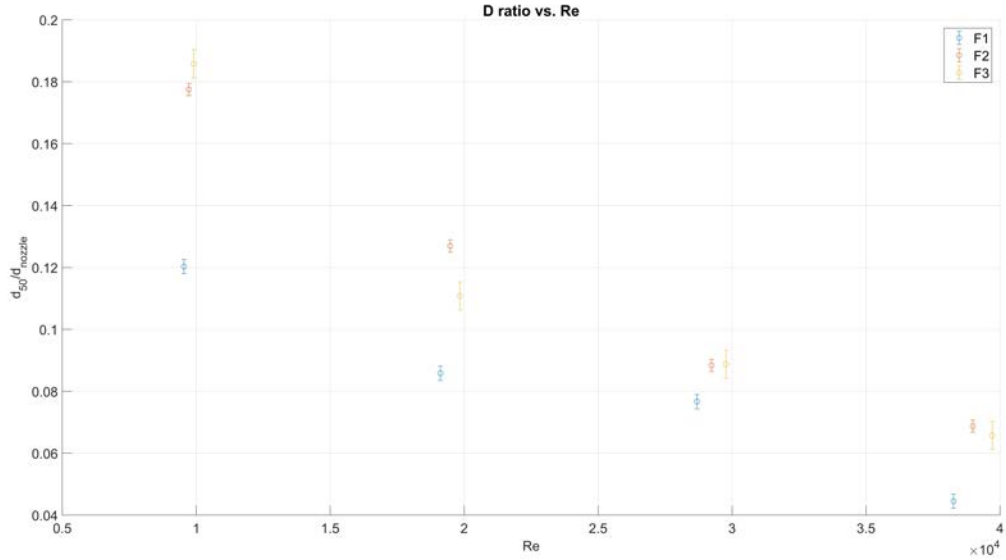

Figure 4.30: D_{50}/d_{nozzle} vs Re. The error bars are representing the std deviation obtained after 3 measurements on three sampling, but on the same powder

4.6.3 Flowability

For all the three emulsions the flowability was measured with the Brookfield powder flow tester. The reference condition was the powder produced with 3.0 l/min of air nozzle. The standard test was used, and the flow curves showing the relation between the unconfined failure stresses and the major principal consolidating stresses are displayed in Fig. 4.31. Apparently, the flowability is not influenced by the quantity of fibers, although a greater percentage of them should increase the easiness of flowing, because this ingredient is the one which should be dried first. There is an outlier for the F3 curve, however the measurement could be not performed again, since the quantity of powder left after the first measurement was not enough, and trying again with the same powder may have introduced some error, since the powder was already subjected to the stress.

4.6.4 Moisture content

Since the aspect of the powder is not oily,, the MC could be measured through a TGA analysis, again taking as reference only the particles produced with 3 l/min. Fig.4.32 shows one example of plot produced after the analysis. The average value of moisture is 3.52 %, which is low enough for a food powder, according to [15].

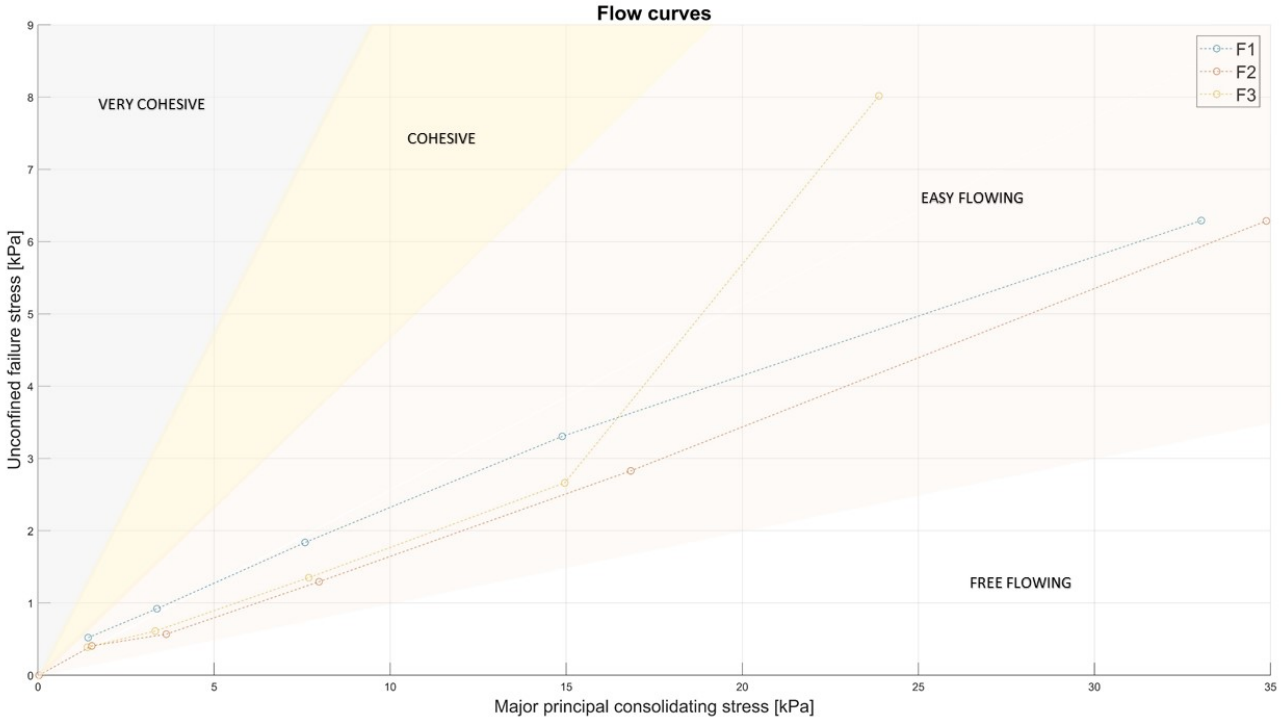

Figure 4.31: Flow curves for the powders produced with 3.0 l/min. Unconfined failure stress vs Major principal consolidating stresses

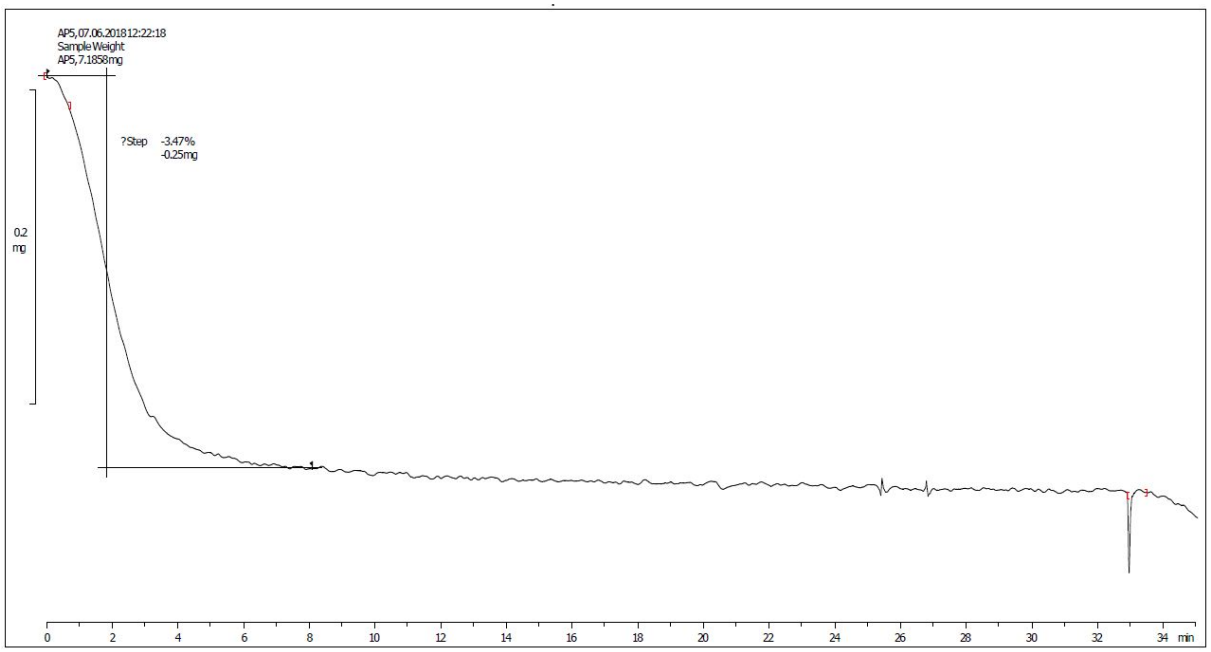

Figure 4.32: Moisture content report

4.6.5 SEM

The particles produced with the condition of 3.0 l/min were also observed through SEM, prior breaking them gently with a spatula. The objective is to look at the powders microstructure, especially around the wall and the inner part of the particles, to verify the encapsulation efficacy. The magnification went from 1000 to 20000, and the three samples analyzed were previously coated with 20 nm of Au, under high-vacuum conditions (10^{-4} Pa). As it can be noticed from Fig. 4.33.a, 4.34.a and 4.35.a, all the particles show some particles inclusion,

which can be addressed as apple fibers. Also the dimension check reinforce the hypothesis made. For the detailed pictures taken around the wall (see Figs. 4.33.b, 4.34.b, 4.35.b), the nanopores can be an indication of the presence of oil (escaped from the wall because of the vacuum applied during coating). The dimension of the pores is compatible with the one found thanks to the Master Sizer measurement, and the pores are appearing in all the three pictures. Moreover, the outer surface is not oily if touched, and the inner surface is not wet nor showing any droplets on it, so the only option is that the oil has been successfully entrapped inside the wall.

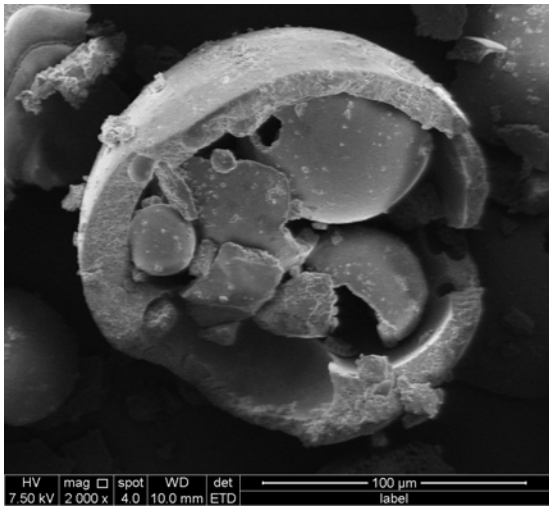

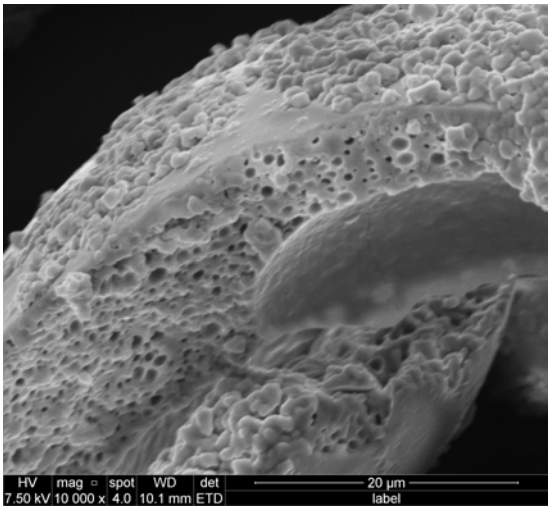

Figure 4.33: a. SEM image of a particle produced from emulsion F1. 3.0 l/min nozzle air b. Details on the wall surface.

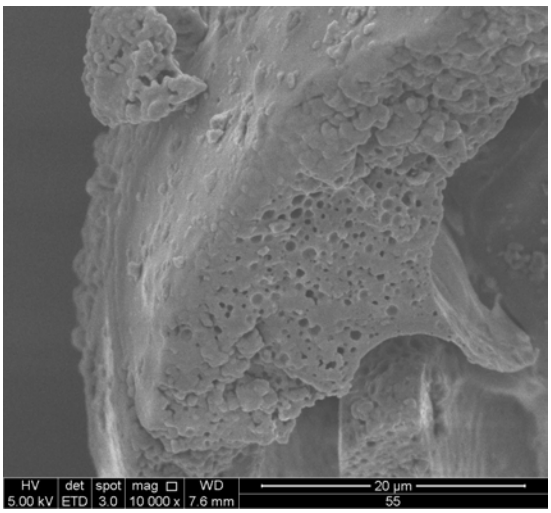

Figure 4.34: a. SEM image of a particle produced from emulsion F2. 3.0 l/min nozzle air b. Details on the wall surface.

4.6.6 Reproducibility

The recipe F1 was replicated to verify the reproducibility of the results. The outcome it's summarized in Appendix A. It can be noticed that the experiment is fully reproducible.

4.7 Experiment 7

The purpose of this experiment is to find a non-artificial surfactant to separate the inner aqueous phase from the oil phase in a double emulsion. The creation of double emulsion is well known, and for this work the

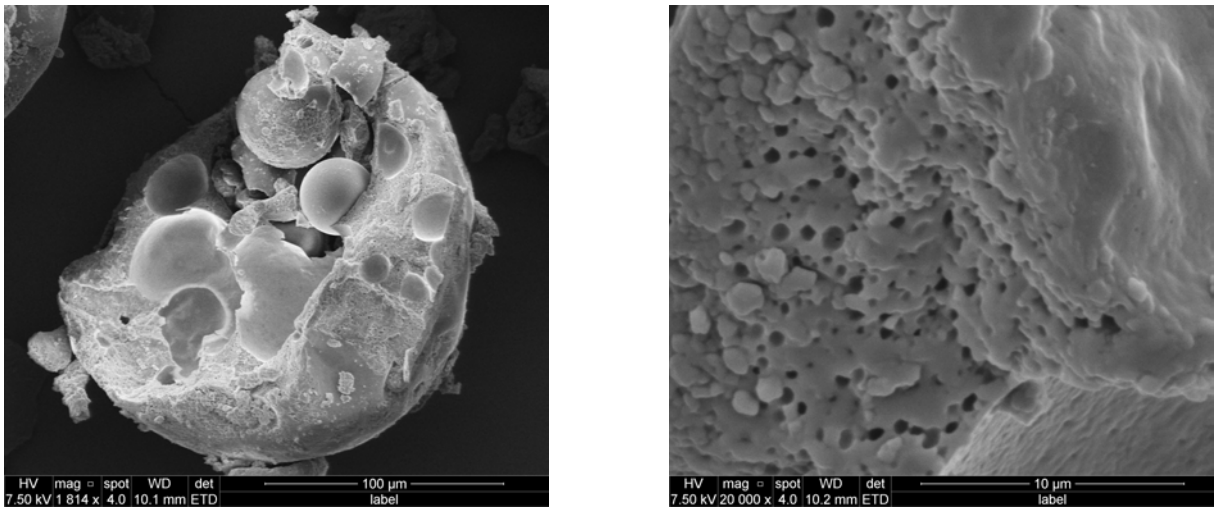

Figure 4.35: a. SEM image of a particle produced from emulsion F3. 3.0 l/min nozzle air b. Details on the wall surface.

Figure 4.36: Final aspect of one of the powder produced.

outer aqueous phase - oil phase interface was previously studied. The material object of this study is the palm stearin, whose property have been described in Ch 2. The major challenge is to reduce the palm stearin in

nano flakes or crystals, since the droplets of oil in the previous emulsion were of that size, and the outer phase should not be altered too much. The objective should be arriving at the production of the same type of powders produced in the previous experiment, by including an aqueous phase inside the oil droplet.

4.7.1 Operating procedure

Palm stearin was melted at 56 ± 2 °C. A solution of 65 % w/w of sugar in water was prepared and heated (54 ± 2 °C). The reason for the sugar addition is related to the viscosity of the water phase, which should be increased to be similar to the oil one, so the droplets breakage will result easier. The melted palm stearin was poured into the water and pre-homogenized with 3 % w/w Tween20 using Silverson RS at 3000 rpm for 2 minutes. The final concentration of the palm stearin in the aqueous medium was 40 % w/w The homogenization step occurred using IKA magic lab (pre heated at 55 ± 1 °C before using it), recirculating the liquid emulsion for 10 minutes, using a rotational speed of 25000 rpm. After that, the crystallization step took place. The emulsion was poured into cold water (5 ± 2 °C) to facilitate crystallization. The ratio emulsion to cold water was 1:2. To use the fat nanoparticles in the emulsion, Tween20 must be removed, otherwise there is no point in using a natural grade surfactant if it contains traces of artificial emulsifier. The diluted emulsion was centrifuged at 4000 rpm for 15 minutes, then most of the water removed. The fat was washed with isopropanol and centrifuged again at 4000 rpm for 10 minutes. The treatment was repeated once with isopropanol and one last time using sunflower oil instead of isopropanol. After the particles were created, the emulsification step was performed: 4 recipes were formulated (see Tab. 4.3). The introduction of Span80 was to assess the quality of the fat as surfactant used alone w.r.t. to its employ with the aid of an artificial emulsifier. The emulsification step was performed with the RS, at 10000 rpm for 10 minutes, using an iced bath to limit the temperature raise.

ID	% Water	% Span80	% Oil	% Palm Stearin
A	21	0	71	4
A+	24.5	0.5	71	4
B	40	0	56	4
B+	39.5	0.5	56	4

Table 4.3: Recipes for the four water in oil simple emulsion tested.

4.7.2 PSD nanoparticles.

The fat nanoparticles produced were measured prior centrifugation and after the treatment, by selecting a refractive index of 1.52 and an absorption factor of 0.01. As it can be noticed from Fig. 4.37, after the centrifugation and the emulsification the size of the crystals did not change considerably: even if there was a caking effect after centrifugation, the nanosize was maintained for at least half of the particles. Please notice that all the PSD measurements for this experiment were done using sunflower oil instead of water as dispersant, since the main phase is now oil. It can be noticed that both the quantity of water and the presence of Span, are not influencing the final particle size of the crystals nor the emulsion water droplets (see Figs. 4.38 - 4.41).

4.7.3 Emulsions stability

What is changing instead is the stability of the emulsion: Fig. 4.42 shows the serum index evolution along with time. The serum index is defined as:

$$SI = \frac{Height\ of\ layer\ of\ emulsion}{Height\ of\ the\ liquid} \tag{4.4}$$

The emulsions with a greater quantity of water released a greater quantity of water, so the serum index is the same. However, also this time, the Span80 effect can be neglected. The emulsions created were all unstable, since the serum index was visibly increasing from the first minute after the emulsification step ended. The hypothesis is that the quantity of water was excessive, so the suggestion for future trials is to reduce its quantity to 5-10 %. All the PSD measurements after the first day were performed by sampling on the stable part. Fig. 4.43 gives an idea about how the separation looks like: the bottom part is constituted by all the water escaped from the fat (or fat and Span80) structure.

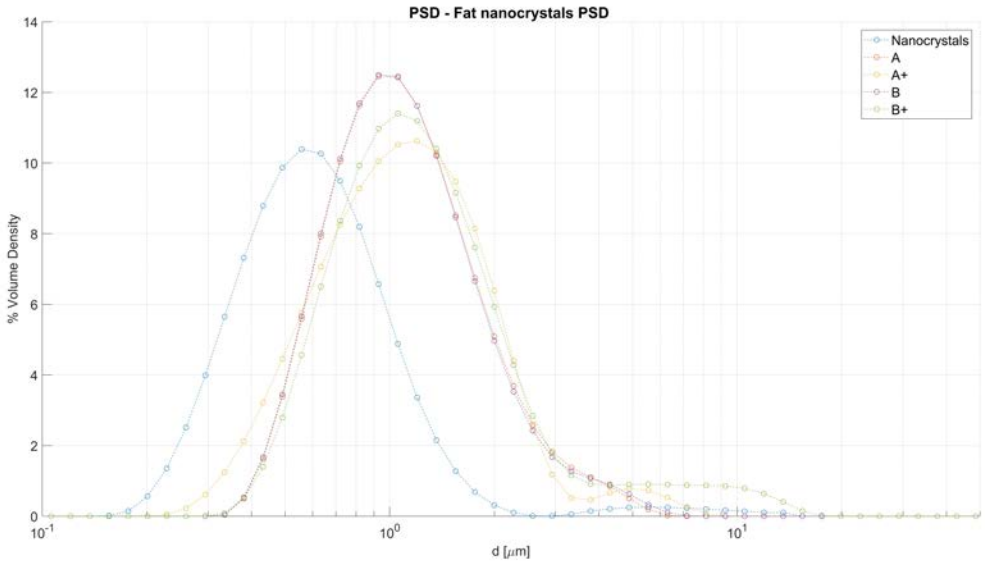

Figure 4.37: PSD for the fat nanoparticles before and after the usage in the water in oil emulsion.

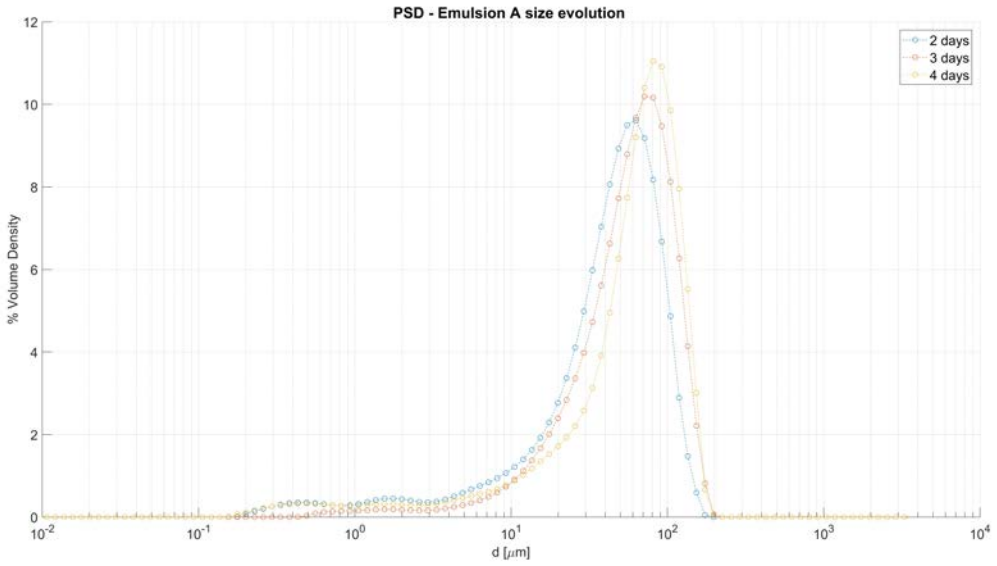

Figure 4.38: PSD evolution for emulsion A

Since the instability is really high, at the moment it has not been possible to create the double emulsion exploiting this fat surfactant, and then proceed with the spray drying.

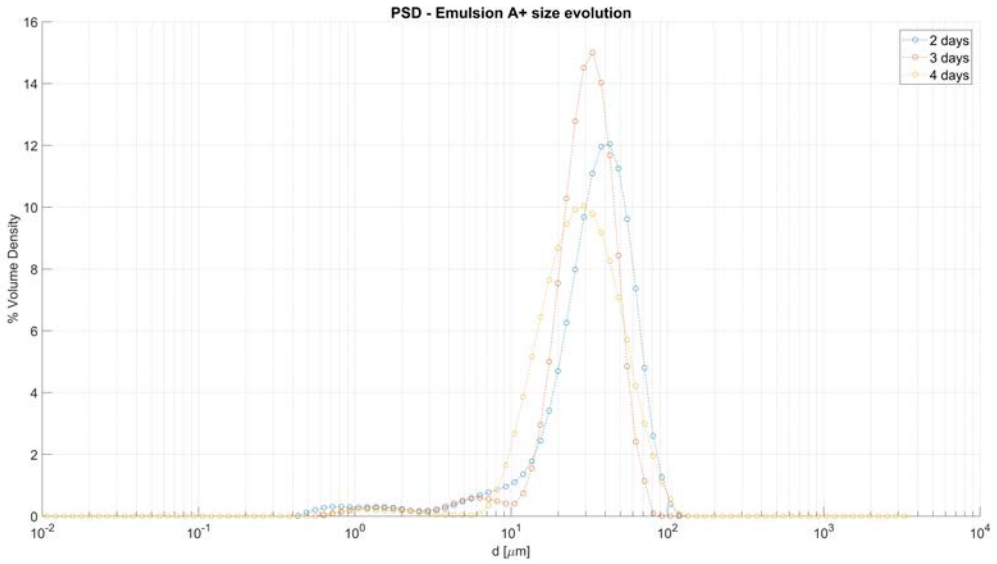

Figure 4.39: PSD evolution for emulsion A+

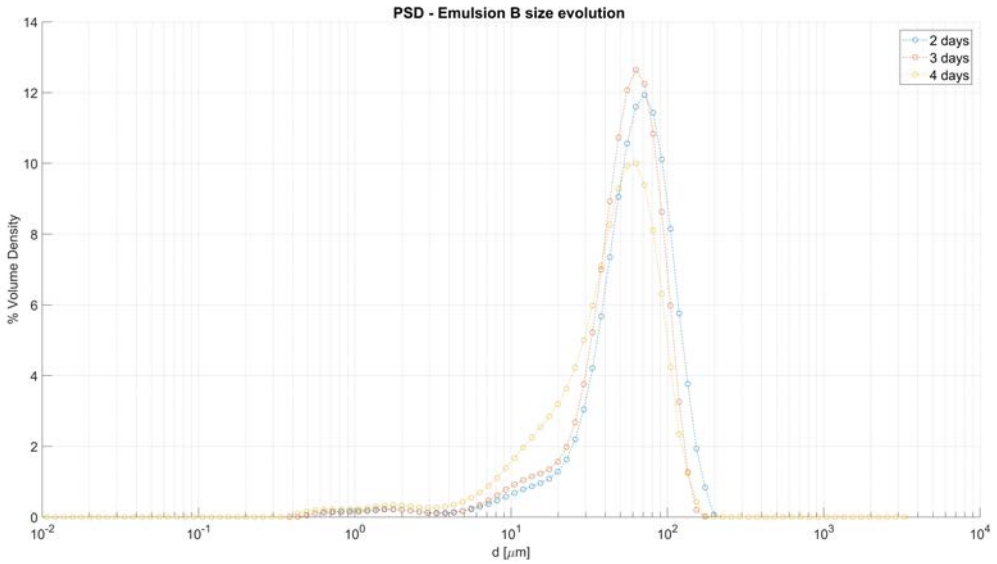

Figure 4.40: PSD evolution for emulsion B

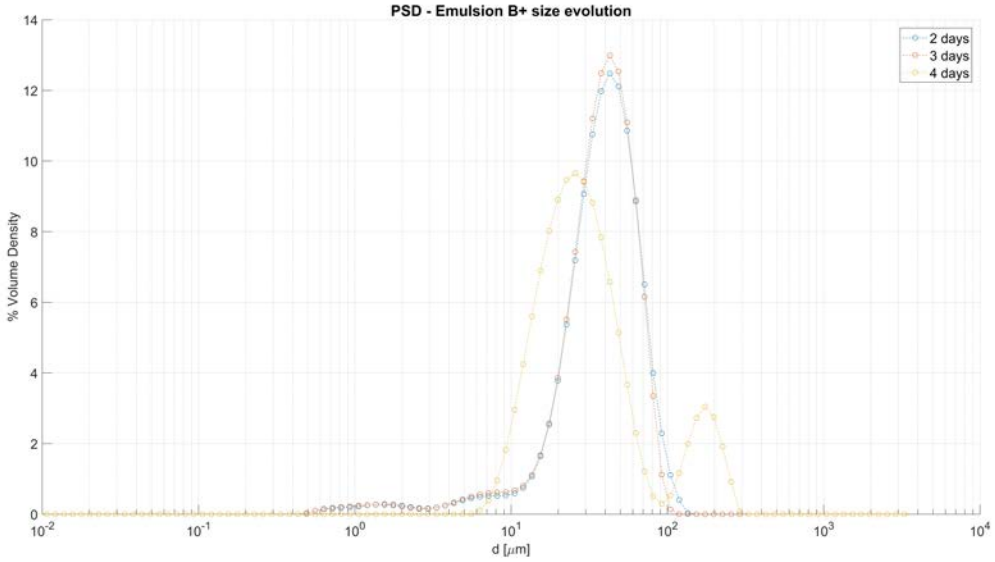

Figure 4.41: PSD evolution for emulsion B+

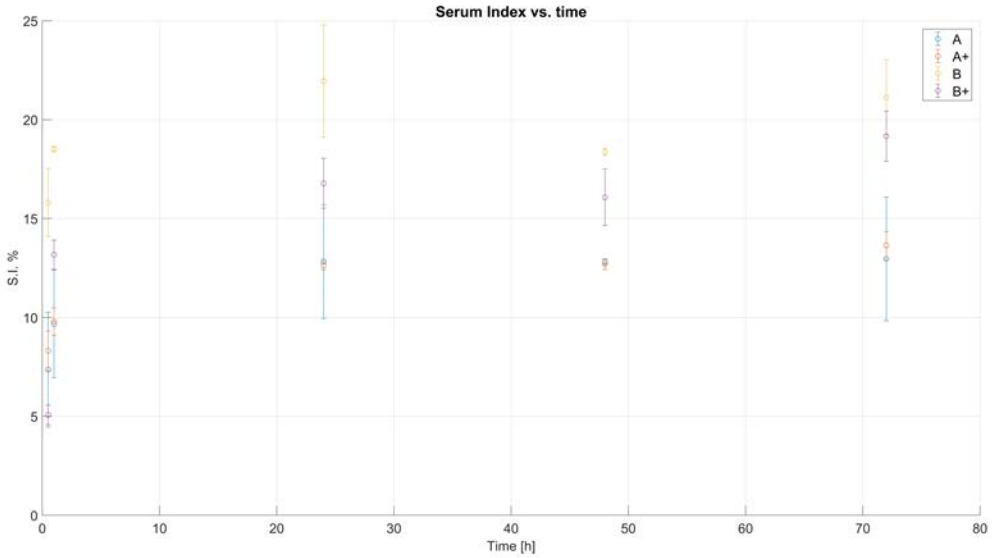

Figure 4.42: Serum index evolution along with time. Standard deviations values are calculated with the values of two different samples.

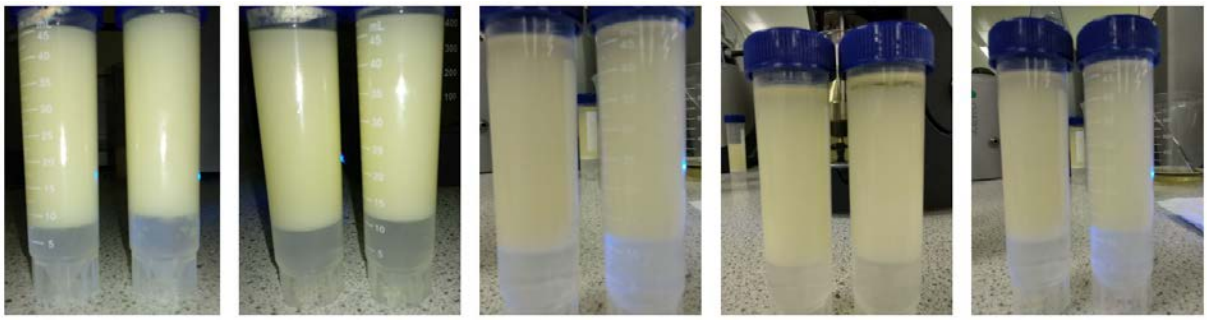

Figure 4.43: Evolution of the emulsion B: instability is noticed even after 30 minutes after its creation.

Chapter 5

Scale up

The last objective of this project is to evaluate the economic feasibility for a large-scale production of the powder produced so far, with the recipe including an average amount of fibre of 5.25 % w/w in the emulsion. All the costs have been estimated using real quotations from different companies and the correlations in [2].

5.1 Batch or continuous?

The first choice is concerning the process category. Although the food industry new trend is the conversion of all existing processes into continuous processes, for this production the only viable option seems to be a semi-batch production. One of the reasons is the need of a periodically cleaning of the spray dryers, due to the accumulation of product on the equipment walls. Another reason is that the production is new, and some batches may be spoiled. Then it would be easier to get rid of the produced powders only for one batch, instead of trying to proceed with the troubleshooting while the plant is still operating, with the risk of losing more than the equivalent of one batch only. All the data regarding the production times, are reported in Tab.5.1, and all the sequence of work can be visualized in the Gannt chart displayed in Fig.5.1. In this chart it can be noticed that the time for transporting the powders requires almost one day. This is due to the pressure drops minimization off the pneumatic system, however, by using a conveyor belt or a screw conveyor, the powders can be transported much quicker. The mixing time of 9 hours is due by the large amount of powders to be added, plus the foaming risk, which must be avoided by adding the powders slowly. Another important choice is regarding the throughput of the plant for which the design is thought. The choice is oriented to a large production for a specialty product, with a quite high cost per unit of mass (€/kg). From this data, the first economical potential EP_0 can be determined, by subtracting the cost of the raw materials to the production cost (plus two approximated evaluations for sterilization and the cleaning of the tanks and the lines). Results are displayed in Tab 5.2.

Number of max worked hours per year:	8760
Number of bank holidays hours:	240
Number of hours for maintenance:	336
Tot number of hours: 8184	8184
Number of days	341
Time for cleaning the equipment	2046
Estimated time lost for spoiled batches: 5%	409.2
Total spraying time	5728.8
Total Hydrating time	2864.4

Table 5.1: Production time estimation

Since there is no recycle nor reaction for this batch production, the plant can be designed in a straightforward way with one level. The Block Flow Diagram is shown in Fig.5.3. For each equipment type, and then for the main piping structures, the annualized cost has been determined, after the equipment has been sized in a way to satisfy the desired throughput.

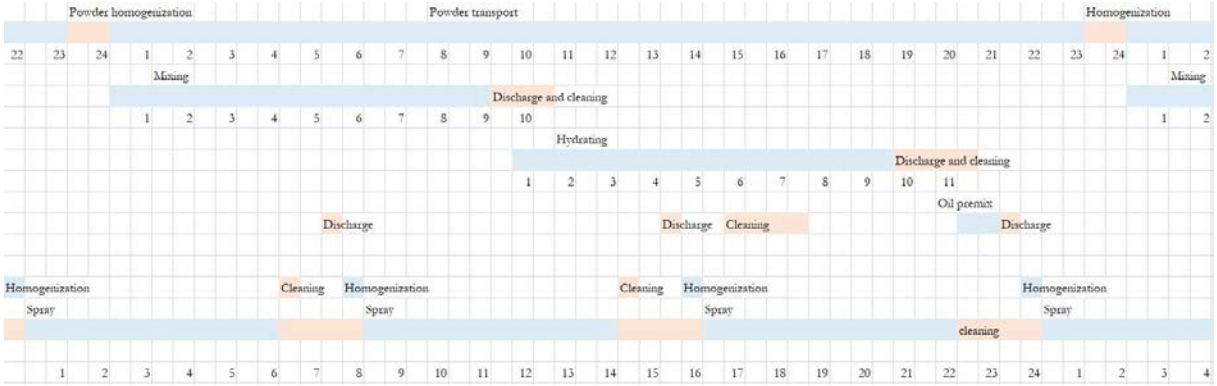

Figure 5.1: Gantt chart. Each square represents 30 minutes.

		Efficiency	0.61
		% powder	0.45
		Price of a kg of product	15.00 €
		Throughput kg/h	1000
		Revenues	85,932,000 €
	Cost [€/kg]	Demand [kg/h]	Cost rate [€/hr]
Emulsion	2.98 €	4000	11,928 €
Sunflower Oil	0.35 €	400	138 €
WPI [€/kg]	11.00 €	840	9,240 €
Apple fiber [€/kg]	2.10 €	210	441 €
Water [€/kg]	0.004 €	2200	9 €
Fibersol-2 [€/kg]	6.00 €	350	2,100 €
			TOT [€/y]
			67,830,711 €
		Cost of washing	477,400 €
		Cost of sterilizing	1,000,000 €
		EP0 [€/y]	25,217,089 €

Table 5.2: EP_0 evaluation

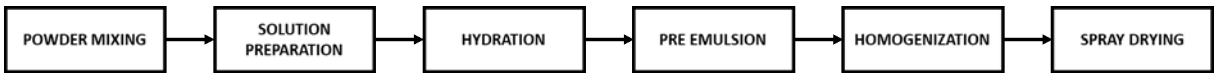

Figure 5.2: Process BFD

5.2 Storage and process vessels.

The first equipment type to be sized is the process vessel. Tab. 5.3 lists all the vessels required by the process, and their volumes. The choice made is to store the quantity for a whole production week, while for the next stages, to process the amount required over a day. After the oil addition, the quantity processed is only the one required for a batch (6 hours of spraying), so the tank size is reduced. For the solid ingredients, it has been decided to store them into a silo, whose dimensions have been decided after the flow ability measurement reported in Fig. 4.3. It can be noticed that the powders have all a good degree of flow ability, the toughest one remains the apple fibre, which is the finest between the three. The rat hole diameter has been determined by the Brookfield flow meter tester (see Ch.2), and according to this value, the dimensions and the ratio between the height H to length L were decided. The ratio between height and length for the tanks containing liquids was decided instead considering the shape of the beaker in which the experimental phase took place, and the average design parameters that are normally employed. For the cost evaluation, the formula in Tab. 5.3 is given by the formula highlighted in yellow, where C_{BM} is the *bare module cost*,the coefficients B_1, B_2 are given by the literature and they change for each type of equipment, F_M is the material factor (in this case stainless steel), F_P is the pressure factor.

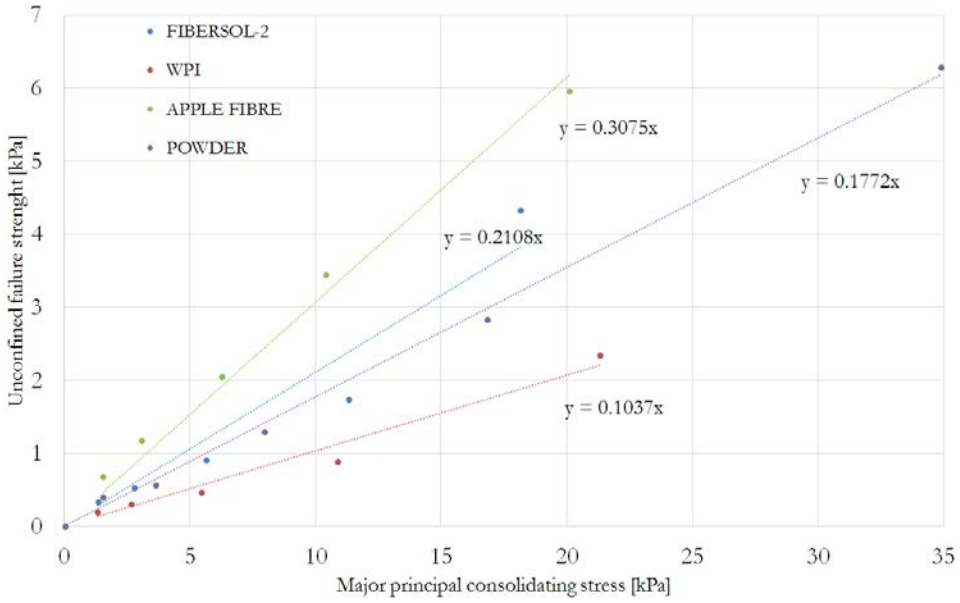

Figure 5.3: Flow test for the single ingredients, compared to the final product

B_1	B_2	F_M	F_P	F_{BM}
2.25	1.82	3.1	1.25	9.3025

$C_{BM} = Cp_0 * F_{BM} = B_1 + (B_2 * F_M * F_P)$

	ID	Strg. weight [kg]	$\rho[kg/m^3]$	V $[m^3]$	H:L	H [m]	L [m]	CP_0	C_{BM}
Sunflower Oil	TK 1	50400	918.00	57.65	2	6.65	3.32	46,117 €	429,009 €
WPI	SI 1	105840	450.00	246.96	5	19.88	3.98	197,568 €	1,837,876 €
Apple fibre	SI 2	26460	400.00	69.46	5	13.03	2.61	39,590 €	368,293 €
Fibersol-2	SI 3	44100	480.00	96.47	5	14.53	2.91	67,528 €	628,180 €
Mixing tank	TK 2	64800	959.11	70.94	2	7.12	3.56	49,658 €	461,948 €
Hydration tank	TK 3	64800	959.11	70.94	2	7.12	3.56	49,658 €	461,948 €
Oil add. Tank	TK 4	72000	955.00	79.16	3	9.68	3.23	55,413 €	515,485 €
Homogenizing Tank	TK 5.1	12000	955.00	13.19	3	5.33	1.78	11,874 €	220,922 €
	TK 5.2	12000	955.00	13.19	3	5.33	1.78		
Feed tank	TK 6.1	24000	955.00	26.39	2.5	5.94	2.38	22,429 €	417,297 €
	TK 6.2	24000	955.00	26.39	2.5	5.94	2.38		
								Annualized cost	**2,629,812.88 €**

Table 5.3: Sizing and cost evaluation for vessels and silos

5.3 Mixing and pumping

5.3.1 Mixing

All the tanks named in Tab.5.3 are provided with a stirring equipment. From the mixing of the ingredients to the stage before spraying, mixing is always relevant to ensure the homogeneity of the product. For the mixing choice a double 6PB turbine has been chosen, for all the tanks, although a Sawtooth disk after the oil addition could have been a good alternative, there's no reason to provide a high shear since the pre-emulsion will remain highly unstable anyway. The impellers diameter has been fixed at 1/3 the tank diameter, while the rotational speed has been set to reach the right Re number ($Re > 104$ for a turbulent regime). It can be noticed how the cost of mixing is even higher than the cost of the tanks, so it is a relevant part of the process. Eq. 5.1 is reporting the formula used for the power consumption for an impeller:

$$P = \rho N_p D^5 N^3 \tag{5.1}$$

Where N_p is the power number, N is the rotational speed, D the impeller diameter and ρ the slurry density.

-	V	H (m)	L (m)	H:L	D (m)	$N_m in$	N	$\rho(kg/m^3)$	N_p	P (W)	h/yr	C_0	F_{BM}	Annualized cost
Mixing tank	70.9	7.12	3.56	2	1.2	2.6066	5	959.11	2.5	745804	3069	1,274,879 €	1.38	586,444 €
Hydration tank	70.9	7.12	3.56	2	1.2	2.6066	5	959.11	2.5	745804	3069	1,274,879 €	1.38	586,444 €
Oil add. Tank	79.2	9.68	3.23	3	1.1	3.1154	6	955.00	2.5	830540	341	1,419,727 €	1.38	653,074 €
Feed tank	26.4	5.94	2.38	2.5	0.8	5.8901	8	955.00	2.5	400556	3069	684,711 €	1.38	314,967 €
	26.4	5.94	2.38	2.5	0.8	5.8901	8	955.00	2.5	400556	3069	684,711 €	1.38	314,967 €
2 x Silverson	-	-	-	-	-	-	-	-	-	6596859	511.5	60,000 €	-	20,000 €
													TOT	2,455,897 €
												Electricity [Wh]		1.07E+10
														962,448 €
												Annualized cost		3,418,345 €

Table 5.4: Sizing and cost evaluation for mixing

5.3.2 Pumping

All the liquids passed through the tanks, starting from the feeding tanks to the spray dryers, are moved through pumps. The pump choice is important to ensure that the pressure drops all along the circuit are won, and the right amount of liquid is moved in time (the right flowrate is provided). The pressure drops through the circuit are calculated according to Eq. 5.16 (Fanning equation), where f is the friction coefficient, calculated in three different ways according to the flow regime, D is the pipe diameter, u is the velocity of the fluid through the pipe, and l is calculated thank to Eq. 5.17

$$h = \frac{\Delta P}{\rho g} = 4f \frac{l}{D} \frac{u^2}{g} \tag{5.2}$$

$$l = \sum_{i=1}^{n} l_i \tag{5.3}$$

The single contributions l_i in the above equation are found in the literature, expressed in terms of kinetic height, and one of them is given by the length of the trait. As shown in Tab.5.5, the regime is laminar in all cases but one: for the exception, f is determined through the *Re* vs Friction group (see Fig.5.4), otherwise f = 8/*Re*. All the pipes are supposed to be built in stainless steel (AISI 304 L), with DIN 11850 which meet the requirements for food industry. Once the pressure drops along the circuit have been calculated, the pump is chosen according to the combination of the flowrate required and the pressure drops: the operation point can be shifted (and then fit the characteristic curve of a specific pump by varying the flowrate: the filling/discharge time for all the tank is quite flexible, and the flowrate capacity can be easily satisfied even if the transfer time for the fluids is less than one hour.

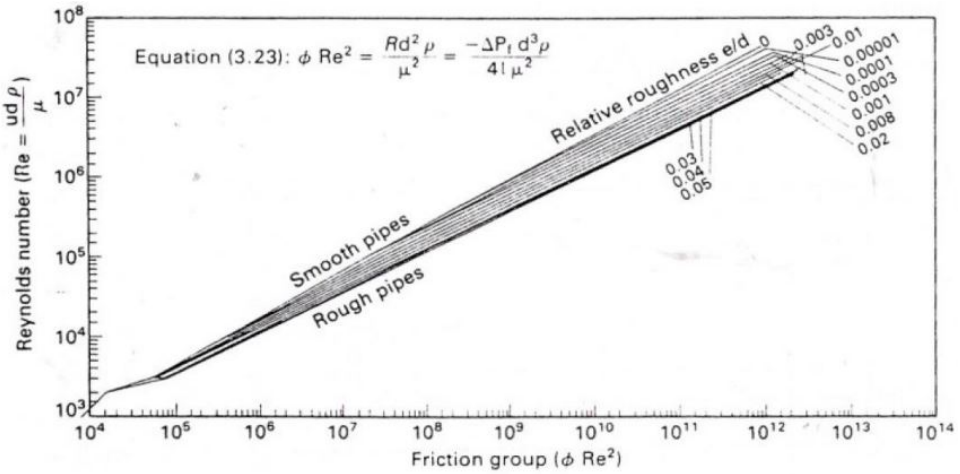

Figure 5.4: Re vs friction group

	Q [l/h]	ρ [kg/m^3]	μ [Pa s]	Re					
Oil to pre emulsion	7200	918.8	0.038	1220.13	f =	0.0068	Number of valves, 1/2 open		3
	d [m]	v [m/s]		1184.06	Circuit lenght [m]	50	Number of 90◦ elbows		4
	0.050	1			H [m.c.l.]	3.72			
	0.052	0.94						kW	kWh/y
					MXLV 32-406 m90 v1-1.5 M			1.5	511.5
	Q [l/h]	ρ [kg/m^3]	μ [Pa s]	Re	f =	0.0002	Number of valves, 1/2 open		3
H_2O	7920	1000	0.001	52925.67	Circuit lenght [m]	40.00	Number of 90◦ elbows		4
	d [m]	v [m/s]		53867.83	H [m.c.l.]	1.7136			
	0.053	1						kW	kWh/y
	0.052	1.04			GXRM 9 v 230/50			0.25	426.25
	Q [l/h]	ρ [kg/m^3]	μ [Pa s]	Re	f =	0.0246	Number of valves, 1/2 open		3
To Hydration section	42400	954.6	0.36	324.72	Circuit lenght [m]	20	Number of 90◦ elbows		4
	d [m]	v [m/s]		382.35	H [m.c.l.]	6.69			
	0.12	1						kW	kWh/y
	0.104	1.39			BNMM 17 HE 230/50 HZ			1.1	562.65
	Q [l/h]	ρ [kg/m^3]	μ [Pa s]	Re	f =	0.0246	Number of valves, 1/2 open		3
To pre emulsification	42400	954.6	0.36	324.72	Circuit lenght [m]	15	Number of 90◦ elbows		4
	d [m]	v [m/s]		382.35	H [m.c.l.]	5.76			
	0.122	1						kW	kWh/y
	0.104	1.386			BNMM 17 HE 230/50 HZ			1.1	562.65
	Q [l/h]	ρ [kg/m^3]	μ [Pa s]	Re	f =	0.027	Number of valves, 1/2 open		6
To Homogenization	35400	954.6	0.36	296.70	Circuit lenght [m]	25	Number of 90◦ elbows		4
(2 PUMPS)	d [m]	v [m/s]		319.22	H [m.c.l.]	7.26			
	0.112	1						kW	kWh/y
	0.104	1.158			BNMM 17 HE 230/50 HZ			1.1	750.2
	Q [l/h]	ρ [kg/m^3]	μ [Pa s]	Re	f =	0.1144	Number of valves, 1/2 open		10
To spray dryers	3933.3	954.6	0.36	69.93	Circuit lenght [m]	15	Number of 90◦ elbows		4
	d [m]	v [m/s]		70.94	H [m.c.l.]	5.81	Entry into T junction		10
	0.053	0.5							
	0.052	0.514						kW	kWh/y
					NMM1/AE 230/50 HZ			0.37	6138
Electricity cost									
€805.61									

Table 5.5: Summary for pressure drops and pumps used in the process. Pump models and costs provided by $Calpeda$®

5.4 Powder handling

The powder supply to the mixing tank takes place to a pneumatic system. First, the powders are carried to reach a powder mixer, with a conical shape, to be homogenized. After that, another fan carries them to the mixing tank, where they are dispersed and partially dissolved in water. Powder transport can be done in different ways. The one proposed has been thought using the concept of dilute phase, which is corresponding typically to high gas velocities, mass flows less than 10^4 kg/h, and low pressure drops.

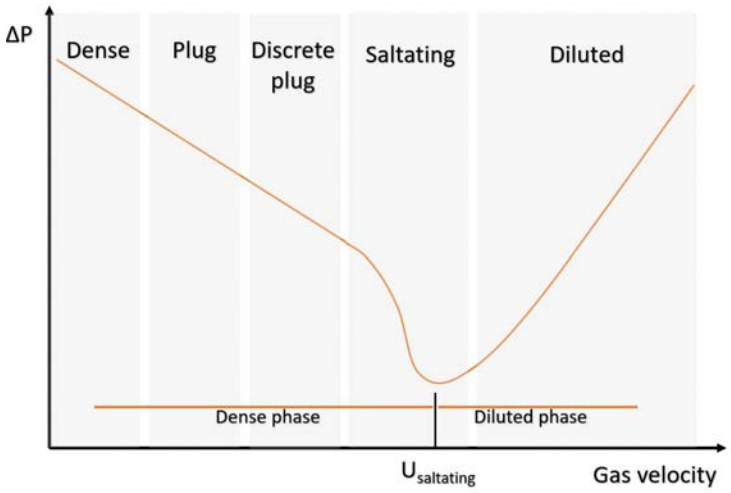

Figure 5.5: Pressure drop variation according to different gas velocities

5.4.1 Pressure drop calculation

The compressors, or the fans, that are carrying the powders must win a certain pressure drop along the line. Here below the e treated as a pure indication. procedure followed to calculate the pressure drop for a transport in a diluted phase is explained. First of all, the saltation velocity is determined through the Eq. 5.4 It is the velocity at which the minimum pressure drop is encountered. Nevertheless, the error of this equation can be up the 50 %, so the value must be treated as a pure indication.

$$\frac{M_p}{\rho_f u_{salt} A} = \frac{1}{10^{1440x+1.96}} \left(\frac{u_{salt}}{\sqrt{gD}}^{1100x+0.25} \right) \tag{5.4}$$

where x is the average particle diameter, M_p the mass flow, A and D the pipe area and diameter, ρ_f the density of the carrier fluid.

$$F_{pw}\ L = \ 0.057\ GL\ \sqrt{gD} \tag{5.5}$$

$$F_{pw} L = \ \frac{2\ f_p\ (1-\varepsilon)}{D} \rho_p u_p^2 L \ \ \text{,} \rho_p \text{ is the particle density, } \varepsilon \text{ the void degree} \tag{5.6}$$

where the velocity of the particle u_p is given by

$$u_p = \ u_g \left(1 - 0.0638\ x^{0.3} \rho_p^{0.5}\right) \tag{5.7}$$

and the friction coefficient is

$$f_p = \ \frac{3}{8} \frac{\rho_g}{\rho_p} \frac{D}{x} C_D \left(\frac{u_f - u_p}{u_p} \right)^2 \tag{5.8}$$

C_D is the drag coefficient. Since it is dependent on the Re number (defined as reported in Eq. 5.7, where x is the average diameter (volume based Sauter diameter), and the viscosity is the one of the air, which is carrying the powder), its value is calculated in three different ways as shown in Tab 5.6 (Shiller and Naumann, 1933), with an accuracy of $\pm 7\%$:

For the velocity of the powder, it is recommended to select a velocity at least equal to (but preferably greater than) the saltation velocity to maintain a diluted phase.

$$Re_p = \ \frac{x\ u\ \rho_f}{\mu} \tag{5.9}$$

Region	**Stokes**	**Intermediate**	**Newton's law**
Re_p **range**	<0.3	$0.3 < Re_p < 500$	$Re_p > 500$
C_D	24/ Re_p	24/ Re_p (1 + 0.15$Re_p^{0.687}$)	0.44

Table 5.6: Re number ranges for single particle drag coefficients

The total pressure drop is given by the summation of different contributions. In the most general case there are:

1. ΔP due to gas acceleration
2. ΔP due to particle acceleration
3. ΔP due to solids to wall friction
4. ΔPdue to gas to wall friction
5. ΔP due to the static head of the solids
6. ΔP due to the static head of the gas

Dividing them between the ones due to horizontal trait and the vertical trait, for this case study:

$$\Delta P_h = \frac{\rho_f \epsilon_H u_{fH}^2}{2} + \frac{\rho_f (1-\epsilon_H) u_{pH}^H}{2} + 2\frac{f_g \rho_p g u^2 L_H}{D} + 2\frac{f_P \rho_P (1-\epsilon_H) u_{pH}^2 L_H}{D} \tag{5.10}$$

$$\Delta P_v = \frac{2 f_g L_v \rho_f u^2}{D} + 0.057 G L_v \left(\sqrt{\frac{g}{D}}\right) + \rho g (1-\epsilon_v) g L_v + \rho_f \epsilon_v g L_v \tag{5.11}$$

ϵ_v is calculated through the solution of the following system. (Eq. 5.10) At the end a second-degree equation is solved (only one solution has a physical meaning in this case).

$$\begin{cases} u_{pv} = \frac{u}{\varepsilon_v} - u_T \\ G = \rho_p (1-\varepsilon_v) u_{pv} \end{cases} \tag{5.12}$$

To find u_T, given a size x, calculate the group

$$C_D \, Re_p^2 = \frac{4}{3} \frac{x^3 \rho_f \, (\rho_p - \rho_f) \, g}{\mu^2} \tag{5.13}$$

Which is constant for a define particle type, so in the plot C_D vs Re_p the curve is a line with slope -2. The velocity U_T, which is the relative velocity between the gas and the particle, is found crossing the line cited above with the curve C_d vs Re. The plots and the calculations are reported in Fig. 5.6 and Tab. 5.7 respectively.

Tranfer time	h	23							
		WPI	Apple f.	Fibersol-2			WPI	Apple f.	Fibersol-2
Tapped density	kg/m^3	1070	864	1234	Chocking: air	kg/s	10.40	10.40	10.40
Amount per line	kg	2520	1890	2100	Actual flow	kg/s	1.21	0.87	0.95
Number of lines		6	2	3	Up	m/s	12.13	9.21	9.77
Flowrate to the double cone	kg/h	109.57	82.17	91.30	fp		0.10	0.92	0.34
u salt	m/s	13.12	9.46	10.58	fg		0.01	0.01	0.01
mean size	μm	104.0	26.1	45.5	ϵ_H		99.9998%	99.9998%	99.9998%
U	m/s	14	10	11	LH	m	20	100	100
Viscosity	Pa s	1.810E-05			L_V	m	20	20	20
Re_p		13.13	1.40	3.78	N_{bends}		4	4	4
C_D		3.44	20.42	8.72	$L_{V,TOT}$	m	50.00	50.00	50.00
D	m	0.3			ϵ_v		99.9998%	99.9998%	99.9998%
Compressor power	kW	200			H	Pa	105025	43737	75207
Number of compressors		6	2	3	V	Pa	527021	425335	607012
Electricity cost		423,522 €	282,348 €	423,522 €	U_T	m/s	0.28	0.01	0.32
Cost of compressors		350,000 €	116,667 €	175,000 €					
TOT COST		1,771,059 €							

Table 5.7: Cost assessment for the transportation from the silos to the powder blender

Bends are included inside the length. Since there's a lack of correlations, a good estimation is attributing an equivalent length of 7.5 m for a single bend. It must be considered that the pipelines carrying the powders

are quite big, and considering the air/powder ratio, it may turn that using a dense phase conveyor is much cheaper (also the purchase of the fans would be avoided), but there's not too much literature about the pressure drops using a dense phase, and the formulas reported in the procedure above would not be accurate enough. After the powders are delivered to the powder mixer, the procedure to be followed to determine the pressure drops for the line that carries them to the tank containing the water, is the same of the one described above. Results are reported in Tab.5.7, together with the costs for the powder mixers: for this equipment, a series of double cone mixers has been chosen. The reason for which a splitting has been done is that there is not a quotation available for very large sizes, and the equipment design might be more expensive than buying multiple machines with a lower size.

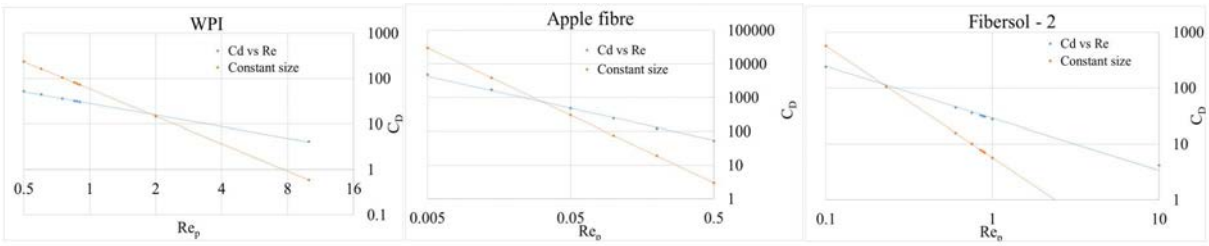

Figure 5.6: Pressure drop variation according to different gas velocities

Tranfer time	h	9			
		Mix			Mix
Tapped density	kg/m^3	1080	Chocking: air	kg/s	10.40
Amount per line	kg	1400	Actual flow	kg/s	1.51
Number of lines		18	U_p	m/s	15.79
Flowrate to the double cone	kg/h	155.556	fp		0.12
u_{salt}	m/s	16.5	fg		0.01
mean size	μm	77.7	ϵ_H		99.99975%
U	m/s	14.0	L_H	m	15
Viscosity	Pa s	1.810E-05	L_V	m	10
Re_p		11.607	N_{bends}		4
C_D		3.436	$L_{V,TOT}$	m	50
D	m	0.3	ϵ_v		99.99979%
compressor power	kW	200	H	Pa	175162
Number of compressors		18	V	Pa	426340
Electricity cost		423,522 €	UT	m/s	0.16
Cost of compressors		350,000 €			
TOT COST		773,522 €			

MIXERS		
Capacity of a mixer	7000	178,123 €
N MIXERS	8	
Tot V	56000	1,424,984 €
h/mixer	341	
kW/mixer	500	
kWh	1364000	122,760 €

Table 5.8: Cost of powder mixing and transport to the mixing tank

5.5 Cooling

The first cooling stage required is after the powders have been added to the ingredients. Before passing the solution to the other tank, for hydration, an ammonia refrigeration cycle cools down the liquid from 20 $°C$ to 5$°C$, since water at 5$°C$ would not be enough to do it (and mixing water with glycol to let it cool down the solution would require an ammonia cycle anyway). Two heat exchangers are required: the first one to cool the solution, the second one to condensate the ammonia after it has been compressed. A schema of the stages can be found in Fig. 5.9, while Tab. 5.8 is displaying the summary of the data used to achieve a cost estimation for this section.

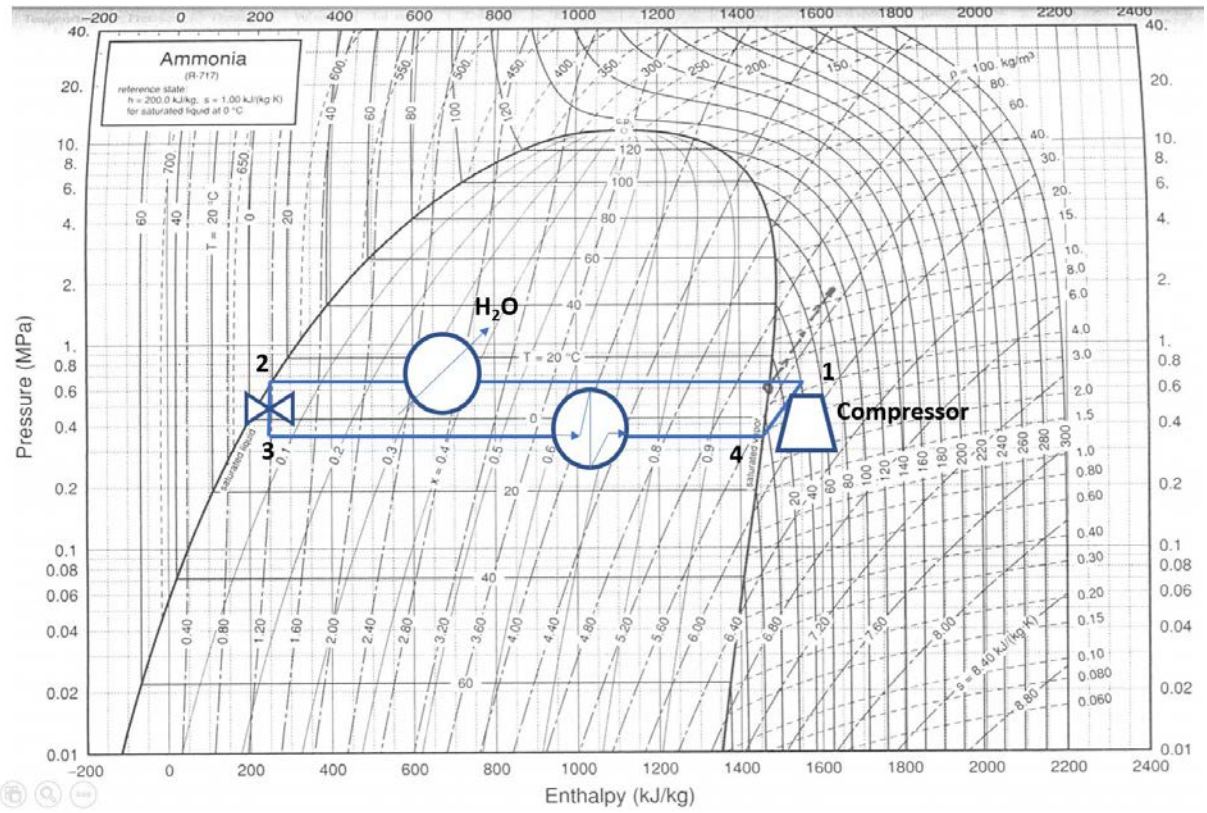

Figure 5.7: Cycle stages. P-H diagram for ammonia - Perry's Chemical Engineers' Hanbook, R.Perry and D.Green, 7th ed.

Thermodyanmic Data			Duty =	-226044000	[J/h]	Condenser NH_3			Condenser purchase cost	55720
H_1 =	1550					ΔT_{ml} =	16.37		Pressure factor	1
H_2 =	275		mNH_3=	190.75	[kg/h]	U =	600.00	$[W/m^2K]$	Material factor	3.1
H_3 =	275		$W_{compression}$ =	22890.53	[kJ/h]	A =	7.04	$[m^2]$	Condenser BM cost (\euro)	377555
H_4=	1460		$C_{compression}$=	1214.34	$[e/yr]$				Condenser annualised cost	125852
p_{IN} =	3.7					Evaporator NH_3			Evaporator purchase cost	55184
p_{OUT} =	7		P_{eff} (hp)=	8.53		ΔT_{ml} =	16.37		Pressure factor	1
Capacity ratio =	1.6396		$C_{compressor}$ =	16009	[€/yr]	U =	600.00	$[W/m^2K]$	Material factor	3.1
T_{IN} =	40	$[°C]$	$C_{ammonia}$ =	477		A =	6.39	$[m^2]$	Evaporator BM cost (e	373929
T_{OUT} =	15	$[°C]$							Evaporator annualized cost	124643
c_{p,H_2O} =	75750	[J/kmolK]	ρ_{H_2O} =	999.75	$[kg/m^3]$		$T_{H_2O,IN}$ [K] =	278.15		
H_{2O} =	10	[K]	V_{H_2O} =	5.92	$[m^3/h]$		$T_{H_2O,OUT}$ [K] =	288.15	TOT =	283282
Cost of water =	0.313	[€/h/m^3]	WC_h =	2	$[e/h]$		$T_{H_2O,MEAN}$ [K] =	283.15		
Q1→2 =	1305	[kJ/kg]	WC =	15088	$[e/h]$					

Table 5.9: Ammonia refrigeration cycle costs

Please notice that no additional heat exchangers have been placed to maintain the temperature at 5 $°C$. The shaft work coming from mixing is somehow transferring some heat to the solution, but it's considered

negligible. The energy balance during the hydration time therefore becomes:

$$mc_p \frac{dT}{dt} = UA\left(T_{amb} - T\right) \tag{5.14}$$

Which can be rearranged in:

$$\frac{dT}{dt} = a + bT \tag{5.15}$$

The solution of the differential equation is:

$$T\left(t\right) = \left(\frac{a}{b} + T_0\right) e^{bt} - \frac{a}{b} \tag{5.16}$$

After 10 hours the result is displayed in Fig.5.8: the temperature increased only by 1.9 degrees. After the oil addition, the estimated temperature is $6.35°C$ (see Eq. 5.15).

$$T_{mix} = \frac{m_1 c_{p1} T_1 + m_2 c_{p2} T_2}{m_1 c_{p1} + m_2 c_{p2}} \tag{5.17}$$

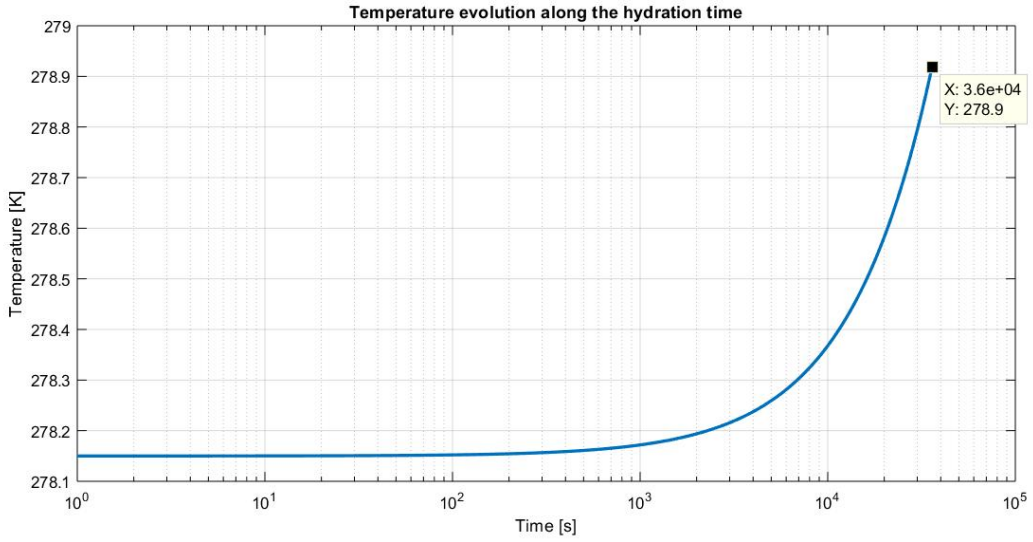

Figure 5.8: Temperature evolution with a good insulation provided by a layer of EPS with graphite around the tank, 10 cm wall thickness

The second cooling stage is after the oil addition. It has been noticed that during homogenization, the temperature increases from 6 $°C$ to 26 $°C$. The objective of this cooling is to let the temperature increase only of $14°C$, from 6 to 20 $°C$. This can be done just with cooling water. The first choice analyzed is a jacketed vessel. Unfortunately, the area required by a jacket cannot be covered by the area of the two tanks available for the homogenization, therefore an external heat exchanger is provided, and this is enough to handle the flowrate coming from both the tanks. The calculations' results are reported in Tab.5.10. The reason for which the pre-emulsion has been split is that the Silverson homogenizer is hard to be scaled up for more than 10^4 litres.

Duty =	-334880000	[J/h]	$T_{H_20,IN}$ =	278.15	K	Cooler purchase cost	77215
$\Delta T_{ml} = \Delta T$	4.6785		$T_{H_20,OUT}$ =	280.15	K	Pressure factor	1
U =	600	$[W/m^2K]$	$T_{H_20,mean}$ =	279.15	K	Material factor	3.1
A =	33.1382	$[m^2]$				Cooler BM cost (€)	523206
c_{p,H_2O} =	75894	[J/kmol K]	ρ_{H_2O} =	1000.97	[kg/m^3]	Cooler annualized cost	174402
$_{H_2O}$ =	2	[K]	V_{H_2O} =	39.67	[m^3/h]		
Cost of water =	0.313	[€/m^3]	WC_h =	12	[€/h]		
			WC =	8469	[€/yr]	TOT =	182871

Table 5.10: Cooling equipment cost - Homogenization section

5.6 Spray drying

Scaling up a spray drier is not immediate. The estimations done in the following section are only hypothesis based on literature data and approximate quotations given by a company, Toption, China. The maximum capacity provided by them is 300 l/min, so to sustain a large throughput, 14 machines must be put in parallel. The air flow has been guessed at the beginning, and then determined through a trial and error procedure. The reasoning is the following: on a lab scale, the air flowrate has been chosen to satisfy the energy balance:

$$\dot{Q}_{given,\ eff} = \dot{m}_{air}\ c_{p,\ air}\ \Delta T_{air} - KA_{col.}\Delta T_{air-amb} \tag{5.18}$$

The second term of the equation is due to the energy loss through the column, where K is equivalent to 1 kcal/hKm^2. It is a quite optimistic estimation, but still realizable, especially in the industry. (Spray drying Handbook, K. Masters). The energy required instead is given by:

$$\dot{Q}_{required} = \dot{m}_{em.} w_{H_2O}\ c_{p,H_2O}(\Delta T_{H_2O} + \lambda_{ev}) + m_{air} MC_{air}(c_{p,H_2O}\Delta T_{H_2O} + \lambda_{ev}) \tag{5.19}$$

Eq. 5.18 takes in account also the air moisture content, in this case fixed at 11% of moisture. Starting from Eq. 5.18 and setting the result equal to the one of Eq. 5.17, the minimum amount of air to be supplied is calculated. After this data is obtained, it is relevant to decide how to provide heating. There are mainly three ways: electricity, direct heating by burning fuel oil, and steam condensation through a heat exchanger. By looking at the simple utilities, the steam turns to be the best solution, therefore the cost of equipment has been calculated only for this alternative (see Tab.5.11 The cost of the spray dryers has been estimated by using the correlation in Fig.5.9.

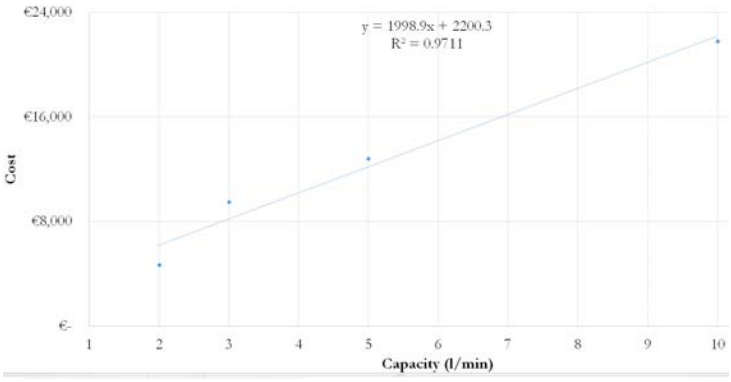

Figure 5.9: Re vs friction group

Sprayed quantity	4000	kg/h
	4202	l/h
Capacity	300	l/h
Number of spray dryers		14
Annualized tot cost		2,808,728 €

	Lab scale	Plant scale
Air flow [l/min]	400	2200000
Liquid flow [kg/min]	3.10E-03	66.67
Fan annualized cost		80,000 €
Electricity cost		1,546,776 €
Air flowrate	132000	m^3/h
Amount air	992514600	kg/y
Energy required	144634190085	KWh/y
kW given	0.35	2766
kW required	0.29	2764
Cost using electricity	13,702,186,429 €	
Cost oil	3,896,018 €	
Cost steam	1,546,014 €	
Tot cost using steam	1,578,531 €	
Heating cost	1,578,531 €	

Capacity l/h	Cost
2	4,680 €
3	9,500 €
5	12,800 €
10	21,800 €
Scaled estimation	
300	601,870 €

STEAM heat exchanger - multiple pipe		
ΔT_{ml} =	154.14	
U =	1000	[W/m^2K]
A =	42.46	[m^2]
Purchase cost	14,396 €	
Pressure factor	1	
Material factor	3.1	
H.E. BM cost	97,549 €	
H.E. annualised cost	32,516 €	

Table 5.11: Cost summary for spray dryers and utilities.

5.7 Economics

In this section the profitability analysis of the plant has been assessed, considering different aspects like the cost of labour, the purchase of the land, hypothesizing that the plant is build ex-novo. The evaluation has been done considering a shut down after 10 years of operations (so the 12^{th} year), with an interest rate of 25 %: being this a new product, the investment for the stakeholders would be quite risky. For each equipment, the bare module cost has been calculated by multiplying the bare module factor FBM times the purchase cost, while the total module cost will be the bare module cost plus an 18 % due to fees and contingencies. The tax has been calculated as the 35 % of the yearly income, payable the following year. Tab.5.12 is summarizing the labour cost, while Tab. 5.14 is displaying the other costs related to the plant and the summary of the cash flows during the years, considering the period cited above.

NUMBER OF EQUIPMENT -$_{FORFLUIDS}$	15
NUMBER OF EQUIPMENT -$_{FORSOLIDS}$	3
GROSS SALARY	40,000 €
$N_{S,fixed}$	4.5
N_{OL}	10.24
N_{OL}'	47
NOL = 6.29 + 31.7 $N_{EQIP,FLUIDS}$ + 0.23 $N_{EQUIP,SOLIDS}$	
NOL' = INT($N_{OL} \cdot N_S$)	
TOT	1,880,000 €

Table 5.12: Cost of labour estimation

From Fig. 5.10 it can be noticed that the discounted payback period is less than 5 years of operations, the cumulative present value after the shut down is equal to 11.66 M€, and the internal rate of return (IRR), defined as:

$$\sum_{n=1}^{n=t} \frac{CF_n}{(i+1)^n} = 0 \tag{5.20}$$

where t is the project life and CF_n the net cash flow. The IRR can be determined by using the goal seeking function, and it turns to be 24.27 %, quite realistic to satisfy a moderate risk investment. At this level of

GRASS ROOT COSTS		
C_{TM}	27,588,798 €	
C_{BMI0}	9,084,617 €	
C_{GR}	32,131,106 €	$C_{GR} = C_{BMI0} + 0{,}5{*}C_{TM}$
Land cost	1,000,000 €	

COST OF MANUFACTURING		
C_{OL}	1,880,000 €	€/yr
C_{UT}	5,080,089 €	€/yr
C_{RM}	67,830,711 €	€/yr
C_{OM}	105,039,393 €	$0.28{*}C_{GR}+2.73{*}C_{OL}+1.23{*}(C_{UT}+C_{RM}+C_{WT})$
C_{OMd}	101,826,283 €	$0.18{*}C_{GR}+2.73{*}C_{OL}+1.23{*}(C_{UT}+C_{RM}+C_{WT})$

REVENUES	
TOT	94,525,200 €

F_{CIL}	31,131,106 €	
SL	3,113,111 €	% salvage value, assumed to be 10% of F_{CIL}
WC	10,084,182 €	% working capital, assumed to be 10% of (F_{CIL} + C_{RM} + C_{OL})
i	20%	% interest rate
dk	4,669,666 €	% depreciation allowance

Table 5.13: Cost summary and salvation value

YEAR	PRE TAX CF	dk	INCOME	TAX	CF	Fd	PV	cum PV
0	- €	- €	- €	- €	- €	-	- €	- €
0	- €	- €	- €	- €	- 1,000,000 €	-	- 1,000,000 €	- 1,000,000 €
1	- 21,791,774 €	- €	- 21,791,774 €	- €	- 21,791,774 €	0.8333	- 18,159,812 €	- 19,159,812 €
2	- 9,339,332 €	- €	- 9,339,332 €	- €	- 9,339,332 €	0.6944	- 6,485,647 €	- 25,645,459 €
2	- €	- €	- €	- €	- 10,084,182 €	0.6944	- 7,002,904 €	- 32,648,363 €
3	9,867,200 €	4,669,666 €	5,197,534 €	- €	9,867,200 €	0.5787	5,710,185 €	- 19,935,274 €
4	19,734,401 €	4,669,666 €	15,064,735 €	5,272,657 €	14,461,743 €	0.4823	6,974,220 €	- 12,961,054 €
5	19,734,401 €	4,669,666 €	15,064,735 €	5,272,657 €	14,461,743 €	0.4019	5,811,850 €	- 7,149,203 €
6	19,734,401 €	4,669,666 €	15,064,735 €	5,272,657 €	14,461,743 €	0.3349	4,843,209 €	- 2,305,995 €
7	19,734,401 €	4,669,666 €	15,064,735 €	5,272,657 €	14,461,743 €	0.2791	4,036,007 €	1,730,013 €
8	19,734,401 €	4,669,666 €	15,064,735 €	5,272,657 €	14,461,743 €	0.2326	3,363,339 €	5,093,352 €
9	19,734,401 €	- €	19,734,401 €	6,907,040 €	12,827,360 €	0.1938	2,486,028 €	7,579,380 €
10	19,734,401 €	- €	19,734,401 €	6,907,040 €	12,827,360 €	0.1615	2,071,690 €	9,651,071 €
11	19,734,401 €	- €	19,734,401 €	6,907,040 €	12,827,360 €	0.1346	1,726,409 €	11,377,479 €
12	19,734,401 €	- €	19,734,401 €	6,907,040 €	12,827,360 €	0.1122	1,438,674 €	12,816,153 €

Table 5.14: Cash flows and present value and cumulative present value evolution. *dk* is due to depreciation, CF is the cash flow, *Fd* is the money depreciation factor, PV is the present value considering the money depreciation, and the cum PV is the cumulative present value, considering the revenues from the beginning

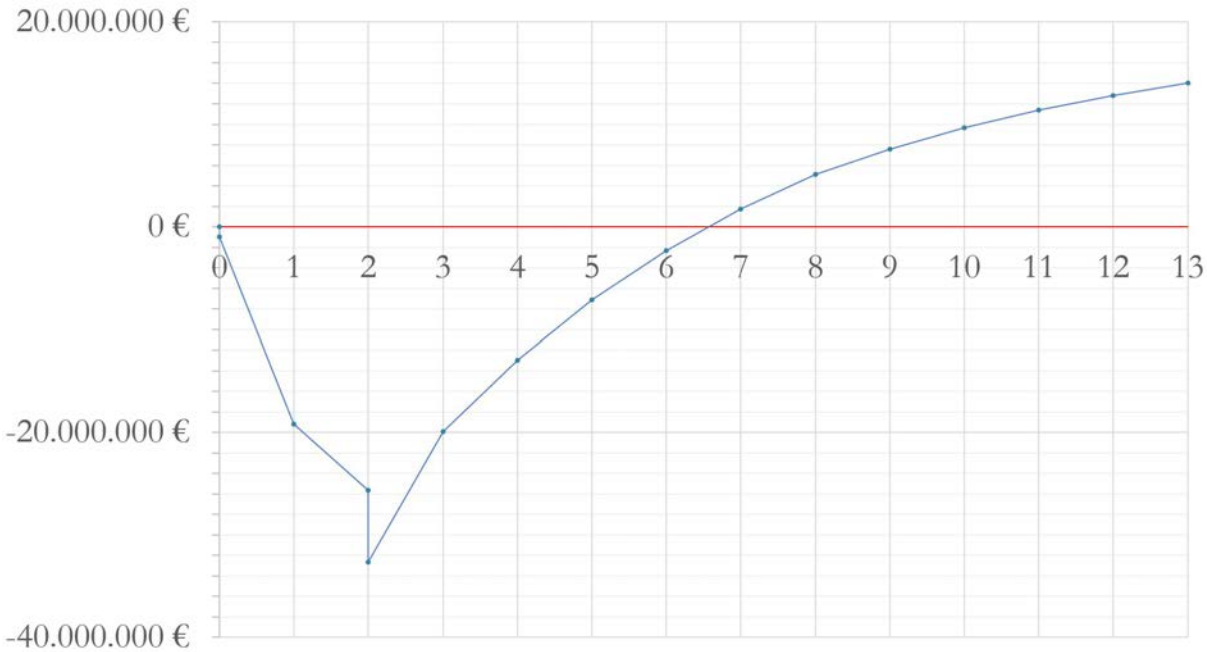

Figure 5.10: Net profit evolution.

evaluation therefore the investment can be considered, since it satisfies the guideline requirements.

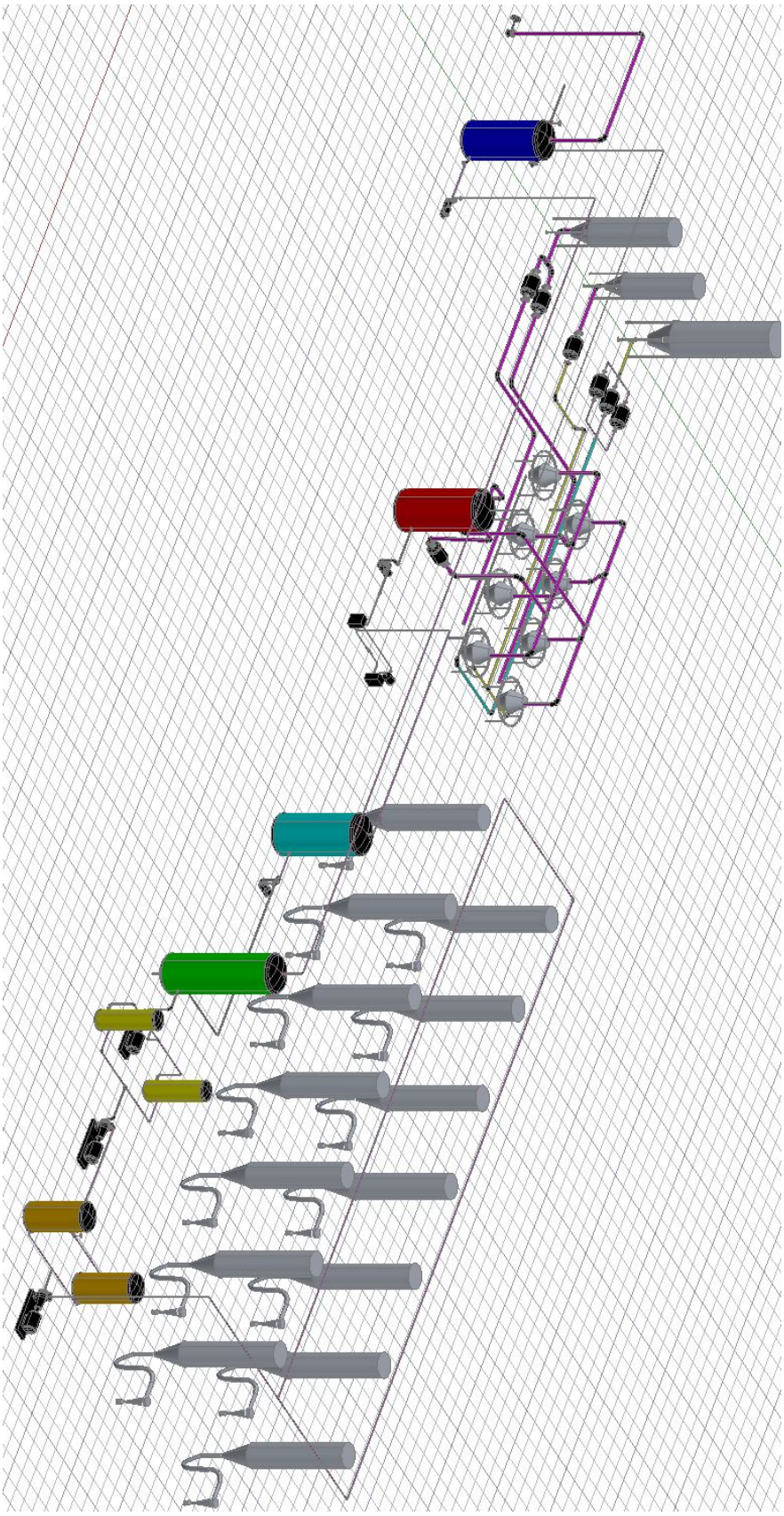

Figure 5.11: Plant model 3D view

Conclusions

The work contained in this thesis involved the usage of different emulsification techniques, already explored and widely described in the literature. The objective was to achieve a good stability for the emulsions for a sufficient time to characterize and process them. To do that, a series of different new ingredients has been tested, combining them in various proportions. The homogenizing equipment used were the high pressure homogenizer and the rotor stator. Unfortunately the first type of equipment presented a limitation regarding the process of insoluble particles contained into the emulsion. However, the second type of device has been revealed to be a good candidate to produce semi-stable emulsions. The rheological studies performed on the emulsions, combined together with the theory of the emulsion stability and the fluid dynamic simulation, allowed to identify the right recipe to obtain a product with a good quality.
The following step was regarding the spray drying operations. After having operated the column to identify the optimal parameters through the centralized controller included in the equipment, different operating conditions were tested. The first change that has been done was increasing the column length, since it was not appropriate for drying emulsions containing a large amount of water. Also the nozzle tip was change after the first trials: to minimize the number of times that the nozzle was clogged because of the presence of solids, the largest available was selected. Even with the largest nozzle, cellulose has been revealed the worst component for the wall materials, but apple fibre behavior was instead acceptable, providing the right conditions. The dimensions of the powders were reaching the microscale, and the wall has been capable to include both the nanodroplets of oil and the dietary fibers as proved with the SEM. Finally, the study about the scale up feasibility, shown a potential capability in generate profits after a reasonable period, considering the product type and the market target. Regarding the spray drying operations, maybe a larger nozzle, or a different type of equipment, considering the limitations of the medium scale equipment used for the experiments, could improve the powder quality and stability. Looking at the production on a large scale, the feasibility of sustain a production of 1 t/h has been proved, considering a positive net profit after 6 years and a half.

Future work

The potential next steps involve the study of the double emulsion creation, to include an aqueous phase inside the oil droplets, and the improvement of the non artificial surfactant made of palm stearin to stabilize the inner interface. Furthermore, studies about the effective capacity of encapsulation manifested by the oil or the internal aqueous phase in the case of double emulsions, must be done. The experiments would include the release in-vitro kinetic studies, to simulate the behaviour of the product in the stomach, and the encapsulation capability measurements. Once the powders will be proved to be effectively well structured under these points of view, the final step before the large scale productions would regard the flowability along time, with a study of the best storage options to prevent caking or arching effects.

Appendix A

REPRODUCIBILITY EXPERIMENT - 3.5 % FIBER CONTENT

l/min	D_{32} µm	std DEV µm	D_{43} µm	std DEV µm	D_{50} µm	std DEV µm
6	33.7	6.8	93.5	48.3	52.9	37.8
4.5	58.6	62.4	113.0	151.3	92.0	128.8
3	64.9	0.2	144.0	49.0	103.0	25.0
1.5	74.1	29.2	232.0	1296.0	131.0	49.0
6	38.9	0.9	79.6	290.7	65.2	0.1
4.5	42.8	62.4	88.4	151.3	69.3	128.8
3	65.7	0.2	158.0	49.0	113.0	25.0
1.5	84.9	29.2	304.0	1296.0	145.0	49.0
6	**36.3**		**86.6**		**59.1**	
4.5	**50.7**		**100.7**		**80.7**	
3	**65.3**		**151.0**		**108.0**	
1.5	**79.5**		**268.0**		**138.0**	

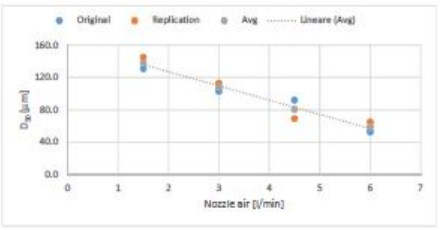

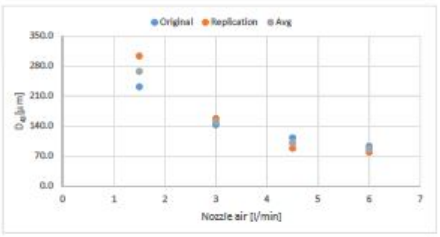

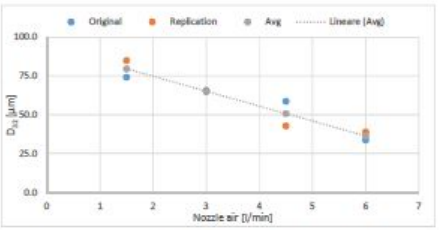

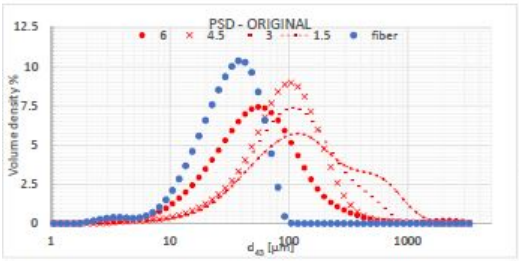

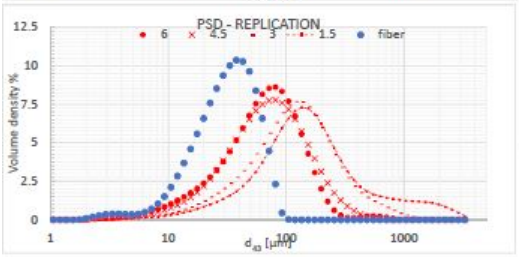

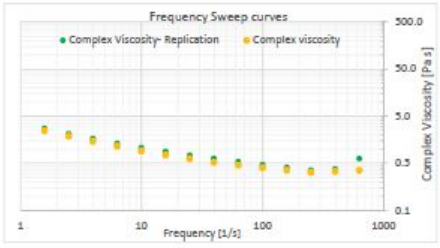

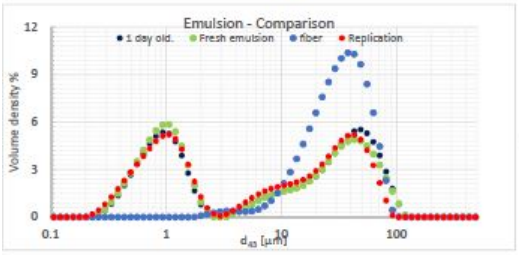

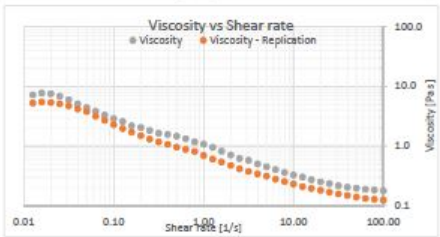

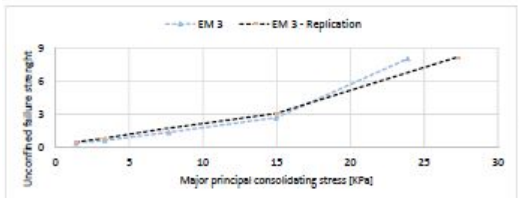

Bibliography

[1] Abbot. *Abbot*. 2018. URL: https://www.stevenabbott.co.uk/practical-surfactants/critcap.php (visited on 09/30/2018).

[2] Turton et al. *Analysis, Synthesis, and Design of Chemical Processes*. 3rd ed. 2008.

[3] María Alejandra Cabrera-Trujillo et al. "Stability of low-fat oil in water emulsions obtained by ultra turrax, rotor-stator and ultrasound homogenization methods". In: *International Journal of Gastronomy and Food Science* 13 (2018), pp. 58–64. ISSN: 1878-450X. DOI: https://doi.org/10.1016/j.ijgfs.2018.06.002. URL: http://www.sciencedirect.com/science/article/pii/S1878450X17301506.

[4] Miete Celus et al. "Structurally modified pectin for targeted lipid antioxidant capacity in linseed/sunflower oil-in-water emulsions". In: *Food Chemistry* 241 (2018), pp. 86–96. ISSN: 0308-8146. DOI: https://doi.org/10.1016/j.foodchem.2017.08.056. URL: http://www.sciencedirect.com/science/article/pii/S0308814617313912.

[5] Marie Chevallier et al. "Aggregated whey proteins and trace of caseins synergistically improve the heat stability of whey protein-rich emulsions". In: *Food Hydrocolloids* 61 (2016), pp. 487–495. ISSN: 0268-005X. DOI: https://doi.org/10.1016/j.foodhyd.2016.06.009. URL: http://www.sciencedirect.com/science/article/pii/S0268005X16302582.

[6] Charikleia Dimakou and Vassiliki Oreopoulou. "Antioxidant activity of carotenoids against the oxidative destabilization of sunflower oil-in-water emulsions". In: *LWT - Food Science and Technology* 46.2 (2012), pp. 393–400. ISSN: 0023-6438. DOI: https://doi.org/10.1016/j.lwt.2011.12.013. URL: http://www.sciencedirect.com/science/article/pii/S0023643811004063.

[7] Bernat Esteban et al. "Temperature dependence of density and viscosity of vegetable oils". In: *Biomass and Bioenergy* 42 (2012), pp. 164–171. ISSN: 0961-9534. DOI: https://doi.org/10.1016/j.biombioe.2012.03.007. URL: http://www.sciencedirect.com/science/article/pii/S0961953412001250.

[8] Qi Fan et al. "Partition and stability of resveratrol in whey protein isolate oil-in-water emulsion: Impact of protein and calcium concentrations". In: *International Dairy Journal* 73 (2017), pp. 128–135. ISSN: 0958-6946. DOI: https://doi.org/10.1016/j.idairyj.2017.06.002. URL: http://www.sciencedirect.com/science/article/pii/S0958694617301358.

[9] FAO. 2018. URL: http://www.fao.org/save-food/resources/keyfindings/en/ (visited on 10/20/2018).

[10] Inga Jurgelane, Valentina Sevjakova, and Liva Dzene. "Influence on illitic clay addition on the stability of sunflower oil in water emulsion". In: *Colloids and Surfaces A: Physicochemical and Engineering Aspects* 529 (2017), pp. 178–184. ISSN: 0927-7757. DOI: https://doi.org/10.1016/j.colsurfa.2017.05.086. URL: http://www.sciencedirect.com/science/article/pii/S0927775717305484.

[11] Kishimoto and al. “Effect of Resistant Maltodextrin on Digestion and Absorption of Lipids”. In: *JOURNAL OF HEALTH SCIENCE* 55 (2009), pp. 445–452. ISSN: 0927-7790. DOI: https://doi.org/10.1019/j.colsurfa.2016.04.020. URL: https://www.researchgate.net/publication/237493925_Effect_of_Resistant_Malt_odextrin_on_Digestion_and_Absorption_of_Lipids.

[12] Sang-Ho Lee et al. “Effects of ultra-high pressure homogenization on the properties and structure of interfacial protein layer in whey protein-stabilized emulsion”. In: *Food Chemistry* 113.1 (2009), pp. 191–195. ISSN: 0308-8146. DOI: https://doi.org/10.1016/j.foodchem.2008.07.067. URL: http://www.sciencedirect.com/science/article/pii/S0308814608009163.

[13] Malvern. *Malvern. Panalytica*. 2018. URL: https://www.alfatest.it/prodotti/mastersizer-3000.

[14] Nameer Khairullah Mohammed et al. “Process conditions of spray drying microencapsulation of Nigella sativa oil”. In: *Powder Technology* 315 (2017), pp. 1–14. ISSN: 0032-5910. DOI: https://doi.org/10.1016/j.powtec.2017.03.045. URL: http://www.sciencedirect.com/science/article/pii/S0032591017302620.

[15] I. Opaliński, M. Chutkowski, and Ali Hassanpour. “Rheology of moist food powders as affected by moisture content”. In: *Powder Technology* 294 (2016), pp. 315–322. ISSN: 0032-5910. DOI: https://doi.org/10.1016/j.powtec.2016.02.049. URL: http://www.sciencedirect.com/science/article/pii/S0032591016300912.

[16] Elli Panagopoulou et al. “Stability of double emulsions with PGPR, bacterial cellulose and whey protein isolate”. In: *Colloids and Surfaces A: Physicochemical and Engineering Aspects* 522 (2017), pp. 445–452. ISSN: 0927-7757. DOI: https://doi.org/10.1016/j.colsurfa.2017.03.020. URL: http://www.sciencedirect.com/science/article/pii/S092777571730256X.

[17] R. Shegokar, K.K. Singh, and R.H. Müller. “Production stability of stavudine solid lipid nanoparticles—From lab to industrial scale”. In: *International Journal of Pharmaceutics* 416.2 (2011). 8th European Workshop on Particulate Systems (EWPS), pp. 461–470. ISSN: 0378-5173. DOI: https://doi.org/10.1016/j.ijpharm.2010.08.014. URL: http://www.sciencedirect.com/science/article/pii/S0378517310006198.

[18] Qian Shen and Siew Young Quek. “Microencapsulation of astaxanthin with blends of milk protein and fiber by spray drying”. In: *Journal of Food Engineering* 123 (2014), pp. 165–171. ISSN: 0260-8774. DOI: https://doi.org/10.1016/j.jfoodeng.2013.09.002. URL: http://www.sciencedirect.com/science/article/pii/S0260877413004548.

[19] S.C. Yang and L.S. Lai. “DRESSINGS AND MAYONNAISE — Chemistry of the Products”. In: *Encyclopedia of Food Sciences and Nutrition (Second Edition)*. Ed. by Benjamin Caballero. Second Edition. Oxford: Academic Press, 2003, pp. 1898–1903. ISBN: 978-0-12-227055-0. DOI: https://doi.org/10.1016/B0-12-227055-X/00364-3. URL: http://www.sciencedirect.com/science/article/pii/B012227055X003643.

[20] Qianyu Ye, Nicolas Georges, and Cordelia Selomulya. “Microencapsulation of active ingredients in functional foods: From research stage to commercial food products”. In: *Trends in Food Science Technology* 78 (2018), pp. 167–179. ISSN: 0924-2244. DOI: https://doi.org/10.1016/j.tifs.2018.05.025. URL: http://www.sciencedirect.com/science/article/pii/S092422441830013X.

[21] Zhong Ye et al. “Soluble dietary fiber (Fibersol-2) decreased hunger and increased satiety hormones in humans when ingested with a meal”. In: *Nutrition Research* 35.5 (2015), pp. 393–400. ISSN: 0271-5317. DOI: https://doi.org/10.1016/j.nutres.2015.03.004. URL: http://www.sciencedirect.com/science/article/pii/S0271531715000627.

[22] Wiley-Intersience New York. *"Bailey's industrial oil & fat products"*. 2005.